Petrogenesis of the Northwest Corner intrusive phases, Dutoitspan kimberlite, South Africa

Adri Hanekom

Thesis submitted in fulfillment of the requirements for the degree of Master of Science

University of Cape Town
July, 2008

DECLARATION

I hereby declare that the work presented in this thesis is my own unless stated otherwise in the text.

Adri Hanekom
July, 2008

ABSTRACT

The Dutoitspan Group 1 kimberlite pipe forms part of the well-known cluster of pipes located in and around the city of Kimberley, South Africa. Eight macroscopically distinct intrusive phases, i.e. D2 Type 2, D2 Type 3, D2/D5, D5, D18, Type 5, D16 and the D16 dyke are present in the Northwest Corner area of the mine. Microscopically they range from macrocrystic to aphanitic hypabyssal (magmatic) kimberlites with varying amounts of opaque minerals, monticellite and phlogopite. Olivine is the dominant macrocryst phase and alteration varies from unaltered to highly serpentinised. These intrusive phases also contain variable amounts of crustal xenoliths.

Major and trace element compositions of the various intrusive phases tend to cluster, indicating relatively clear geochemical differences between the intrusive phases. Across the various intrusive phases, compositions are variable (major elements: 21.0-37.9 wt % MgO, 26.3-41.2 wt % SiO_2, Mg# 0.86-0.91, 0.81–2.00 wt % TiO_2, 1.36-6.61 wt % Al_2O_3, 3.85-16.9 wt % CaO, 7.0-9.1 wt % FeO*, 0.73–3.65 wt % K_2O; trace element ratios: Zr/Nb 1.33 – 2.34, Nb/Ta 18.4 - 24.6). In terms of REE abundances, La/Sm_n ratios are restricted (4.9 - 5.8), but La/Yb_n ratios vary considerably (57 – 197) and indicate that all samples are highly enriched in LREE relative to HREE.

The whole rock compositions of a number of the intrusive phases are significantly influenced by crustal contamination, i.e. negatively correlated SiO_2 and MgO, a broadly positive correlation between P_2O_5 and MgO, high K_2O, and low FeO*. In contrast, the aphanitic and relatively uncontaminated macrocrystic show major element compositions and correlations opposite to that of the crustally contaminated intrusive phases.

The significant influence of olivine concentration is shown by the relatively high Mg-number and Ni, Co and Cr content of a single intrusive phase. Primitive mantle-normalised patterns for the majority of samples in this study show strong negative K, Hf and Ti anomalies. These anomalies are more subdued in samples that show increased crustal dilution. The Pb, Sr and P contents are variable not only between the different intrusive phases but also between samples within a given intrusive phase. A positive Pb anomaly is common for the crustally contaminated intrusive phase samples.

Crustal contamination and late stage alteration had a significant effect on the major and trace element compositions of some of the Dutoitspan intrusive phases. Approximately 60 % of the samples were therefore eliminated from the study based on the degree to which their whole rock compositions were affected by alteration or contamination. These include all samples from the Type 5, D5 and D16 intrusive phases and, with the exception of a single sample, all D18 samples.

The majority of Dutoitspan samples have been affected by mantle xenolith entrainment, i.e. increased MgO, SiO_2 and Ni abundances and dilution of REE and other incompatible trace element abundances. In contrast, no evidence of the effects of crystal fractionation was found. Following Becker & le Roex (2006), the intrusive phase compositions were corrected for peridotite entrainment by using an average Kimberley garnet lherzolite comprising ~68 % olivine, ~23 % orthopyroxene, ~3 % clinopyroxene, ~5 % garnet and <1 % phlogopite. The Dutoitspan samples, which contain 10 % - 25 % olivine macrocrysts, are therefore calculated to have entrained ~15 % - 35 % garnet lherzolite.

By correcting for peridotite entrainment, an average close-to-primary magma was calculated for each of the intrusive phases: D2 Type 3, D2 Type 2, D2/D5, D18 and the Dyke. The major element compositions of these close-to-primary magmas show a restricted but significant range: ~25-31 wt % SiO_2, ~27-36 wt % MgO, ~9-16 wt % CaO, ~1.2-4.3 wt % K_2O, ~0.6-2.6 wt % Al_2O_3 and Mg# ~0.85-0.90 with ~781-1376 ppm Ni and ~139-284 ppm La.

Using equations for non-modal batch melting and assuming low degrees of partial melting (F = 1%) of a metasomatised garnet lherzolite, compositions of source regions in equilibrium with close-to-primary Dutoitspan kimberlites are calculated. A characteristic feature of the calculated source region compositions is the depleted HREE abundances relative to chondrite. The low HREE abundances, and the high Mg-number and high Ni content of the inferred primary magmas suggest derivation of the primary magmas from a refractory source that had experienced a prior depletion event. The strong enrichment in incompatible trace elements suggests subsequent metasomatic enrichment of the source, prior to kimberlite formation.

TABLE OF CONTENTS

LIST OF FIGURES

LIST OF TABLES

1 INTRODUCTION

1.1 Kimberlite

Kimberlite is a rare rock type in comparison with rocks like basalt, granite and other igneous rocks. It is however of interest to a diverse group of earth scientists as it may contain diamonds and is the transporter of xenoliths from the upper mantle, providing a means to study this largely unknown portion of the earth.

Two types of kimberlites can be distinguished based on differences between their ages, mineralogy, petrography, mantle xenocryst content, isotopic character and whole rock geochemistry, i.e. Group I and Group II (e.g. Smith *et al.*, 1985b; Skinner, 1989; Mitchell, 1995). Group I kimberlites generally compare well with Wagner's (1914) basaltic kimberlite, are rich in olivine and contain monticellite, serpentine and calcite. Group II kimberlites are mica-rich and similar to the micaceous lamprophyric kimberlite described by Wagner (1914). Group I kimberlites are found all over the world and are generally younger than the Group II kimberlites that to date, have only been found in southern Africa and were primarily classified as kimberlite due to the presence of diamonds.

The following definition of a Group 1 kimberlite is quoted from Woolley et al. (1996) The definition is after Mitchell (1995) and incorporates earlier definitions by Mitchell (1979, 1986, 1994), and Clement *et al.* (1984):

"Group-I kimberlites consist of volatile-rich (dominantly CO_2) potassic ultrabasic rocks commonly exhibiting a distinctive inequigranular texture resulting from the presence of macrocrysts (a general term for large crystals, typically 0.5-10 mm in diameter) and, in some cases, megacrysts (larger crystals, typically 1-20 cm) set in a fine-grained matrix. The assemblage of macrocrysts and megacrysts, at least some of which are xenocrystic, includes anhedral crystals of olivine, magnesian ilmenite, pyrope, diopside (in some cases subcalcic), phlogopite, enstatite and Ti-poor chromite. Olivine macrocrysts are a characteristic and dominant constituent in all but fractionated kimberlites. The matrix contains a second generation of primary euhedral to subhedral olivine, which occurs together with one or more of the following primary minerals: monticellite, phlogopite, perovskite, spinel (magnesian ulvöspinel - magnesiochromite - ulvöspinel - magnetite solid solutions), apatite, carbonate and serpentine. Many kimberlites contain a late-stage poikilitic mica belonging to the barian phlogopite -

kinoshitalite series. Nickeliferous sulfides and rutile are common accessory minerals. The replacement of earlier-formed olivine, phlogopite, monticellite and apatite by deuteric serpentine and calcite is common. Evolved members of the Group may be poor in, or devoid of, macrocrysts and composed essentially of second-generation olivine, calcite, serpentine and magnetite, together with minor phlogopite, apatite and perovskite."

Clement and Skinner (1985) proposed a textural-genetic classification for kimberlites that is basically divided into the following three groups: crater facies, diatreme facies, and hypabyssal facies kimberlite. This classification largely corresponds to the vertical zones of kimberlite pipes, i.e. crater zones, diatreme zones and root zones that were recognised by Dawson (1971) and Hawthorne (1975). The root zone is irregularly shaped and contains hypabyssal kimberlite and breccias. Pipe related dykes and sills crosscut or occur in close proximity to the pipes.

This deep, steep-sided type of kimberlite body that occurs mainly in southern Africa, is only one of three types proposed by Field and Scott Smith (1999) and was named Class 1 by Skinner and Marsh (2004). Class 2 pipes are shallow and comprise only the crater zone, which is infilled with volcaniclastic kimberlite (e.g. the majority of pipes found in Canada); Class 3 pipes are small and steep-sided and mainly infilled with re-sedimented volcaniclastic kimberlite or less frequently, with hypabyssal kimberlite (e.g. the Jwaneng pipe in Botswana) (Field and Scott Smith, 1999).

1.2 Scope of Study

The Dutoitspan kimberlite pipe is located in Kimberley, South Africa and is a Class 1 kimberlite of the Group I variety. It contains both diatreme and hypabyssal facies kimberlite (Clement, 1982). Samples were collected from a portion of the pipe known as the Northwest Corner (see Section 2.2 for discussion on sample locality), which composes predominantly of hypabyssal facies kimberlite. The intention of this study is to:

i. Analyse suitable – the hypabyssal varieties – samples for major and trace elements, and compare variations of these elements between the various intrusive phases. Diatreme facies kimberlites are extremely altered and contaminated (Becker and le Roex, 2006) and therefore analyses of these facies are avoided as far as possible for the purpose of this study.

ii. Derive a close-to-primary kimberlite magma composition for the Dutoitspan kimberlite by evaluating and isolating the effects of late stage alteration, crustal contamination, peridotite entrainment and crystal fractionation.

iii. Develop semi-quantitative models to identify petrogenetic processes and source region characteristics.

iv. Compare the geochemistry of samples from this study and the petrogenesis of the Northwest Corner intrusive phases with the recent studies on the petrogenesis of the Kimberley pipes by le Roex *et al*. (2003).

2 GEOLOGICAL SETTING

2.1 Regional Geology

The Dutoitspan kimberlite pipe forms part of the well-known cluster of pipes located in and around the city of Kimberley, South Africa (Figure 2.1). This cluster of pipes, which also includes the De Beers, Kimberley, Wesselton and Bultfontein pipes, represents the type locality of kimberlite.

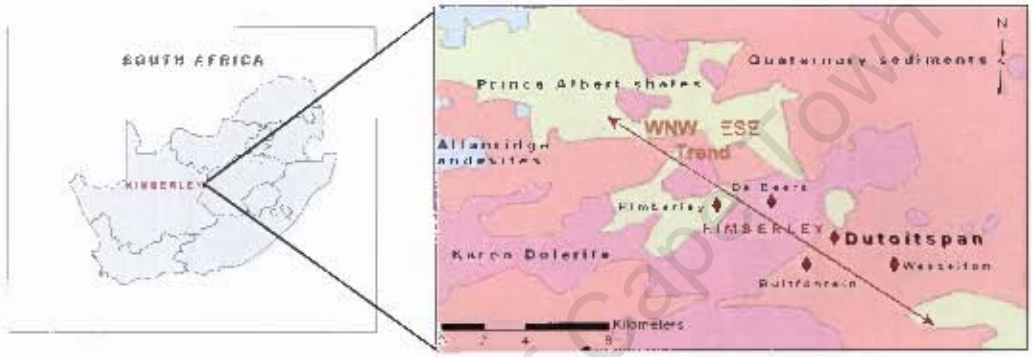

Figure 2.1. Locality plan of Dutoitspan Mine, Kimberley, indicating geological formations in the area as well as the five well known kimberlite pipes (red symbols). Notice the approximate WNW – ESE linear trend of the five major pipes.

At present, the surface area in the vicinity of Kimberley is covered by recent red sand and calcrete, with numerous outcrops of Karoo-age dolerite. It was, however, the underlying formations and the dolerite intrusions that had an apparently significant influence on the emplacement and assemblage of the kimberlite pipes in the area. Tankard *et al.* (1982) suggested that these formations were formed during five stages of crustal evolution (Table 2.1).

The granitic basement was formed during the first stage of evolution (Table 2.1). In the vicinity of Kimberley these basement rocks consist predominantly of amphibolitic and granitic gneiss with locally extensively developed talc schist. Numerous pegmatite veins crosscut these rocks (Clement, 1982).

Sediments and volcanic rocks, including the Ventersdorp andesitic lavas, buried the basement rocks during the second stage of crustal evolution (Table 2.1). Measured from surface, the depth to the unconformable contact between the Ventersdorp Supergroup and the underlying Archaean Basement Complex is approximately 350 m at Dutoitspan mine (Clement, 1982).

Table 2.1. Summary of geological evolution of southern Africa (after Tankard *et al.*, 1982).

	Age (Ma)	Evolutionary Stage	
Phanerozoic	0	After Gondwana	Tertiary – Recent Deposits
		The Gondwana Era	Karoo volcanics
			Karoo Sequence
			Cape folding
	500		Cape Supergroup
Late Proterozoic	1000	Proterozoic orogenic activity	Metamorphism, and intrusion of younger rocks
Middle Proterozoic	1500		Waterberg Group
Early Proterozoic	2000		Bushveld Complex
		Early Proterozoic supracrustal development	Transvaal & Griqualand West Sequences
	2500		Ventersdorp Supergroup
Late Archaean			Witwatersrand Supergroup
			Pongola Sequence
Middle Archaean	3000	Archaean crustal development	Development of granitic crust
	3500		
Early Archaean			
	4000		

The third stage occurred during the Proterozoic Eon (Table 2.1). It was characterised by tectonic activity, during which deformation, as well as the intrusion of granitoid rocks and the partial melting of older rocks, occurred.

During phase four, the Gondwana Era (Table 2.1), the quartzitic sandstones and shales of the Cape Supergroup were deposited. This was followed by continental glaciation and, amongst others, the formation of the Dwyka tillites, which form the base of the Karoo Supergroup. Dolerite dykes and sills intruded the sediments that filled the Karoo basin after the period of glaciation. It should be noted that the Cape Supergroup does not occur in the Kimberley area and that, due to extensive erosion after the emplacement of the Kimberley kimberlite pipes, only Dwyka-aged Karoo rocks are preserved.

From surface to approximately 100 to 120 m below surface, the country rock surrounding the Dutoitspan pipe comprises of horizontally bedded black and grey shales of the Carboniferous Dwyka Group. As noted earlier, areally extensive dolerite sills are present within the shales and are up to 30 m thick. In places these sills have prevented the kimberlite magma from reaching surface resulting in kimberlite sills and blind intrusions (Clement, 1982).

Fragmentation of Gondwanaland occurred during the Post-Gondwana era, the fifth stage of crustal evolution. Following the formation of the South Atlantic ocean, numerous kimberlite pipes, including Dutoitspan, were intruded during the early Cretaceous. The Kimberley group of kimberlites appear to be linearly aligned in a broad west-northwest – east-southeast direction (Clement, 1982) (Figure 2.1) and are dated to be 86 ± 3 Ma in age (Allsopp and Barrett, 1975), using the Rb-Sr method on phlogopite.

2.2 Local Geology

After being discovered in 1869, development of the Dutoitspan mine began in 1871. Opencast mining ceased in 1902 when a shaft was sunk and underground mining began. Production has been predominantly focused on the higher grade, eastern section of the pipe and the last production level was at the 870 m Level.

A bulk sampling project of an area known as the Northwest Corner (NWC) on 760 m Level (Figure 2.2) began in June 2001. The aim of this project was to determine the economic viability to mine the area given that a new treatment plant, capable of handling lower grade material, has also been built in Kimberley. The scope of the project included the development of a 4 x 4 m tunnel to produce at least 12 x 550 ton bulk samples.

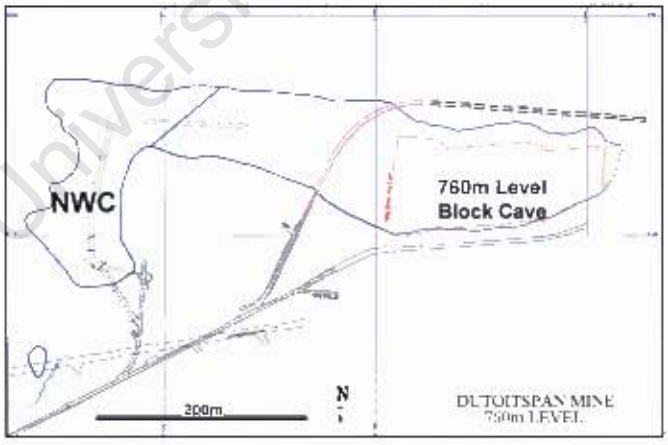

Figure 2.2. Plan view of Dutoitspan on 760 m Level with sampling tunnel in NWC (figure courtesy of Kimberley Mines Survey Department).

The mine sampling project exposed at least 7 different kimberlite types of the known 18 (Clement, 1982) present in the Dutoitspan pipe. The sampling tunnel cuts across these 7 types and affords an opportunity to study them in detail.

Clement (1982) conducted a detailed investigation into the geology of the Dutoitspan kimberlite. His interpretation of the NWC is illustrated in Figure 2.3 (a). His classification of each of the Dutoitspan kimberlite facies is preceded by a *D* and followed by a number depicting the sequential intrusion of the facies.

A map of the same area, dated 1967 and signed by C.D. Hallam, was however found to be more consistent with observations made during recent work done by various geologists, including the author. As seen in Figure 2.3 (b), the geology of the NWC is much more complex than indicated by Clement (1982). Since it can be assumed that Clement (1982) had access to Hallam's map, it is speculated that he might have combined some of the facies based on diamond grade. In recent years geologists working at Dutoitspan mine have adopted the use of a combination of Clement (1982) and Hallam's (1967) classification as shown in Figure 2.4. This classification was also adopted in the present study.

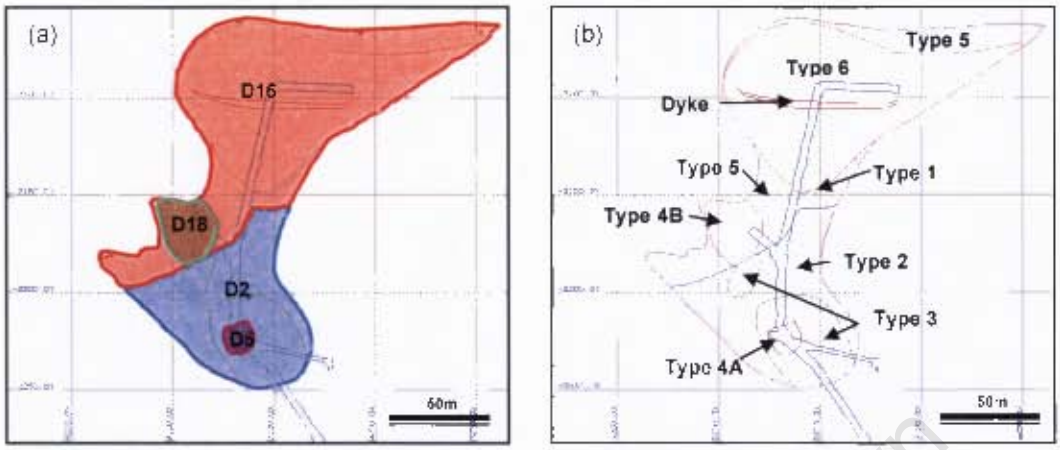

Figure 2.3. (a) Clement's (1982) and (b) Hallam's (1967) interpretation of the geology of the NWC, Dutoitspan.

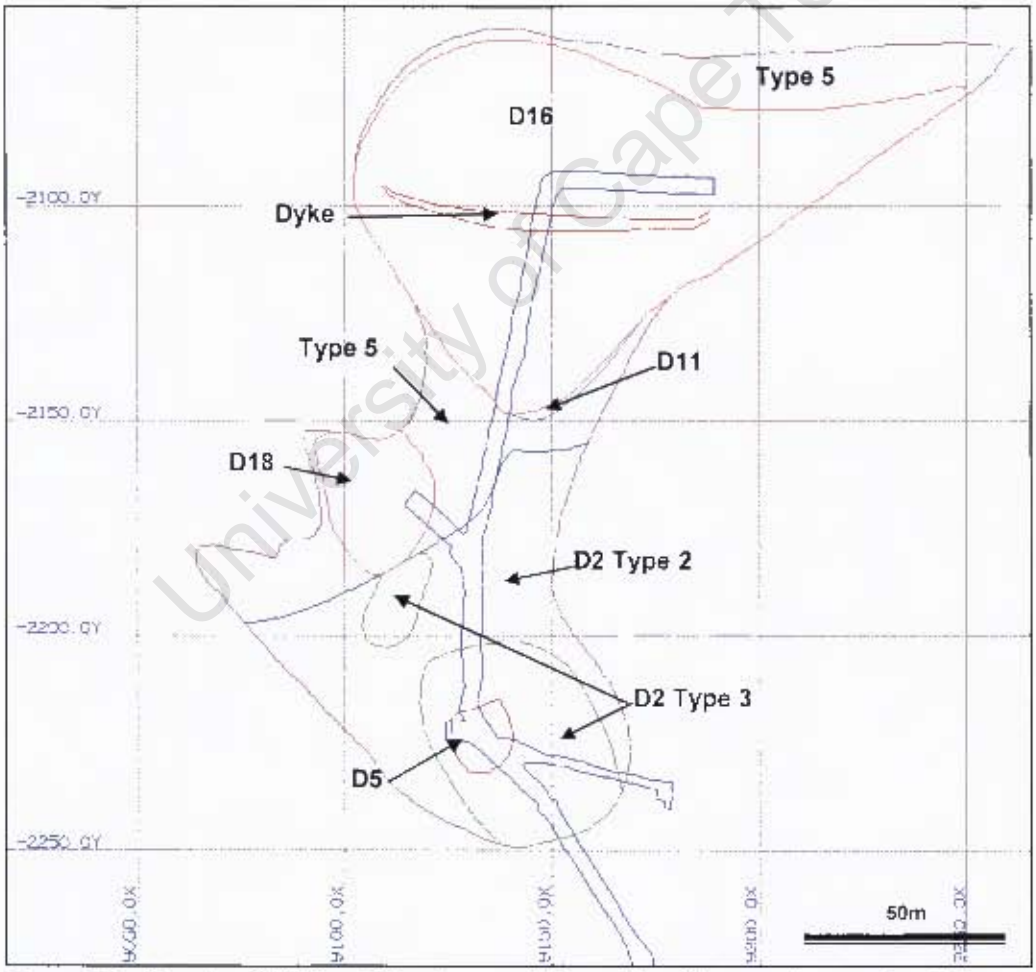

Figure 2.4. Plan view of NWC on 740 m Level with the position of the sampling tunnel on 760 m Level superimposed. This is a combination of mapping done by Clement (1982) and Hallam (1967) on 740m Level.

2.2.1 Sampling

During the recent bulk sampling project the area was mapped in detail as exposed by the sampling tunnels. Representative samples were collected during mapping for both petrographic (see chapter 4 and Appendix A) and whole rock chemistry analysis (see chapter 5) in an attempt to characterise the different intrusions. The letter 'P' in a sample number refers to a petrographic sample, whereas the letter 'W' refers to a sample collected for whole rock geochemistry analysis. The basic sample numbers, without the letters 'P' or 'W' are listed in Table 2.2 and their positions are indicated in Figure 2.5.

Table 2.2. Sample numbers and positions of samples collected during the study. The locations of the samples are indicated by their distance from the nearest survey peg, where '+' indicates a northerly direction or east in the case of the D16 samples.

Sample Number	Intrusive Phase	Location
NWCD2T3-01	D2 Type 3	N4213-10.6m, Left
NWCD2T3-02	D2 Type 3	N4213-3.6m, Left
NWCD2T3-03	D2 Type 3	N4213+0m, Left
NWCD2T3-04	D2 Type 3	N4223+9.5m, Left
NWCD2T3-05	D2 Type 3	N4228+1.6m, Left
NWCD2D5-01	D2/D5 Aphanitic contact	N4213+2.9m, Left
NWCD2D5-02	D2/D5 Aphanitic contact	N4223+7.4m, Left
NWCD5-01	D5	N4213+5.1m, Left
NWCD5-02	D5	N4213+8.1m, Right
NWCD5-03	D5	N4213+11.5m, Right
NWCD5-04	D5	N4223+1.5m, Left
NWCD5-05	D5	N4213+17.7m, Left
NWCD2T2-01	D2 Type 2	N4228+9.5m, Left
NWCD2T2-02	D2 Type 2	N4228+13.8m, Left
NWCD2T2-03	D2 Type 2	N4228+18.3m, Left
NWCD2T2-04	D2 Type 2	N4228+22.4m, Left
NWCD2T2-05	D2 Type 2	N4228+26.4m, Right
NWCD18-01	D18	N4233+5.5m, Left (in breakaway)
NWCD18-02	D18	N4233+11.1m, Left (in breakaway)
NWCD18-03	D18	N4233+2.2m, Right
NWCD18-04	D18	N4233+6.1m, Left
NWCD18-05	D18	N4233+9.0m, Left
NWCT5-01	Type 5	N4233+14.7m, Right
NWCT5-02	Type 5	N4233+17.1m, Right
NWCT5-03	Type 5	N4233+18.5m, Left
NWCT5-04	Type 5	N4233+20.6m, Left
NWCT5-05	Type 5	N4233+21.6m, Right
NWCD16-01	D16	N4235+13.5m, Left
NWCD16-02	D16	N4238-1.0m, Left
NWCD16-03	D16	N4238+21.4m, Left
NWCD16-04	D16	N4241+10.3m, Left
NWCD16-05	D16	N4243+4.2m, Left
NWCD16-06	D16	N4243+36.0m, Left
NWCD16Dyke-01	Dyke in D16	N4241+0m, Right
NWCD16Dyke-02	Dyke in D16	N4243+26.6m, Right

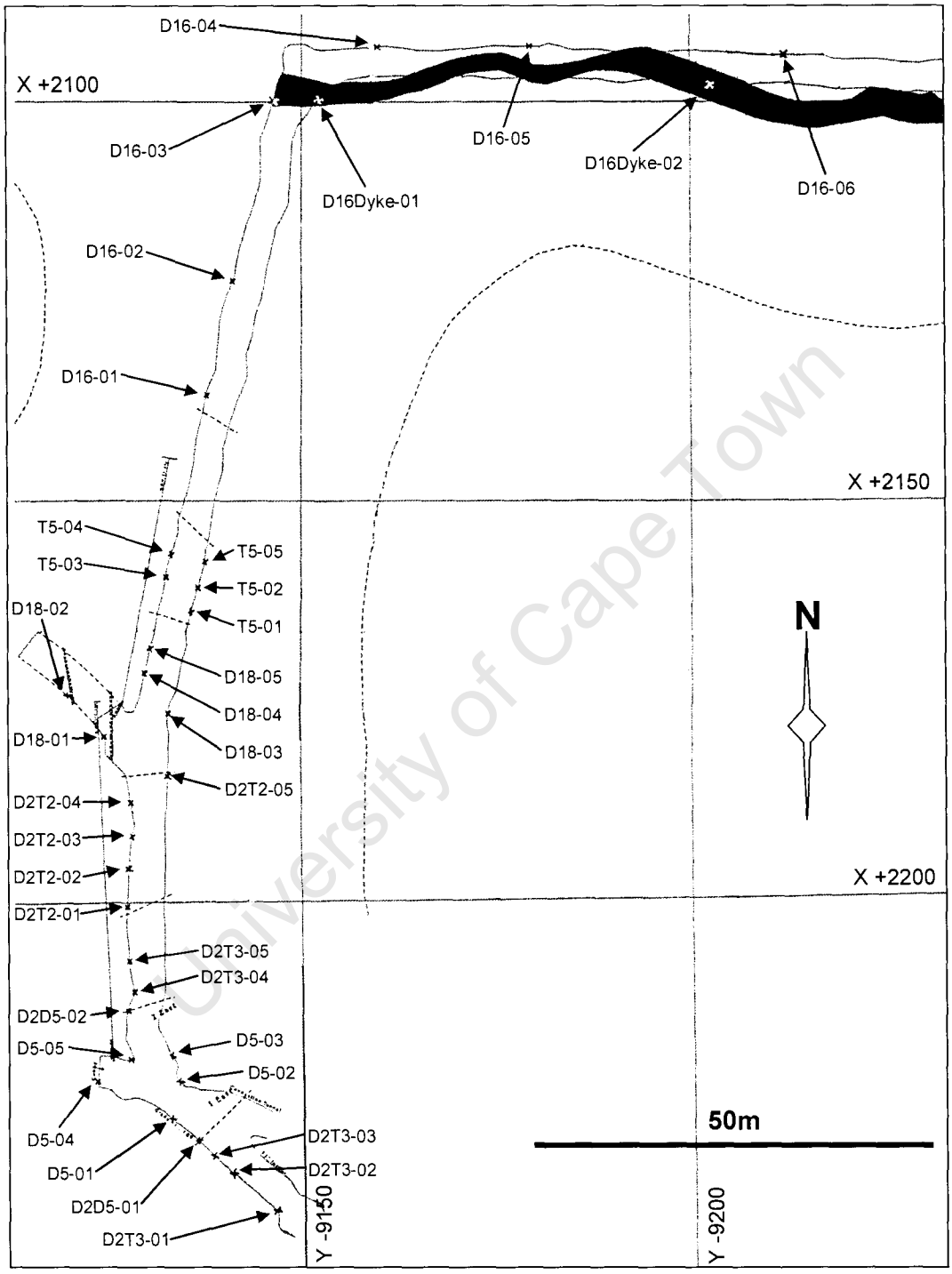

Figure 2.5. Locality plan of the North West Corner sampling tunnel indicating the positions of samples collected for whole rock chemistry and petrographic analyses. Also note the position of the dyke crosscutting the D16 facies.

3 PREVIOUS WORK

The first diamond recovered from kimberlite was found on the Dutoitspan farm in November 1869 (Janse, 1995). This discovery led to a diamond rush and four more economically viable kimberlite pipes, namely Bultfontein, De Beers, Kimberley and Wesselton, were found. During the more than 130 years of diamond mining in the Kimberley area, numerous researchers have included the geological aspects of the Dutoitspan kimberlite pipe in their studies.

The focus of this chapter is to provide the reader with brief summaries of previous work related to the present study. These summaries are chronologically noted below. Note that details of these and other studies are discussed in more detail where applicable in the sections to follow.

According to Clement *et al.* (1984), it was **Lewis (1887)** who introduced the term kimberlite into geological literature to describe the host-rock of diamond from the type locality Kimberley, South Africa.

Wagner, P.A. (1914) conducted a major study of "The diamond fields of Southern Africa", which he concluded with "The origin of kimberlite". Herein he notes that the composition of kimberlites suggests a deep-seated origin and that their similarity over an extensive area on the South African Plateau indicates that the same geological conditions prevailed at the time of formation of the various pipes. He suggested that kimberlite magma may be produced by the relief of pressure on potential fluid zones of peridotite, which underlie the granitic basement of southern Africa at an unknown depth. He also noted that the low temperature gradient (measured in certain Johannesburg mines) implies an abnormal thickness of solid crust beneath the South African Plateau, now widely known as the Kaapvaal Craton.

Allsopp *et al.* (1969) determined the age of the Dutoitspan kimberlite to be approximately 80 Ma, and **Allsopp and Barrett (1975)** determined an age of 84 ± 3 Ma using the Rb-Sr method on phlogopite. An age of 82 ± 3 Ma was determined by **Green (1985)** using the fission-track technique on zircon.

Snowden (1981) studied the D2 and D5 intrusive phases of the Dutoitspan kimberlite pipe (see Section 2.2) by analysis of their petrography, mineral chemistry and whole rock geochemistry. Some of the conclusions of this study are summarised below:

i. The D2 intrusive phase is a monticellite kimberlite that has a chilled margin where in contact with the gneissic granite country rock and is intruded by the D5 intrusive phase, a phlogopite kimberlite.
ii. Whole rock geochemistry suggests that the kimberlite magmas originate from the partial melting of mantle material in the presence of a fluid enriched in lithophile elements.
iii. The phlogopite type kimberlite shows a reduced concentration of lithophile elements relative to the monticellite type kimberlite since it was subjected to a larger degree of partial melting.
iv. The monticellite contact rock rapidly froze without being significantly affected by contamination with crustal material and is therefore highly enriched in REE, Nb and Sr.

C.R. Clement studied the kimberlite pipes in the Kimberley area, including the Finsch and Koffiefontein pipes, over several years and presented his findings in a Ph.D. thesis (**Clement, 1982**). He suggested that primary minerals crystallised during two stages: in the upper mantle before intrusion and near surface after intrusion, and that the general crystallization sequences during the two periods are:

i. pre-intrusion – ilmenite/spinel/perovskite/rutile, olivine, diopside, phlogopite;
ii. post-intrusion – ilmenite/spinel/perovskite, diopside, monticellite, apatite, phlogopite, calcite and serpentine.

He also suggested that olivine phenocrysts crystallized in the upper mantle before inclusion of olivine xenocrysts originating from upper mantle peridotite. Variations in the whole rock element contents of the Kimberley pipes are ascribed to batch-mixing of magma. The addition of average upper mantle enriched these batches in olivine and orthopyroxene to different extents.

McCandless (1999) noted that there is enough geochemical and geophysical evidence to suggest that subducted oceanic lithosphere extends far beneath continental lithosphere and contains sufficient volatiles for initiating deep-mantle magmatism. He proposed that the spatial-temporal trends in southern African kimberlite magmatism

(and those in North America) can be linked with changes in convergence velocity between oceanic and continental lithospheric plates over the last 200 Ma.

A major study with regard to the petrogenesis of the Group 1 Kimberley kimberlites, which include the Dutoitspan kimberlite, is that by **le Roex *et al.* (2003)**. They have shown that the whole rock major and trace element compositions of hypabyssal kimberlites can be used to estimate their close-to-primary magma compositions. It was proposed that kimberlite is produced by a small degree (~1 %) of melting of a metasomatised source and originates from a sub-lithospheric source region. It was also suggested that the primary magmas originate from an upwelling mantle plume given the similarity between the incompatible element ratios of kimberlites and ocean island basalts.

As noted in Section 1.2 results from the present study will be compared with the abovementioned study by le Roex *et al.* (2003).

4 PETROGRAPHY

In this section the various intrusive phases encountered during the NWC bulk sampling project are discussed based on macro- and microscopic observations. Detailed descriptions of each of the thirty-five samples collected during this study are enclosed in Appendix A and the reader is referred to Section 2.2.1 in Chapter 2 for sample positions. Note that modal abundances were determined by visual estimation. This method is preferred over point counting based on the variability of the macrocrystic composition of kimberlites over a few centimetres (e.g. le Roex *et al.*, 2003).

A brief discussion of previous work by Hallam (1967) and Clement (1982) are noted in Section 2.2 of Chapter 2 and will therefore not be repeated here. The textural-genetic classification system of Clement and Skinner (1985) is used in this chapter to describe and classify the samples in this study. As will be shown below, all samples in this study are hypabyssal facies kimberlites and include macrocrystic, segregationary and aphanitic textured kimberlite (Clement and Skinner, 1985). The macrocrystic varieties are characterised by anhedral grains of predominantly olivine macrocrysts. The crystallisation of minerals in irregular pools or patches imposes a segregationary texture on the kimberlite. Aphanitic kimberlites are microporphyritic rocks that lack macrocrystic olivine. It should be noted that gradations between the textures may occur (Clement and Skinner, 1985).

The bulk sampling tunnel was mapped in detail as its development progressed and the contacts between the various intrusive phases are indicated in Figure 4.1. Note that the extrapolations of these contacts are inferred from their angles with the tunnel and maps of levels above 760 m Level.

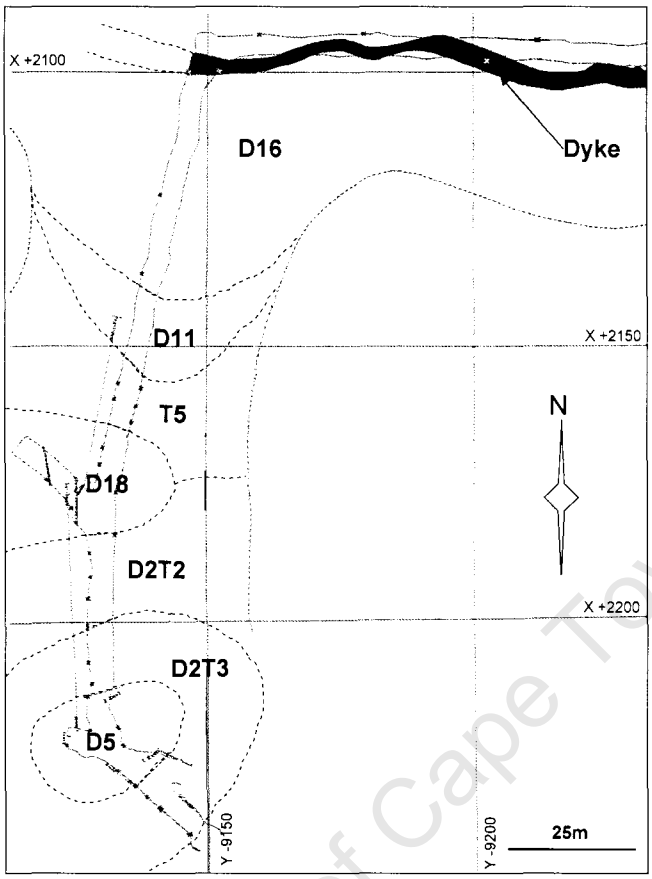

Figure 4.1. Plan view of NWC on 760 m Level, indicating the contacts between the various intrusive phases. Note that extrapolations of the contacts outside of the tunnel are inferred.

4.1 D2 Type 3 - macrocrystic opaque- and monticellite-rich hypabyssal kimberlite and D2/D5 – aphanitic opaque- and monticellite-rich hypabyssal kimberlite

On 760 m Level the D2 Type 3 intrusive phase (Figure 4.2a & b) is in sharp contact with the surrounding amphibolite and granite-gneiss country rock. It is a hard, dark grey to black hypabyssal kimberlite (Clement and Skinner, 1985), which contains highly carbonatised, creamy-green or –pink xenoliths (5-80 mm in size, but on average 10-20 mm). Reaction rims occur around some of the xenoliths. The xenoliths are crustal in origin - cores of shale, dolerite and basement granite-gneiss are recognisable in a number of the xenoliths.

From the contact with the surrounding country rock to approximately 5 m inside the kimberlite, where a few calcite veins were observed, the D2 Type 3 intrusive phase contains approximately 5 % highly carbonatised xenoliths. The abundance of xenoliths increases to between 10 and 15 % in the following 5 m, and decreases again to ~5 % for approximately 0.80 m. The last half meter before the contact with the D5 intrusive

phase, which cuts through the middle of the D2 Type 3 intrusive phase, is aphanitic (Clement and Skinner, 1985) on a macroscopic scale and contains rare vertical flow bands of olivine (Figure 4.3 & 4.4). Microscopically it is classified as a micro-porphyritic kimberlite due to the presence of abundant small olivines. This kimberlite surrounds the D5 kimberlite. Clement (1982) has described a similar phenomenon, 3 to 6 m in width, on higher levels.

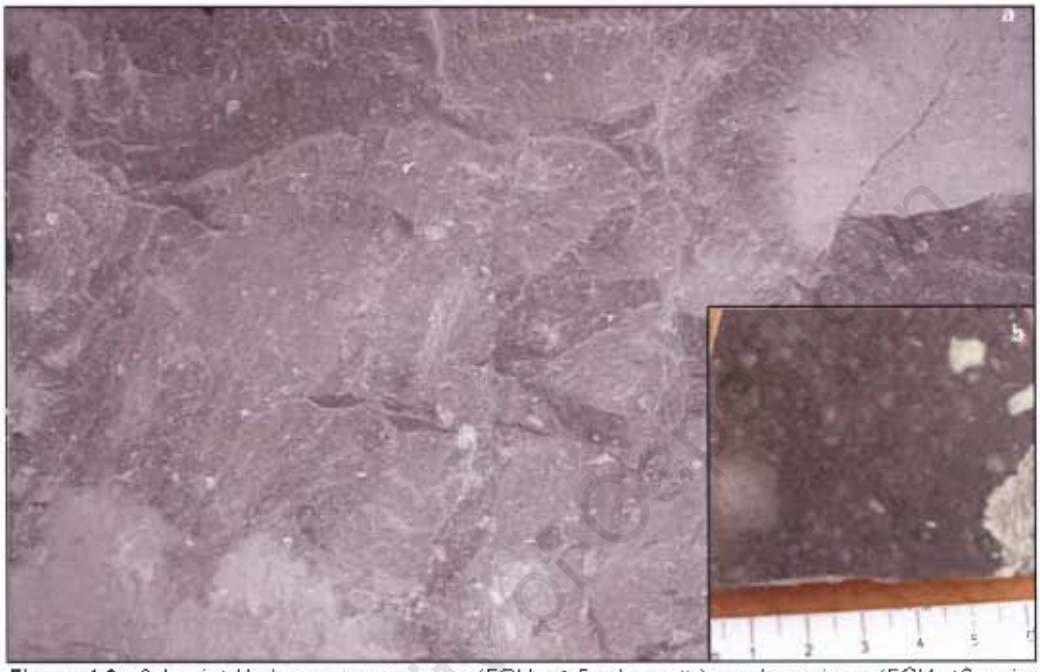

Figure 4.2a & b. (a) Underground exposure (FOV: ±1.5 m) and (b) hand specimen (FOV: ±6 cm) of D2 Type 3 intrusive phase. Note lack of large and abundant xenoliths in comparison with intrusive phases such as the D5 kimberlite

Fresh olivine macrocrysts, on average 3-7 mm and up to 20 mm in size, are common. Microscopically they increase slightly in abundance towards the contact with the D5 intrusive phase, whereas the phenocrysts decrease in quantity and average size. The same applies to the other side of the D5 intrusive phase as one progresses towards the contact with the D5. At approximately 20 % modal abundance, monticellite is the most abundant groundmass phase. Spinels are common, whereas phlogopite phenocrysts, perovskite and apatite occur in lesser amounts. Pools of carbonate occur regularly throughout the matrix. The serpentine and clay contents increase slightly towards the contact with the D5 intrusive phase.

On the northern side of the D5 intrusive phase, the D2 Type 3 is similar in appearance to that described above and contains approximately 10 % xenoliths. A concentration of these carbonatised xenoliths occurs in a near vertical line approximately 7 m from the contact with the D5 intrusive phase.

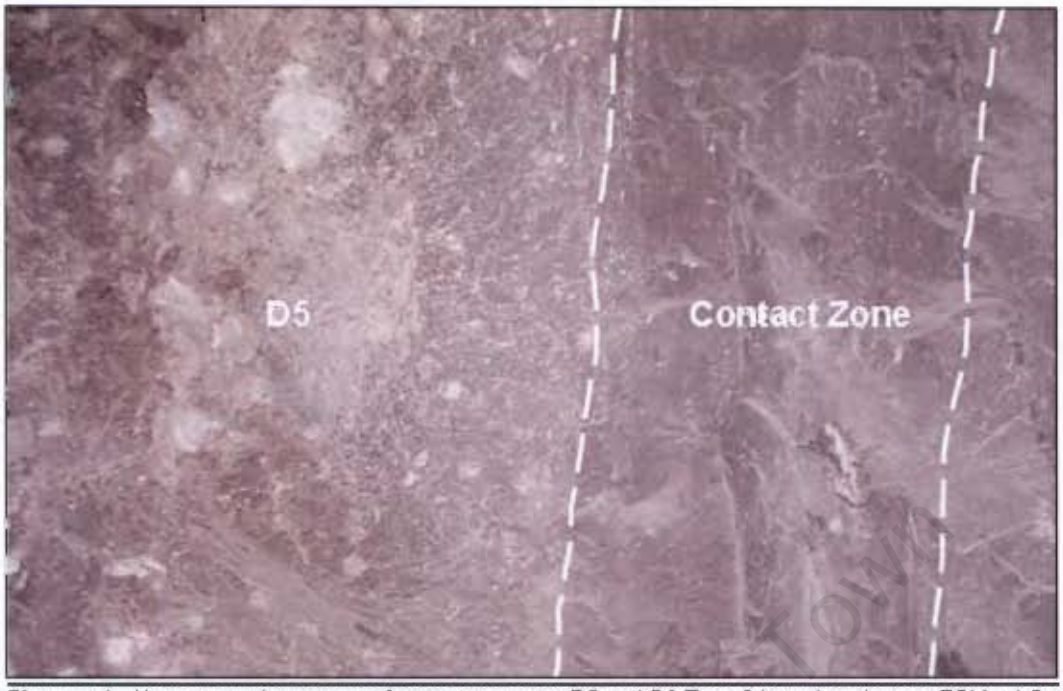

Figure 4.3. Underground exposure of contact between D5 and D2 Type 3 intrusive phases (FOV: ±1.5 m).

Figure 4.4. This sample was taken from the contact zone between the D2 Type 3 and the D5 intrusive phases and contains alternating flow bands of black aphanitic kimberlite (in the centre of the sample shown here) and macrocrystic kimberlite which contains only very rare completely altered xenoliths. FOV: 9 cm.

4.2 D5 - macrocrystic monticellite- and phlogopite-rich hypabyssal kimberlite

As mentioned above, the D5 intrusive phase (Figure 4.3 & 4.5) cuts through the middle of the D2 Type 3 and has an approximate diameter of 20 m on 760 m Level. It is speckled in appearance and is pinkish brown in colour due to the relatively high abundance of phlogopite. It contains approximately 25 % highly carbonatised xenoliths. The number of xenoliths decreases to approximately 10 % towards the outer 3-5 m rim of the D5 kimberlite. Subangular to subrounded xenoliths of up to 200 mm in size were observed. On average, however, they are smaller than 40 mm. Although the xenoliths are generally highly carbonatised and whitish or brownish in colour, a few cores of granite-gneiss, shale and dolerite were recognised by their distinctive macroscopic characteristics. Rare, predominantly unaltered, black shale xenoliths

were also observed. The D5 kimberlite contains abundant altered olivine and phlogopite macrocrysts.

Microscopically the matrix of this rock is orange-brown in colour. It contains abundant fairly fresh olivine macrocrysts with serpentinised rims. The olivine phenocrysts are partly to completely serpentinised. A number of phlogopite macrocrysts that have been partly resorbed and are surrounded by secondary spinel, occur regularly throughout the matrix. The matrix consists of clay, perovskite, laths of phlogopite phenocrysts, spinel, and apatite. Stubby prisms of diopside occur as aggregates in some areas of the matrix. Clay is the main base mineral phase, followed by serpentine and some carbonate. The carbonate is most abundant towards the centre of the intrusion.

The xenoliths have been completely altered to clay and carbonate. They are often surrounded by phlogopite and perovskite. A xenolith consisting almost entirely of phlogopite with some ilmenite, possibly a MARID (3.7 mm), has been observed.

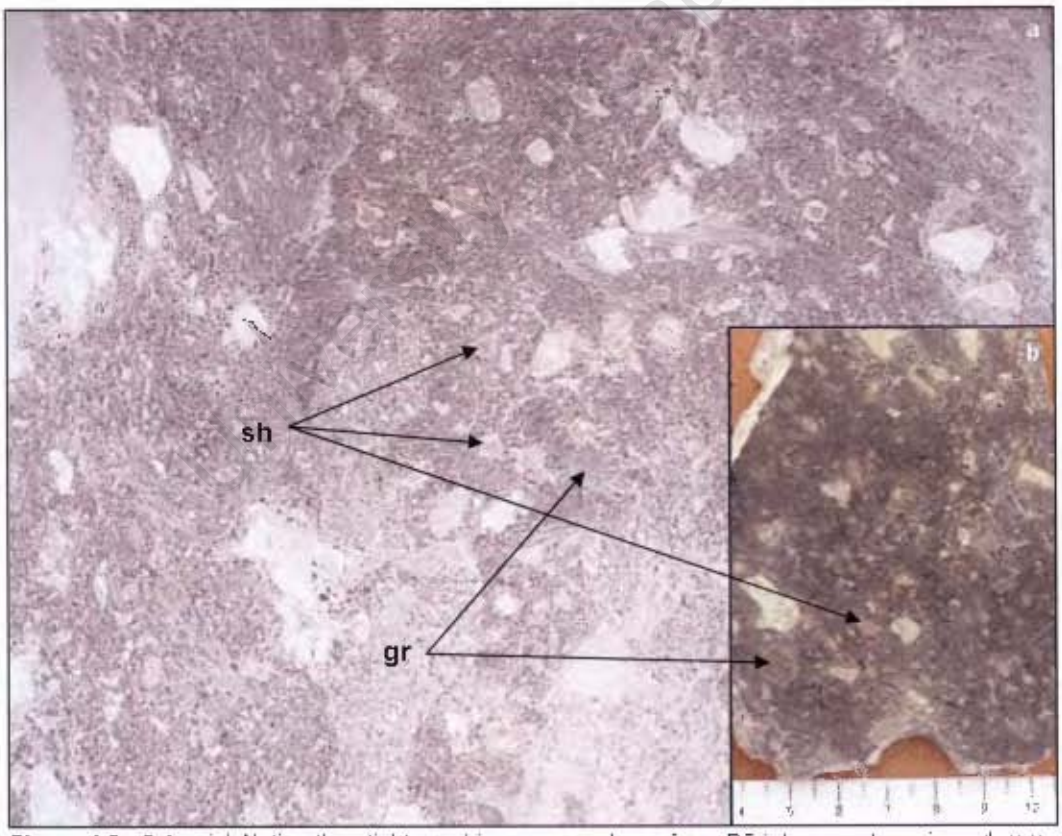

Figure 4.5a & b. (a) Notice the slightly pinkish brown colour of the D5 intrusive phase in underground exposure (FOV: ±60 cm). This can be attributed to the abundance of macrocrystic and groundmass phlogopite (also observed in thin section). Many of the xenoliths have a pinkish brown rim and some (possibly shale sh) are completely pinkish-brown in colour. Others (possibly basement granite) have a greenish colour. (b) The same features are observed in the hand specimen (FOV 7 cm).

4.3 D2 Type 2 - macrocrystic altered monticellite kimberlite of the hypabyssal type

The contact between the D2 Type 3 and D2 Type 2 intrusive phases is sharp. The D2 Type 2 is a hard, dark grey, macrocrystic hypabyssal kimberlite (Clement and Skinner, 1985), which contains approximately 50 % olivines (Figure 4.6). It is homogenous in appearance and contains very rare carbonatised xenoliths and kelyphytic garnets.

On a microscopic scale the D2 Type 2 is a macrocrystic kimberlite that contains abundant anhedral to subhedral, fresh, rounded olivine macrocrysts, which are partly altered to serpentine and chlorite in some cases. A number of these macrocrysts have been recrystallised. Fresh olivine phenocrysts are also highly abundant. Some are slightly altered to serpentine. The most dominant groundmass minerals are euhedral to subhedral monticellite and spinel. Perovskite occurs quite commonly in the matrix. Rare, completely altered, crustal xenoliths, including shale and dolerite, were observed as well. In many cases they are almost completely oxidised whilst some have been altered to clay. Rare phlogopite macrocrysts, which have been completely resorbed, were also found. Very few rounded ilmenite macrocrysts occur. The base minerals are irregular carbonate and serpentine. The carbonate increases in modal abundance towards the contact with the D18 intrusive phase, whereas fresh monticellite decrease in this direction.

An autolith (1.3 mm) was observed in one of the thin sections. It is similar in appearance to the surrounding kimberlite except that it contains fewer oxides and the olivines are more altered.

Figure 4.6. The D2 Type 2 intrusive phase contains large olivine macrocrysts and no xenoliths. FOV 7 cm.

4.4 D18 – macrocrystic diopside-bearing phlogopite-rich hypabyssal kimberlite

The D18 kimberlite is in sharp contact with the D2 Type 2 intrusive phase (Figure 4.7). It is the older of the two intrusions as dykes of the latter cross cuts the D18 kimberlite. The D18 intrusive phase is very similar in appearance to the D5 intrusive phase as was also indicated by Hallam (1967) who named the two intrusive phases Type 4B kimberlite and Type 4A kimberlite, respectively (Figure 4.7 & 4.8 and Figure 4.5a & b).

A few horizontal joint planes, approximately 1-2 m in length, occur randomly in the kimberlite and are filled with lighter grey, brown or greenish soft kimberlitic material.

Amphibolite schist, which occurs very rarely in the D5 kimberlite, forms a more prominent part of the xenolith suite of the D18 intrusive phase. MARID-suite xenoliths also occur. The olivines vary from fresh to slightly altered. In some areas they are golden in colour, which is a characteristic feature of the Type 5 kimberlite discussed below. The D18 kimberlite is greyish-brown rather than typically pinkish-brown near the contact with the Type 5 intrusive phase.

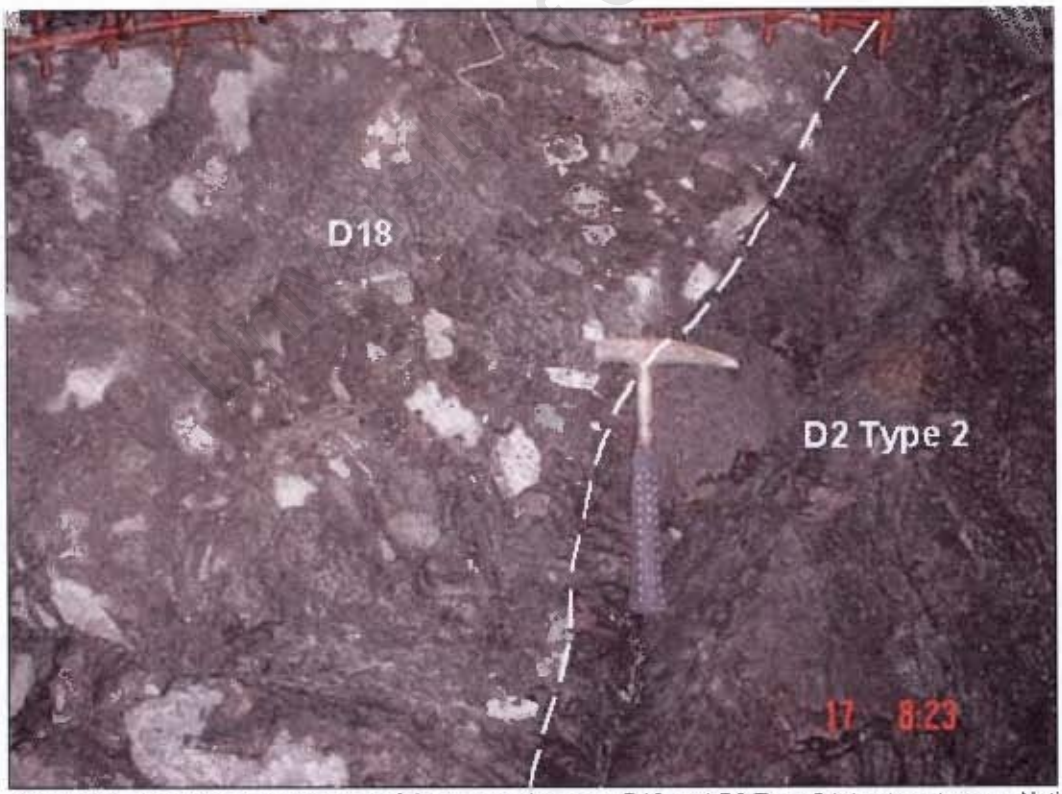

Figure 4.7. Underground exposure of the contact between D18 and D2 Type 2 intrusive phases. Notice the abundance of country rock fragments in the D18 kimberlite, compared to almost no xenoliths in the D2 Type 2 kimberlite.

Microscopically this macrocrystic kimberlite breccia contains abundant slightly altered olivine macrocrysts. A number of these olivines have an orange colouration due to alteration. In rare instances the olivines have been recrystallised. Slightly altered phlogopite macrocrysts occur regularly throughout the matrix. Some of these phlogopites are kink banded, whereas others have been almost completely altered to ilmenite. The olivine phenocrysts are partly to completely altered to serpentine. Perovskite and spinel are common in the matrix. The matrix is very rich in groundmass phlogopite and rare apatite was observed. Carbonate is the most abundant base mineral and sometimes occurs as segregationary pools. Serpentine and clay are also common in the greenish matrix. The subrounded to subangular xenoliths are mostly completely altered to carbonate and phlogopite and are of crustal origin. Only dolerites are recognisable as xenoliths.

Figure 4.8. Note the similarity in macroscopic appearance of the D18 to the D5 intrusive phases (Figure 4.5b)

4.5 Type 5 – segregationary textured phlogopite-bearing hypabyssal kimberlite

The exposure of the Type 5 intrusive phase in the sampling tunnel is approximately 11 m in width. The contact between the Type 5 and the D18 intrusive phases is sharp and sinuous. The most distinguishing features of this kimberlite are its segregationary texture (Clement and Skinner, 1985) and the dull golden colour of the altered olivines (Figure 4.9 & 4.10). It also has been subjected to some degree of stress, as is evident from the presence of strained phlogopite macrocrysts and schist, as well as lens-like structures. These vertically elongated lenses are carbonatised towards their edges.

The Type 5 kimberlite is less competent than any of the intrusive phases described above. It is purplish-grey in colour and contains abundant, predominantly unaltered xenoliths. These include black and khaki coloured shale, dolerite, granite-gneiss and schist. Autoliths are also present.

Microscopically this macrocrystic kimberlite breccia is segregationary in texture with abundant pools of carbonate and some serpentine. The matrix is clay rich and contains abundant diopside as well as some apatite. Perovskite is common and opaque oxides, including spinel and ilmenite, occur as well. The opaque oxides are most abundant towards the centre of the intrusion. The abundant olivine macro- and phenocrysts are almost completely altered to serpentine and are yellowish-green to dark yellow in colour. Rare twinned phenocrysts of olivine were observed. Slightly altered phlogopite macrocrysts are common in the matrix but decrease in abundance towards the contact with the D11 kimberlite (described below). Some of these are kink-banded. The xenoliths are partly to completely altered and are predominantly composed of shale and amphibolite.

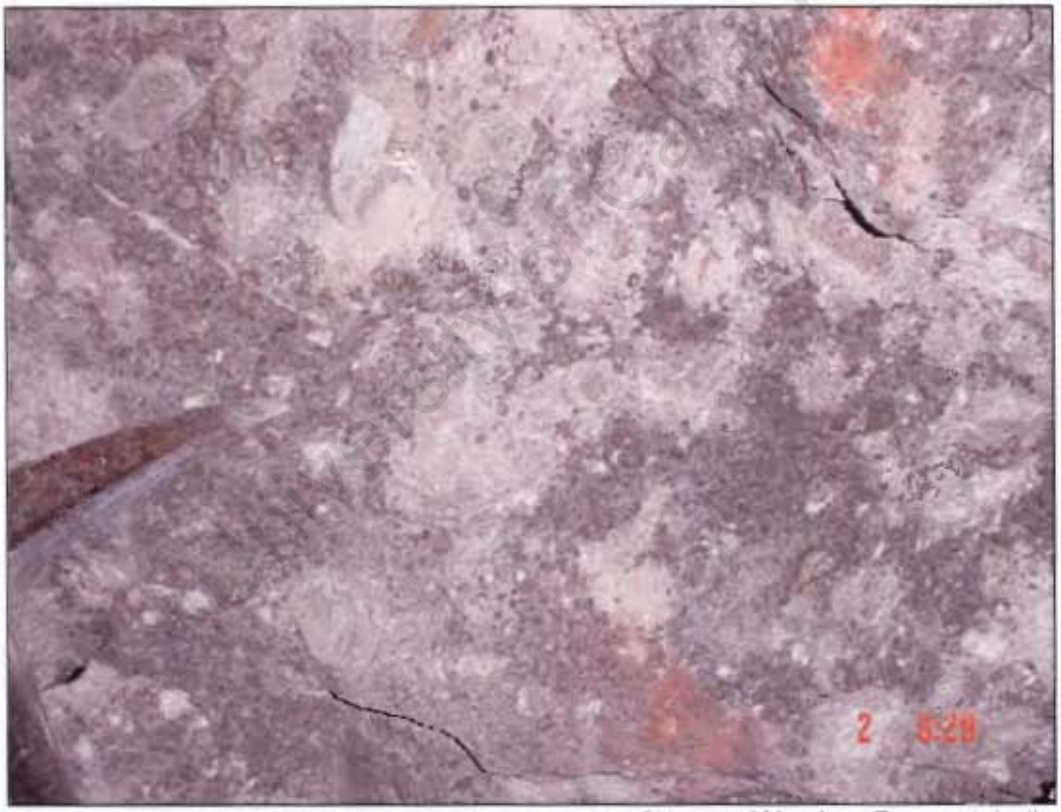

Figure 4.9. Note the segregationary texture (Clement and Skinner, 1985) of the Type S kimberlite in underground exposure, as well as the golden colour of the olivines.

Figure 4.10. The segregatonary texture and golden olivines are also noticeable in this hand specimen of the Type 5 intrusive phase. FOV 6 cm.

4.6 D11 intrusive phase

The D11 is a volcaniclastic kimberlite and does not form part of the present study. A brief macroscopic description is however included below.

The contact between the D11 and Type 5 intrusive phases is sharp. In this exposure of the D11 kimberlite, it is a soft grey kimberlite containing abundant (~50 %) relatively large (up to 1.2 m) xenoliths close to the contact with the Type 5 kimberlite. The xenolith suite is composed predominantly of intact dolerite and shale, and lesser amounts of granite-gneiss, schist and rare Ventersdorp lava, recognised by its amygdaloidal texture. Autoliths of a darker colour than the matrix of the D11 intrusive phase, are present. Rare lapilli-sized pyroclasts and peridotite occur. Some ilmenites were observed. Xenolith size and abundance decrease further away from the contact.

4.7 D16 – macrocrystic diopside-bearing hypabyssal kimberlite

The contact between the D16 (Figure 4.11) and the D11 intrusive phases is gradational over approximately 5 m. The D16 intrusive phase is a grey kimberlite that contains abundant highly altered macrocrystic olivine (~20 %), which are greenish-black in colour with, in some cases, a fresher core. Smaller elongated olivines are ubiquitous (2 mm width, 4 mm length). Abundant xenoliths, similar to that of the D11 kimberlite occur. Basement granite-gneiss xenoliths are completely carbonatised and approximately 2 cm in size, giving the D16 intrusive phase a characteristic white speckled appearance when observed from a distance. Xenoliths of shale, dolerite and schist are largely unaltered. The black and khaki coloured shale fragments are angular, while the remainder of the xenoliths are subrounded

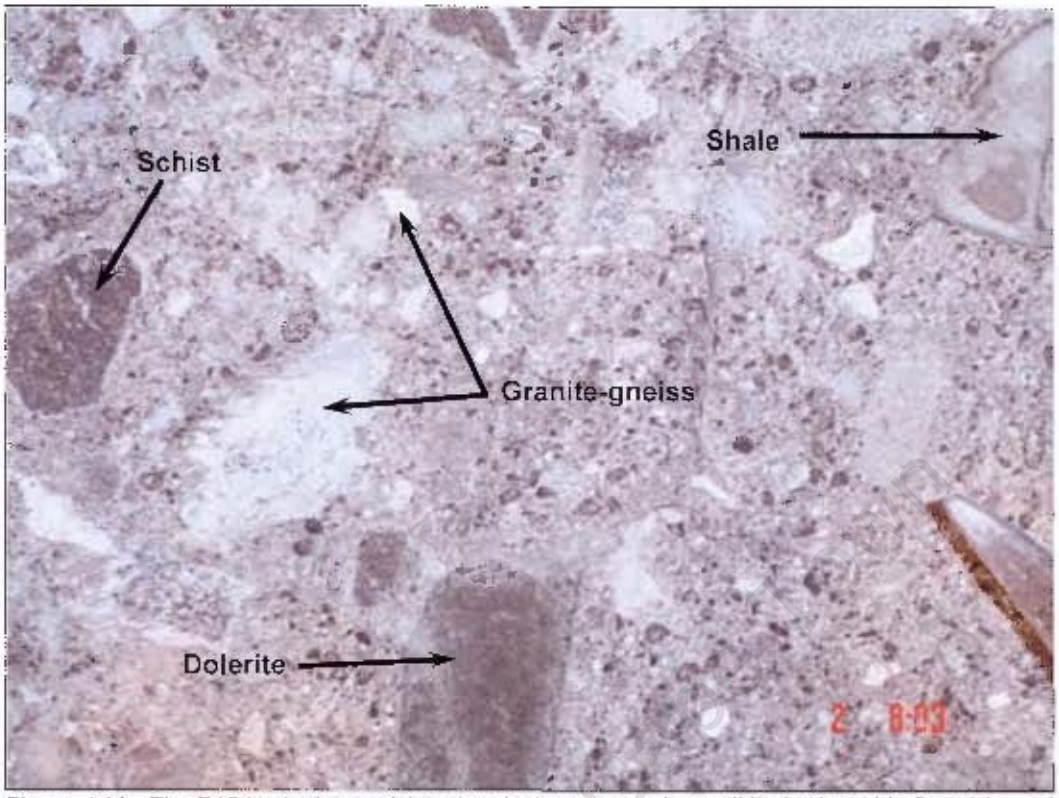

Figure 4.11. The D16 kimberlite contains abundant country rock xenoliths (indicated in figure) in a wide range of sizes, up to ±500 mm, and varying degrees of alteration, as seen here.

The D16 kimberlite is not homogenous in appearance. In some parts of the underground exposure it is similar in appearance to the segregationary textured Type 5 intrusive phase described above, which is purplish-grey in colour and contains golden coloured olivines (Figure 4.12).

An approximately 1 m section in the D16 kimberlite is similar in appearance to the D11 intrusive phase, as it contains approximately 70 % large rounded boulders of Karoo xenoliths, including shale and dolerite, as well as basement granite-gneiss. Approximately 15 % smaller xenoliths, predominantly carbonatised basement granite-gneiss, occur as well. Olivines are subrounded to elongate. A kelyphytic garnet, characterised by its thick black rim, and an autolith, with a darker coloured matrix than the surrounding D16 kimberlite matrix, were also observed.

Where the D16 intrusive phase has the appearance of the Type 5 intrusive phase, it contains ~30 % xenoliths, including peridotite, MARID-suite xenoliths, autoliths and schist. The dolerite xenoliths (50-400 mm, ~40 %) regularly have white alteration rims and approximately 40 % white basement granite-gneiss are present. Xenoliths of shale and/or siltstone (~10 %) are deformed in appearance. Olivine macrocrysts, up to 30 mm in size, occur. They are golden in colour and a number of them have fresh cores.

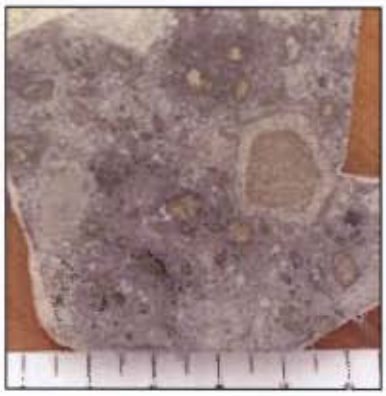

Figure 4.12. In hand specimen the D16 looks very similar to the Type 5 kimberlite described above. Scale in cm.

Microscopically the D16 intrusive phase looks similar to the Type 5 intrusive phase in that the olivines are also dark yellow in colour and its texture is segregationary to globular segregationary (Clement and Skinner, 1985). Again the xenoliths are partly to completely altered. The shales show zonal alteration and are carbonatised in some instances, while the dolerites and amphibolites are fairly fresh. Spinel and perovskite do occur in the matrix but in lesser amounts than in Type 5 kimberlite. Microlitic diopside occurs on the rims of the xenoliths and olivines as well as in the matrix. Serpentine is the main base mineral whilst carbonate is less abundant.

4.8 Dyke in D16 - aphanitic to macrocrystic hypabyssal kimberlite

An approximately 2 m wide dyke cuts through the D16 intrusive phase and runs along the sampling tunnel. It is very similar in appearance to the D2 Type 3 intrusive phase as it is dark grey in colour, macrocrystic and contains approximately 5 % carbonatised xenoliths (Figure 4.13). In some areas the olivines are highly altered or nearly absent, in which case it is aphanitic or micro-porphyritic in appearance.

The two samples collected from the dyke in the sampling tunnel are different in appearance. One thin section is very similar in appearance to that of the D2 Type 2 kimberlite in that it contains abundant opaque oxides and monticellite. The olivine macrocrysts are less abundant, however.

The thin section of the second sample contains a large xenolith (14 mm), which is almost completely altered to carbonate. The matrix contains considerably less opaque oxides, including spinel and ilmenite, than the sample above, and the olivines are highly altered. Most of the sample has been carbonatised. Perovskite occurs commonly. Laths of diopside and/or apatite occur as well. Isotropic pools of serpentine are plentiful.

Based on the observations above, the second sample will be discarded from the remainder of the study with the exception of a brief discussion on its major and trace element content in Chapter 5.

Figure 4.13. This hand specimen of the dyke in D16 is very similar in appearance to samples of D2 Type 2/3 intrusive phases.

5 WHOLE ROCK GEOCHEMISTRY

It is evident, through petrographic analyses, that the various intrusive phases of the Northwest Corner, which are dissimilar in macroscopic appearance, are also diverse on a microscopic scale. In an attempt to determine to what extent these differences are manifested in their chemical compositions, the whole rock geochemistry of the samples was determined.

Thirty-five samples were collected for analyses (see chapter 2 for sample positions). The following sample preparation process was followed to minimize the effect of xenolithic and weathered material on the major and trace element analyses. A hydraulic splitter was used to split samples into smaller pieces with an average size of ~5cm and an attempt was made to remove all weathered surfaces. The samples were subsequently jaw-crushed to reduce the size of individual pieces to ~1cm.

Visible fragments of secondary veins, mantle and crustal xenoliths, and xenocrysts were manually removed from the samples. The remains of these samples were then powdered in a carbon steel Sieb swing mill for one minute.

The xenolithic material of an additional three samples was not removed to compare their results with those of the 'xenolith-free' samples of the same intrusive phases. These samples were selected from the crustally contaminated facies of D5, D18 and Type 5 and labelled D5-02WN, D18-03WN and T5-02WN respectively.

Results of the major and trace element analyses are reported in Table 5.1 and are discussed below. Details of the analytical techniques are reported in Appendix B. The chemical compositions of each of the intrusive phases are compared with those of the study by le Roex *et al.* (2003). The latter is a major study with regard to the petrogenesis of the Group 1 hypabyssal Kimberley kimberlites (see Chapter 3). This study includes samples from the Dutoitspan kimberlite, and will be referred to as the range of Kimberley data.

5.1 Major Elements

Studies of kimberlite major element chemistry have shown that their compositions may be strongly affected by crustal xenoliths accumulated by the kimberlite during emplacement. The contamination index (C.I.) introduced by Clement (1982) has been

widely used (e.g. Price *et al.*, 2000, Taylor *et al.*, 1994) in an attempt to calculate the extent of crustal contamination and weathering. The calculation is as follows:

$$C.I. = \frac{SiO_2 + Al_2O_3 + Na_2O}{MgO + 2K_2O}$$

A high C.I. (>1) usually indicates extensive weathering and/or contamination with crustal xenoliths characteristically being enriched in SiO_2, Al_2O_3 and Na_2O and less enriched in MgO and K_2O (Clement, 1982). A C.I. of less than 1 generally indicates the lack of influence of crustal contamination or weathering. It should be noted that high degrees of serpentinisation may also increase the C.I. of a given sample since it is associated with a decrease in MgO and an increase in volatiles in a closed system (Coetzee, 2005, and references therein). It is therefore, important to not look at the C.I. of a sample independently from its petrographic analyses.

The C.I. of all the samples in the present study was determined and is reported in Table 5.1. The relationship between these C.I.'s and each of the major elements correlated with crustal xenoliths, is illustrated in Figure 5.1.

5.1.1 D2 Type 3 intrusive phase

The major element composition of the D2 Type 3 kimberlite is well constrained with SiO_2 contents ranging from ~30.2 to ~31.8 wt % and MgO contents ranging from ~30.1 to ~33.3 wt % (Table 5.1; Figure 5.2 (a)). Mg-numbers (atomic Mg / (Mg + Fe^{2+}) with Fe_2O_3 / FeO = 0.15) are high and range between 0.89 and 0.90. The remaining major elements also show little variation (Al_2O_3 ~2.39 - ~3.18 wt %; TiO_2 ~1.34 - ~1.56 wt %; CaO ~8.37 - ~10.00 wt %; FeO* ~8.41 - ~9.11 wt %). Samples D2T3-03W and -04W do, however, show an approximate 2 wt % increase in MgO and slightly higher SiO_2 contents relative to the remaining samples. These two samples also have slightly lower Al_2O_3, TiO_2, CaO and FeO* (total Fe) contents in comparison with the remaining three samples. Sample D2T3-01W, which shows the highest CaO concentration, also has a high CO_2 contents (3.89 wt %) in relation to that of the remaining samples (1.21 – 1.63 wt %). The major element compositions of the majority of the D2 Type 3 samples correlate well with that of the Kimberley kimberlites from le Roex *et al.* (2003) with the exception of samples D2T3-03W and -04W that show slightly higher MgO concentrations and plot marginal to the Kimberley range of data.

The C.I. of this intrusive phase ranges between 0.91 and 0.96 (Figure 5.1; Table 5.1), indicating relatively little contamination by crustal xenoliths and a low degree of

serpentinisation. This correlates well with macro- and microscopic estimates of crustal dilution, i.e. approximately 5 – 10%.

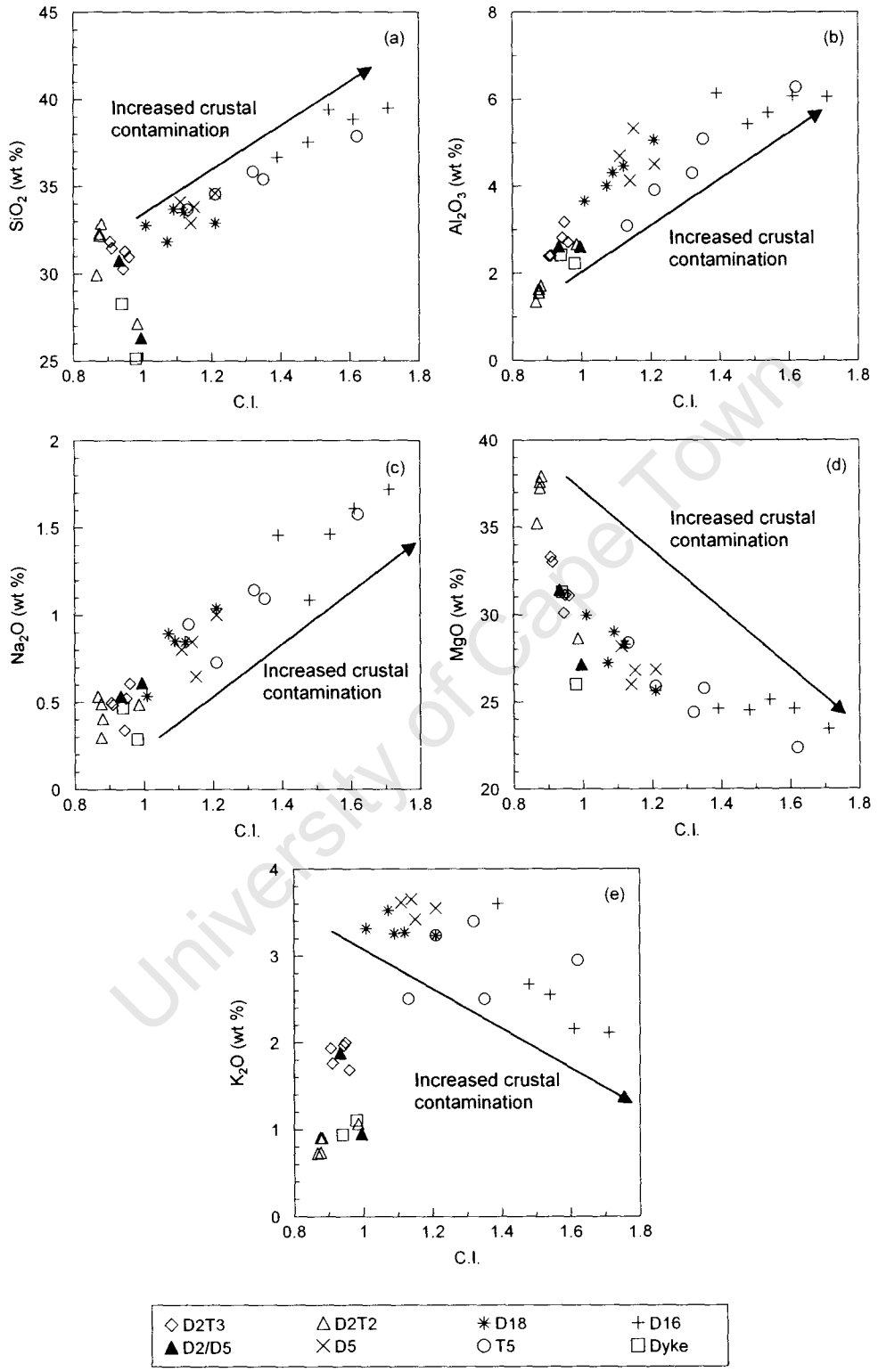

Figure 5.1. Major elements of the NWC kimberlite intrusive phases, that correlate with crustal xenoliths, are plotted here against C.I.

Table 5.1 Bulk-rock major and trace element analyses of the Northwest Corner area, Dutoitspan kimberlite.

	D2 Type 3 - Macrocrystic					D2/D5 - Aphanitic	
Sample #	D2T3-01W	D2T3-02W	D2T3-03W	D2T3-04W	D2T3-05W	D2D5-01W	D2D5-02W
Major Elements (wt %)							
SiO_2	30.2	31.3	31.4	31.8	30.9	30.7	26.3
TiO_2	2.82	3.18	2.40	2.39	2.72	2.62	2.60
Al_2O_3	1.53	1.56	1.34	1.36	1.54	1.56	2.00
Fe_2O_3	8.77	9.07	8.42	8.41	9.11	9.21	8.21
MnO	0.148	0.156	0.147	0.141	0.152	0.151	0.173
MgO	30.1	31.1	33.0	33.3	31.1	31.4	27.1
CaO	10.0	9.85	8.37	8.88	9.50	9.56	16.9
Na_2O	0.339	0.522	0.484	0.496	0.607	0.534	0.610
K_2O	1.97	2.00	1.76	1.93	1.68	1.88	0.947
P_2O_5	1.88	1.06	2.40	2.34	1.67	1.70	4.50
SO_3	0.012	0.010	0.012	0.010	0.013	0.013	0.015
Cr_2O_3	0.267	0.251	0.270	0.263	0.248	0.257	0.356
NiO	0.145	0.147	0.157	0.167	0.156	0.165	0.110
L.O.I.	10.4	8.73	8.76	7.22	9.50	9.18	9.30
H_2O^-	0.593	0.522	0.574	0.501	0.384	0.443	0.571
Total	99.2	99.4	99.6	99.2	99.3	99.4	100
Mg#	0.885	0.885	0.898	0.899	0.885	0.885	0.881
CO_2	3.89	1.22	1.57	1.21	1.63	3.57	2.94
H_2O^+	6.24	7.29	6.95	5.83	7.70	5.41	6.10
C.I.	0.944	0.949	0.911	0.906	0.960	0.933	0.995
Trace Elements (ppm)							
Sc	11.1	11.1	10.1	9.59	11.2	15.7	17.8
V	132	93.2	103	89.7	100	143	199
Cr**	1835	1724	1851	1802	1703	1762	2444
Co	73.6	78.3	76.1	77.6	73.7	61.0	62.1
Ni**	1142	1159	1239	1314	1229	1297	866
Cu	69.1	48.0	60.6	63.1	75.9	215	112
Rb	114	96.6	102	82.8	77.8	54.2	74.5
Sr	2040	1045	1989	2053	1406	2448	2019
Y	16.5	15.3	13.5	13.2	15.4	23.7	25.7
Zr**	352	341	340	339	360	576	569
Nb**	196	202	172	175	179	247	276
Ba	1867	1162	1340	1162	1196	1080	1592
La	167	155	147	142	147	244	268
Ce	329	331	301	293	310	510	539
Pr	34.9	35.7	32.2	31.5	33.5	54.2	60.4
Nd	133	135	123	120	127	208	230
Sm	17.8	17.7	16.2	15.9	16.8	27.8	30.4
Eu	4.43	4.38	3.92	3.89	4.22	6.77	7.40
Gd	11.0	10.5	9.87	9.53	10.5	16.6	18.1
Tb	1.13	1.09	0.97	0.97	1.07	1.67	1.84
Dy	4.91	4.63	4.10	4.05	4.55	7.00	7.67
Ho	0.682	0.641	0.565	0.556	0.651	0.965	1.06
Er	1.34	1.22	1.05	1.05	1.24	1.86	2.02
Tm	0.146	0.140	0.115	0.111	0.137	0.196	0.213
Yb	0.731	0.729	0.568	0.562	0.690	0.955	1.09
Lu	0.092	0.086	0.071	0.068	0.085	0.114	0.119
Hf	6.13	6.29	5.51	5.39	5.75	9.32	9.58
Ta	7.96	8.40	7.17	7.48	7.52	11.1	12.0
Pb	10.6	6.92	9.22	7.74	7.92	4.81	11.1
Th	17.3	17.7	14.8	14.8	16.4	24.7	27.2
U	5.28	4.43	4.41	4.63	3.96	6.06	6.80
Zr/Nb	1.80	1.69	1.98	1.94	2.01	2.34	2.06
La/Nb	0.849	0.769	0.853	0.809	0.820	0.990	0.969
Ba/Nb	9.52	5.76	7.79	6.64	6.69	4.38	5.76
Nb/Ta	24.6	24.0	24.0	23.4	23.8	22.3	23.1
Ce/Pb	30.9	47.8	32.6	37.8	39.1	106	48.4
La/Sm_n*	6.04	5.64	5.84	5.75	5.65	5.66	5.69
La/Yb_n*	163	153	185	181	153	183	177

LOI: loss on ignition; Mg#: atomic $Mg/(Mg+Fe^{2+})$ with $Fe_2O_3/FeO=0.15$; * - normalised to chondrite; ** - trace elements analysed by XRF, all other trace elements analysed by ICP-MS

Table 5.1 Continued

	D2 Type 2 - Macrocrystic					D5 - Macrocrystic			
Sample #	D2T2-01W	D2T2-02W	D2T2-03W	D2T2-04W	D2T2-05W	D5-02W	D5-03W	D5-04W	D5-05W
Major Elements (wt %)									
SiO_2	27.1	32.9	32.3	32.2	29.9	32.9	33.8	34.6	34.1
TiO_2	2.17	0.96	0.88	0.83	0.81	1.15	1.05	1.00	1.03
Al_2O_3	2.66	1.71	1.64	1.56	1.36	4.12	5.32	4.50	4.69
Fe_2O_3	8.69	8.30	8.04	8.04	7.64	7.25	6.96	6.97	7.50
MnO	0.185	0.142	0.144	0.135	0.128	0.124	0.113	0.116	0.109
MgO	28.6	37.9	37.3	37.6	35.2	26.0	26.8	26.8	28.2
CaO	16.7	8.43	8.04	7.66	7.44	7.91	6.37	6.79	6.47
Na_2O	0.486	0.404	0.296	0.491	0.534	0.846	0.647	1.00	0.803
K_2O	1.06	0.903	0.906	0.735	0.727	3.65	3.42	3.55	3.61
P_2O_5	3.91	1.38	1.63	1.64	2.17	4.08	1.25	1.46	3.32
SO_3	0.022	0.009	0.018	0.014	0.010	0.020	0.009	0.009	0.008
Cr_2O_3	0.369	0.346	0.318	0.296	0.301	0.211	0.232	0.203	0.216
NiO	0.119	0.199	0.195	0.197	0.188	0.132	0.144	0.132	0.147
L.O.I.	6.99	5.79	7.24	7.40	13.2	9.92	11.08	10.44	7.18
H_2O^-	0.348	0.247	0.298	0.258	0.348	1.52	2.15	2.00	1.66
Total	99.5	99.6	99.2	99.0	99.9	99.8	99.3	99.6	99.0
Mg#	0.881	0.911	0.912	0.913	0.912	0.889	0.896	0.896	0.894
CO_2	2.18	2.02	1.97	1.58	5.62	1.77	2.71	2.37	0.91
H_2O^+	4.69	3.69	5.16	5.73	7.31	7.41	7.28	7.15	5.73
C.I.	0.985	0.881	0.876	0.876	0.867	1.14	1.15	1.21	1.11
Trace Elements (ppm)									
Sc	6.83	9.02	9.74	10.9	10.3	10.4	10.9	8.14	9.28
V	63.1	95.2	76.3	51.5	101	244	259	226	194
Cr**	2529	2372	2178	2029	2067	1453	1606	1404	1487
Co	70.0	80.9	85.7	81.6	80.1	63.6	66.3	62.3	72.5
Ni**	933	1563	1535	1551	1479	1045	1145	1050	1165
Cu	29.8	43.8	40.1	44.9	15.9	27.4	29.0	33.6	73.6
Rb	39.0	65.4	54.0	55.0	55.9	123	125	131	232
Sr	1027	1469	1276	2112	778	1125	1549	911	1869
Y	10.5	11.0	10.4	10.6	10.6	10.8	10.2	11.2	9.91
Zr**	266	239	218	246	179	236	231	219	199
Nb**	138	129	121	142	110	113	117	118	118
Ba	774	1046	1198	1067	1568	1497	1547	2005	1890
La	121	116	126	137	84.8	92.9	105	92.2	95.2
Ce	248	241	258	263	200	196	206	200	211
Pr	26.6	25.8	27.4	27.5	22.2	21.3	21.9	21.6	23.1
Nd	101	98.2	103	103	86.8	81.5	83.7	83.3	87.7
Sm	13.3	12.8	13.3	13.3	11.6	10.9	11.0	11.1	11.8
Eu	3.23	3.21	3.22	3.23	2.86	2.65	2.68	2.68	2.83
Gd	7.90	7.83	7.76	7.79	7.04	6.69	6.54	6.89	7.08
Tb	0.798	0.795	0.783	0.778	0.723	0.703	0.675	0.722	0.718
Dy	3.27	3.30	3.20	3.24	3.10	3.03	2.96	3.17	3.09
Ho	0.445	0.444	0.429	0.439	0.418	0.429	0.414	0.451	0.433
Er	0.842	0.846	0.823	0.827	0.789	0.842	0.825	0.929	0.835
Tm	0.087	0.091	0.087	0.087	0.084	0.097	0.098	0.106	0.100
Yb	0.448	0.427	0.430	0.423	0.396	0.494	0.498	0.574	0.488
Lu	0.051	0.054	0.047	0.051	0.049	0.065	0.065	0.071	0.064
Hf	3.94	3.70	3.50	3.81	3.12	3.82	4.03	3.87	3.36
Ta	5.10	5.27	5.38	5.24	4.95	4.67	6.12	5.44	6.05
Pb	4.56	9.40	8.42	10.7	19.4	13.0	11.1	13.6	8.67
Th	11.8	12.5	13.1	13.8	12.3	10.7	10.9	11.3	11.9
U	3.08	3.58	3.12	4.20	2.56	3.26	3.97	3.26	2.91
Zr/Nb	1.93	1.86	1.81	1.73	1.63	2.08	1.98	1.85	1.69
La/Nb	0.882	0.903	1.039	0.965	0.772	0.819	0.898	0.781	0.806
Ba/Nb	5.62	8.13	9.9	7.50	14.3	13.2	13.3	17.0	16.0
Nb/Ta	27.0	24.4	22.5	27.2	22.2	24.3	19.1	21.7	19.5
Ce/Pb	54.4	25.6	30.6	24.6	10.3	15.0	18.5	14.7	24.3
La/Sm_n*	5.90	5.84	6.09	6.69	4.72	5.50	6.15	5.36	5.22
La/Yb_n*	195	195	210	233	153	135	151	115	140

LOI: loss on ignition; Mg#: atomic Mg/(Mg+Fe2+) with Fe2O3/FeO=0.15; * - normalised to chondrite; ** - trace elements analysed by XRF, all other trace elements analysed by ICP-MS

Table 5.1 Continued

	D18 - Macrocrystic					Type 5 - Macrocrystic				
Sample #	D18-01W	D18-02W	D18-03W	D18-04W	D18-05W	T5-01W	T5-02W	T5-03W	T5-04W	T5-05W
Major Elements (wt %)										
SiO_2	32.7	32.9	31.8	33.7	33.5	35.8	37.9	33.7	35.4	34.5
TiO_2	1.27	1.21	1.44	1.28	1.31	1.35	1.56	1.37	1.20	1.22
Al_2O_3	3.65	5.06	4.00	4.30	4.46	4.30	6.28	3.09	5.07	3.91
Fe_2O_3	8.03	8.08	7.75	8.05	7.90	7.41	7.69	7.71	7.77	7.51
MnO	0.125	0.139	0.139	0.140	0.133	0.124	0.128	0.127	0.132	0.131
MgO	30.0	25.6	27.2	29.0	28.3	24.4	22.3	28.4	25.8	25.9
CaO	6.99	9.03	8.02	6.48	7.66	6.63	4.98	6.11	5.55	6.86
Na_2O	0.536	1.04	0.893	0.852	0.848	1.14	1.57	0.948	1.09	0.73
K_2O	3.31	3.24	3.52	3.25	3.27	3.40	2.95	2.51	2.50	3.24
P_2O_5	0.752	1.25	1.66	1.89	1.45	1.37	0.613	1.53	1.25	1.36
SO_3	0.010	0.007	0.011	0.010	0.014	0.013	0.009	0.016	0.013	0.018
Cr_2O_3	0.214	0.199	0.217	0.229	0.230	0.204	0.156	0.231	0.247	0.222
NiO	0.151	0.127	0.134	0.144	0.149	0.118	0.100	0.138	0.134	0.135
L.O.I.	10.19	10.63	11.46	8.80	9.58	9.63	8.05	11.61	10.44	10.90
H_2O^-	1.25	1.48	1.39	1.21	1.20	3.16	4.86	2.29	3.00	2.41
Total	99.2	100	99.7	99.3	100	99.1	99.1	99.7	99.6	99.1
Mg#	0.893	0.877	0.888	0.890	0.889	0.881	0.867	0.892	0.882	0.886
CO_2	4.02	4.10	3.93	2.25	3.15	2.14	1.18	2.64	1.78	3.01
H_2O^+	5.57	5.80	6.76	6.06	5.91	6.15	5.10	7.75	7.25	6.70
C.I.	1.009	1.21	1.072	1.09	1.12	1.32	1.62	1.13	1.35	1.21
Trace Elements (ppm)										
Sc	9.63	11.0	10.6	10.5	10.5	12.4	12.4	13.8	14.7	12.7
V	81.7	166	116	183	112	98.4	106	91.7	97.9	82.1
Cr**	1475	1373	1501	1579	1580	1419	1086	1601	1716	1538
Co	76.1	66.8	68.4	63.3	68.7	63.2	58.7	71.0	69.5	67.0
Ni**	1192	1005	1064	1136	1175	944	801	1098	1073	1077
Cu	22.3	24.0	54.2	37.7	41.3	44.9	57.1	50.1	49.4	45.3
Rb	148	95.0	154	124	106	102	124	98.5	89.5	110
Sr	2178	2658	2360	2093	1579	1084	430	956	980	888
Y	12.7	14.6	14.1	11.8	12.9	13.5	11.1	12.7	11.4	14.0
Zr**	303	273	303	316	298	280	207	310	248	162
Nb**	142	121	171	141	135	141	108	154	120	121
Ba	1320	1260	1677	1626	1376	987	672	1049	984	859
La	109	109	129	113	115	113	60.5	126	104	106
Ce	237	221	283	230	242	236	126	261	215	222
Pr	25.9	23.9	31.0	24.9	26.2	25.7	13.9	28.0	23.0	23.9
Nd	99.5	91.9	120	95.1	101	98.6	54.5	108	89.0	92.8
Sm	13.5	12.7	15.5	12.5	13.7	13.3	8.1	14.4	11.9	12.4
Eu	3.29	3.14	3.74	3.06	3.42	3.32	2.02	3.60	2.96	3.11
Gd	8.05	7.97	9.05	7.72	8.45	8.08	5.47	8.54	7.36	7.54
Tb	0.836	0.840	0.939	0.797	0.881	0.848	0.610	0.890	0.745	0.805
Dy	3.60	3.83	4.06	3.46	3.82	3.84	2.88	3.82	3.37	3.72
Ho	0.518	0.577	0.577	0.496	0.535	0.550	0.437	0.532	0.474	0.560
Er	1.05	1.26	1.19	1.02	1.06	1.15	1.01	1.00	0.94	1.22
Tm	0.119	0.147	0.133	0.116	0.117	0.137	0.121	0.113	0.110	0.142
Yb	0.666	0.858	0.693	0.629	0.596	0.772	0.750	0.585	0.562	0.767
Lu	0.081	0.114	0.089	0.079	0.075	0.102	0.100	0.068	0.078	0.083
Hf	5.19	4.45	5.10	4.73	5.08	4.88	4.22	5.62	4.48	3.64
Ta	7.01	6.26	9.18	6.18	7.19	7.55	5.89	8.20	6.43	6.84
Pb	4.07	11.2	11.2	10.6	11.8	3.25	4.18	2.32	4.88	3.85
Th	12.8	11.0	22.5	10.9	11.7	12.1	7.1	13.2	11.1	11.7
U	3.49	3.38	4.09	3.02	3.28	3.19	2.00	3.45	2.95	3.93
Zr/Nb	2.14	2.26	1.77	2.25	2.20	1.99	1.91	2.01	2.08	1.33
La/Nb	0.769	0.899	0.755	0.804	0.847	0.800	0.557	0.814	0.869	0.876
Ba/Nb	9.32	10.4	9.79	11.6	10.2	6.99	6.20	6.79	8.22	7.08
Nb/Ta	20.2	19.3	18.7	22.8	18.8	18.7	18.4	18.8	18.6	17.7
Ce/Pb	58.2	19.8	25.2	21.7	20.6	72.7	30.2	112.8	44.1	57.7
La/Sm_n*	5.21	5.52	5.38	5.83	5.41	5.49	4.81	5.63	5.62	5.55
La/Yb_n*	117	90.8	134	129	138	105	57.8	154	133	99.4

LOI: loss on ignition; Mg#: atomic Mg/(Mg+Fe2+) with Fe2O3/FeO=0.15; * - normalised to chondrite; ** - trace elements analysed by XRF, all other trace elements analysed by ICP-MS

Table 5.1 Continued

	D16 - Macrocrystic						Dyke - Macrocrystic		Xenoliths not removed		
Sample #	D16-01W	D16-02W	D16-03W	D16-04W	D16-05W	D16-06W	D16D-01W	D16D-02W	D5-02WN	T5-02WN	D18-03WN
Major Elements (wt %)											
SiO_2	39.5	39.4	36.7	38.8	37.5	41.2	28.2	25.1	33.6	35.7	32.1
TiO_2	1.20	1.22	1.30	1.24	1.23	1.54	2.13	1.44	0.91	1.56	1.31
Al_2O_3	6.05	5.69	6.14	6.07	5.43	6.61	2.42	2.22	4.44	5.72	4.27
Fe_2O_3	7.67	7.81	7.57	7.71	7.85	7.59	9.80	7.46	6.42	8.10	7.46
MnO	0.13	0.12	0.13	0.13	0.12	0.12	0.17	0.13	0.11	0.13	0.14
MgO	23.4	25.1	24.6	24.6	24.5	21.0	31.3	26.0	24.3	20.7	26.3
CaO	4.90	3.85	4.53	4.51	5.57	5.20	11.3	9.19	7.53	6.07	8.46
Na_2O	1.72	1.47	1.46	1.61	1.09	1.90	0.47	0.29	1.16	1.40	0.81
K_2O	2.11	2.55	3.60	2.16	2.67	2.48	0.93	1.10	3.54	2.71	3.70
P_2O_5	0.61	0.59	0.44	0.78	0.79	0.60	1.36	1.66	1.54	0.67	1.67
SO_3	0.017	0.013	0.008	0.009	0.009	0.010	0.008	0.073	0.014	0.008	0.010
Cr_2O_3	0.17	0.17	0.19	0.17	0.16	0.16	0.24	0.21	0.18	0.15	0.22
NiO	0.12	0.14	0.12	0.14	0.12	0.10	0.13	0.12	0.12	0.09	0.12
L.O.I.	7.72	7.22	8.60	7.30	7.53	6.62	6.27	19.28	10.42	9.51	11.36
H_2O^-	4.46	4.38	4.43	4.42	4.43	4.35	4.40	5.38	5.10	6.63	1.98
Total	99.8	99.7	99.8	99.7	99.0	99.5	99.2	99.7	99.4	99.1	99.9
Mg#	0.87	0.88	0.88	0.88	0.88	0.86	0.88	0.89	0.89	0.85	0.89
CO_2	0.6	0.4	1.4	0.4	0.9	0.6	2.3	6.3	2.3	1.8	3.7
H_2O^+	5.5	5.4	5.5	5.4	3.9	4.8	2.8	8.3	6.0	4.8	6.6
C.I.	1.71	1.54	1.39	1.61	1.48	1.92	0.94	0.98	1.25	1.64	1.10
Trace Elements (ppm)											
Sc	11.4	9.49	9.93	9.49	9.70	11.2	15.4	9.83	9.27	12.8	11.3
V	93.5	84.6	60.6	83.9	135	109	67.7	138	243	139	114
Cr**	1203	1174	1310	1148	1064	1084	1665	1524	1298	1055	1515
Co	63.3	68.9	63.9	67.9	66.5	60.1	78.7	70.4	62.1	63.5	65.6
Ni**	943	1148	986	1098	941	783	1066	988	996	743	981
Cu	52.1	56.8	44.0	45.3	45.0	57.0	59.6	62.3	24.3	57.2	50.0
Rb	106	118	177	105	160	100	38.0	82.2	126	120	156
Sr	502	521	394	520	1176	521	932	1224	1182	600	2448
Y	10.6	11.6	11.8	10.3	9.9	11.0	19.2	12.5	11.2	13.4	13.6
Zr**	154	162	175	148	171	171	366	228	227	205	303
Nb**	77.6	82.0	97.1	86.2	79.4	92.0	199	126	112	92.0	149
Ba	601	606	901	555	1190	587	797	1179	2080	693	1648
La	54.9	56.7	61.5	56.3	56.1	56.8	171	100	94.8	62.8	111
Ce	114	118	126	117	114	117	362	210	193	130	229
Pr	12.7	13.1	13.8	12.9	12.5	12.9	39.7	23.3	21.2	14.4	24.9
Nd	50.3	52.2	54.9	50.9	49.6	49.1	154	91.4	80.9	56.1	95.5
Sm	7.49	7.88	8.14	7.39	7.17	7.19	21.1	12.7	10.8	8.54	13.0
Eu	1.83	1.94	2.06	1.85	1.71	1.80	5.24	3.26	2.80	2.19	3.26
Gd	5.00	5.23	5.50	5.02	4.71	4.93	13.2	8.37	7.01	5.88	8.22
Tb	0.558	0.598	0.620	0.557	0.521	0.563	1.369	0.860	0.727	0.686	0.856
Dy	2.70	2.92	3.06	2.65	2.54	2.66	5.82	3.67	3.18	3.28	3.75
Ho	0.418	0.458	0.462	0.405	0.398	0.421	0.804	0.522	0.448	0.517	0.536
Er	0.960	1.02	1.05	0.908	0.933	1.02	1.66	1.09	0.978	1.25	1.16
Tm	0.126	0.122	0.129	0.112	0.118	0.135	0.169	0.114	0.109	0.154	0.130
Yb	0.710	0.689	0.749	0.644	0.690	0.842	0.880	0.615	0.594	0.928	0.690
Lu	0.097	0.091	0.097	0.086	0.101	0.111	0.104	0.069	0.073	0.122	0.087
Hf	3.14	3.20	3.52	2.78	3.47	3.75	6.69	4.36	3.98	4.16	5.01
Ta	4.13	4.76	4.79	4.55	4.23	5.35	9.98	7.01	5.23	5.11	6.72
Pb	3.12	2.72	4.92	5.23	6.07	6.76	5.45	8.54	16.2	6.32	11.9
Th	7.38	7.76	7.75	8.03	6.49	7.08	19.2	9.85	10.5	8.15	11.6
U	1.60	1.89	2.85	2.89	1.51	1.66	4.37	2.86	3.59	2.10	3.36
Zr/Nb	1.99	1.97	1.80	1.72	2.15	1.86	1.83	1.81	2.02	2.23	2.04
La/Nb	0.708	0.691	0.634	0.654	0.707	0.618	0.856	0.793	0.843	0.683	0.747
Ba/Nb	7.75	7.38	9.3	6.45	15.0	6.38	4.00	9.4	18.5	7.53	11.1
Nb/Ta	18.8	17.2	20.3	18.9	18.8	17.2	20.0	18.0	21.5	18.0	22.1
Ce/Pb	36.5	43.5	25.5	22.3	18.7	17.3	66.5	24.6	11.9	20.6	19.3
La/Sm_n*	4.74	4.64	4.88	4.92	5.05	5.10	5.22	5.09	5.64	4.75	5.49
La/Yb_n*	55.5	59.0	58.9	62.7	58.4	48.4	139	117	114	48.6	115

LOI: loss on ignition; Mg#: atomic Mg/(Mg+Fe2+) with Fe2O3/FeO=0.15; * - normalised to chondrite; ** - trace elements analysed by XRF, all other trace elements analysed by ICP-MS

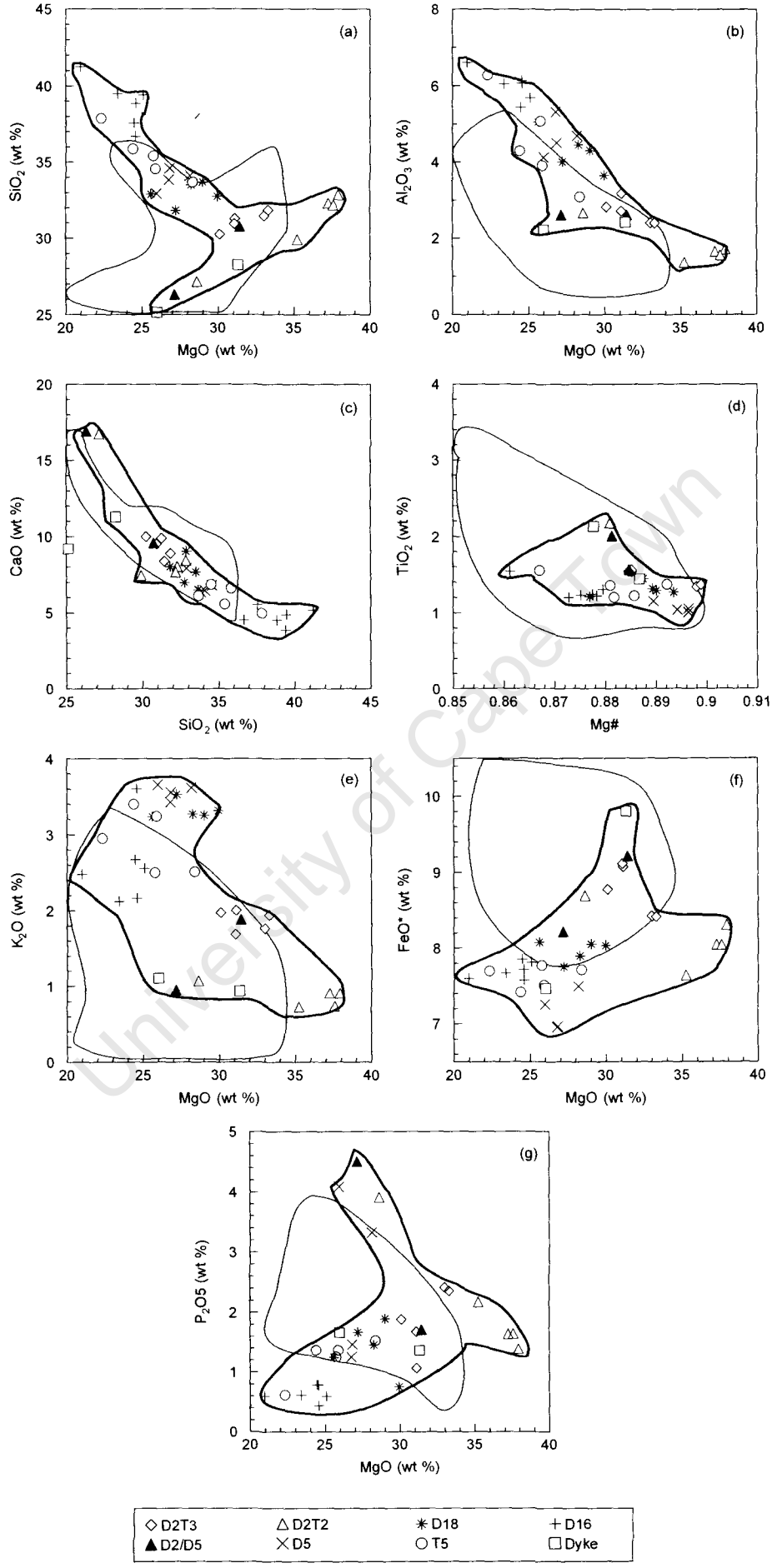

Figure 5.2. Selected major element variation diagrams for the NWC kimberlite intrusive phases. Shaded areas indicate range of Kimberley data from le Roex *et al.* (2003).

5.1.2 D2/D5 intrusive phase

The two samples representing this intrusive phase are aphanitic and are on average depleted in SiO_2, and slightly enriched in TiO_2, CaO and FeO*, relative to the remaining samples in this study (Table 5.1). This is with the exception of the SiO_2 content of the kimberlite dyke in the D16 intrusive phase. Their major element compositions are, however, quite different from one another with sample D2D5-01W containing ~30.7 wt % SiO_2, ~31.4 wt % MgO (Mg# = ~0.89) and ~2.62 wt % Al_2O_3, whereas sample D2D5-02W has a SiO_2 content of ~26.3 wt %, ~27.1 wt % MgO content (Mg# = ~0.88) and ~2.60 wt % Al_2O_3. Their FeO* and K_2O contents vary by ~1 wt %, with sample D2D5-01W having the highest contents (Table 5.1), and their TiO_2 contents by ~0.4 wt %. Sample D2D5-02W is highly enriched in CaO (~16.9 wt %) but contains less CO_2 (~2.94 wt % vs. 3.57 wt %) than sample D2D5-01W. There is also a notable difference in their P_2O_5 contents with sample D2D5-01W containing ~1.7 wt % and sample D2D5-02W containing ~4.5 wt % (Figure 5.2). The high P_2O_5 content suggests an accumulation of apatite. This was not observed, however, due to the high abundance of opaque oxides, which made the examination of the groundmass of either of the samples difficult. A modal abundance of 1 % apatite was estimated for both samples. The major element compositions of both samples fall well within the Kimberley range of major element compositions, with the exception of the CaO concentration of sample D2D5-02W (Figure 5.2).

Sample D2D5-01W has a C.I. of 0.93 and sample D2D5-02W one of 1.00 (Figure 5.1; Table 5.1). Microscopically, these two samples contain similar amounts of crustal xenoliths to the D2 Type 3 kimberlite samples discussed above and the similarity between their contamination indices is expected.

5.1.3 D2 Type 2 intrusive phase

Samples D2T2-02W, -03W and -04W of the macrocrystic D2 Type 2 intrusive phase have very similar major element contents (Figure 5.2) with their SiO_2 contents ranging from ~32 to ~33 wt % and their MgO contents ranging from ~37 to ~38 wt %; sample D2T2-02W having the highest SiO_2 and MgO, and sample D2T2-04W the lowest. Sample D2T2-01W contains ~5 wt % less SiO_2 and ~9 wt % less MgO than the three samples mentioned above and, as seen in Figure 5.2, has a major element composition very similar to aphanitic sample D2D5-02W (see 5.1.2). Sample D2T2-05W has a SiO_2 content of ~29.9 wt % and a MgO content of ~35.2 wt % and therefore trends towards the D2 Type 3 samples (see 5.1.1). The D2 Type 2 samples have higher MgO contents in comparison with the Kimberley samples (le Roex *et al.*, 2003) and therefore plot outside of the shaded

area in the majority of graphs shown in Figure 5.2. The Al_2O_3 contents of samples D2T2-02W, -03W, -04W and -05W range between ~1.36 and ~1.71 wt %, whereas their CaO contents range between 7.44 and 8.43 wt % (Table 5.1). These four samples all have a Mg# of 0.91. In contrast, the Al_2O_3 and CaO contents of sample D2T2-01W are raised relative to the remaining samples. Sample D2T2-01W also shows raised TiO_2, K_2O and FeO* contents and has a Mg# of 0.88. The CO_2 content of sample D2T2-05W is high (5.62 wt %) in relation to the other D2 Type 2 samples (1.58 – 2.18 wt %).

The D2 Type 2 samples have an average C.I. of 0.86 with the exception of sample D2T2-01W that has a C.I. of 0.97 (Figure 5.1; Table 5.1). This is slightly lower than those of the two intrusive phases discussed above although their country rock xenolith abundances are apparently similar.

5.1.4 D5 intrusive phase

The MgO and K_2O contents of the D5 samples vary within a restricted range, with MgO increasing slightly from sample D5-02W (~26 wt %) to sample D5-05W (~28 wt %), and K_2O ranging between 3.42 and 3.65 wt %. The Mg# of these samples ranges between 0.89 and 0.90 and their SiO_2 content from ~33 to ~35 wt % with sample D5-02W having the lowest SiO_2 contents and sample D5-04W the highest. Al_2O_3 contents vary between ~4.12 wt % and 5.32 wt % with sample D5-03W having the higher Al_2O_3 content. FeO* varies between 6.96 wt % and 7.50 wt %, TiO_2 between ~1.00 wt % and ~1.15 wt %, and CaO between 6.37 wt % and 6.79 wt % with sample D5-02W containing 7.91 wt % CaO. The CO_2 concentrations of the samples range between 0.91 wt % (sample D5-05W) and 2.71 wt % (sample D5-03W). The D5 samples show slightly elevated SiO_2, Al_2O_3 and K_2O, and slightly lower FeO* contents in comparison with the Kimberley data (le Roex *et al.*, 2003; Figure 5.2).

The C.I. of the D5 intrusive phase varies between 1.02 and 1.08 (Figure 5.1; Table 5.1). This increase is ascribed to a higher country rock xenolith abundance (~14 %) in comparison with the intrusive phases discussed above.

5.1.5 D18 intrusive phase

The MgO contents of the D18 samples range from 25.6 to 30.0 wt % and they have an average Mg# of 0.89, whereas their SiO_2 contents range from 31.8 to 33.7 wt %. Samples D18-03W, D18-04W and D18-05W were collected in the main tunnel with sample D18-04W having the highest SiO_2 content. The first sample collected in the breakaway has the

MgO content of all the D18 samples, whereas the second sample has the lowest MgO content. Al_2O_3 shows a broad negative correlation with MgO and ranges from 3.65 to 5.06 wt %. TiO_2 ranges from 1.21 to 1.44 wt % and K_2O ranges from 3.24 to 3.52 wt % with sample D18-03W having the highest amount of both elements. FeO* varies between 7.75 and 8.08 wt %; whereas CaO ranges from 6.48 to 9.03 wt % with sample D18-02W having the highest contents in both these elements. Sample D18-02W also shows the highest CO_2 concentration (4.10 wt %). The D18 samples show slightly elevated Al_2O_3 and K_2O relative to the Kimberley samples (Figure 5.1).

The C.I. of the D18 intrusive phase varies between 0.94 and 1.09 (Figure 5.1; Table 5.1). It shows more varied abundances of crustal xenoliths in comparison with the D5 intrusive phase but the average dilution is similar (~13 %).

5.1.6 Type 5 intrusive phase

The Type 5 samples show a negative correlation between MgO and SiO_2 contents, with MgO ranging between 22.3 and 28.4 wt % and SiO_2 ranging between 33.7 and 37.9 wt %. The MgO and SiO_2 contents show a wider range than that of the other macrocrystic intrusive phases thus far discussed. Samples T5-01W and -02W have MgO and SiO_2 compositions closer to the D16 samples, whereas the remaining Type 5 samples plot closer to the D18 samples discussed under 5.1.5. Similar to that of the D18 samples, Al_2O_3 also shows a broad negative correlation with MgO, and ranges from 3.09 to 6.28 wt %. The Mg# of these samples varies between 0.87 and 0.89. TiO_2 ranges between 1.20 and 1.56 wt % with sample T5-02W having the highest contents and sample T5-04W the lowest. FeO* varies between 7.41 and 7.77 wt % (sample T5-01W and sample T5-04W, respectively); whereas CaO ranges between 4.96 and 6.86 wt % (sample T5-02W and sample T5-05W, respectively). There is a relatively good positive correlation between the CO_2 and CaO contents of the samples with sample T5-02W having the lower CO_2 content (1.18 wt %) and sample T5-05W having the higher CO_2 content (3.01 wt %). This correlation may be attributed to the presence of secondary calcite. K_2O ranges from 2.50 to 3.40 wt % with sample T5-04W having the lowest contents and sample T5-01W the highest. Some of the Type 5 samples show slightly elevated SiO_2, Al_2O_3 and K_2O, and slightly lower FeO* contents in comparison with the Kimberley samples (Figure 5.2).

The C.I. of the Type 5 intrusive phase ranges between 1.08 and 1.45 (Figure 5.1; Table 5.1), where higher C.I. values correlates with increased xenolith abundance, e.g. sample T5-02W contains ~39 % country rock xenoliths and has a C.I. of 1.45.

5.1.7 D16 intrusive phase

The D16 intrusive phase has on average the lowest MgO and highest SiO_2 contents of all the intrusive phases in this study, with MgO ranging from 21.0 to 25.1 wt % and SiO_2 ranging from 36.7 to 41.2 wt %. The Mg# varies from 0.86 to 0.88. The samples with the highest MgO (and highest Mg#) and lowest SiO_2 occur towards the centre of the intrusion. Al_2O_3 ranges between 5.43 and 6.61 wt % and show a broad negative correlation with MgO (Figure 5.2), whereas CaO varies between 3.85 and 5.57 wt % with sample D16-02W having the lowest contents and sample D16-05W the highest. Sample D16-02W has the lowest and sample D16-03W the highest CO_2 content (0.4 wt % vs. 1.4 wt %). The TiO_2 contents of the D16 samples ranges between 1.20 and 1.54 wt %. FeO* contents also vary within a restricted range from 7.57 to 7.85 wt %, whereas K_2O ranges from 2.11 to 3.60 wt %, the latter being anomalously high. The SiO_2 and Al_2O_3 content of the D16 samples are slightly elevated in comparison with the Kimberley samples, whereas they show less FeO* than the latter (Figure 5.2).

The C.I. of the D16 intrusive phase varies between 1.24 and 1.72 (Figure 5.1; Table 5.1) indicating the influence of the abundant country rock xenoliths observed macroscopically, i.e. generally 30 % and up to 70 % in places.

5.1.8 Dyke in D16 intrusive phase

There is a notable difference in the major element contents of samples D16D-01W and D16D-02W (Table 5.1, Figure 5.2) collected from the dyke crosscutting the D16 intrusive phase with sample D16D-01W being more enriched in most major elements relative to sample D16D-02W. Sample D16D-02W however shows a higher K_2O, P_2O_5, SO_3 and CO_2 contents, as well as a higher C.I. of 0.96 (Figure 5.1) and a higher Mg# of 0.89. The major element compositions of the two samples correlate well with the Kimberley data from le Roex *et al.* (2003; Figure 5.2). The CaO content of sample D16D-02W is however slightly lower than that of the Kimberley samples.

5.1.9 Summary: Major Elements

Major element compositions of the different intrusive phases tend to cluster (Figure 5.2), indicating relatively clear geochemical differences between the intrusive phases. Across the various intrusive phases, compositions are variable, with MgO contents ranging from ~21.0 to ~37.9 wt % and SiO_2 contents from ~26.3 to ~41.2 wt % (Figure 5.2a). These two components are positively correlated in the case of the aphanitic and country rock xenolith

(CRX) -poor macrocrystic varieties, with the micro-porphyritic intrusive phases being most depleted in SiO_2 and MgO. Crustally contaminated samples show a negative correlation, with the most contaminated varieties having the highest SiO_2 and lowest MgO contents. The Mg# (atomic $Mg/(Mg+Fe^{2+})$; Fe_2O_3/FeO ratio set at 0.15) ranges from 0.86 to 0.91 and show a largely negative relationship with TiO_2 (~0.81 – ~2.00 wt %; Figure 5.2c), similar to that of Al_2O_3 (~1.36 - ~6.61 wt %) and MgO (Figure 5.2b). The aphanitic and the macrocrystic D2 Type 2 samples, however, show a positive correlation between Al_2O_3 and MgO. The negative correlation between CaO and SiO_2 is well defined, with the former ranging from ~3.85 to ~16.9 wt %, with the aphanitic samples having the highest CaO content. The D18 samples show the highest average CO_2 content (3.49 wt %) and the D16 samples the lowest (0.72 wt %), whereas the CO_2 concentrations of the Kimberley samples range between 1.0 and 12.1 wt %. Although samples from a given intrusive phase are relatively well clustered, both FeO* (~7.0 - ~9.1 wt %) and K_2O (~0.73 – 3.65 wt %) show poor correlations with MgO. The crustally contaminated samples generally have lower abundances of FeO* and higher amounts of K_2O compared to the aphanitic and CRX-poor macrocrystic varieties. P_2O_5 shows a negative correlation with MgO in the case of the CRX-poor D2 Type 2 intrusive phase and aphanitic D2/D5 contact zone and a broad positive correlation in the case of the crustally contaminated samples, with the most contaminated varieties being most depleted in P_2O_5 (Figure 5.2). The exceptions are the broadly negative correlation of these components in the xenolith-rich D5 intrusive phase and their seemingly positive correlation in the xenolith-poor D2 Type 3.

Disregarding the anomalous 28.6 wt % MgO and 2.66 wt % Al_2O_3 values of sample D2T2-01W, the macrocrystic D2 Type 2 has the highest average MgO content at ~37 wt % and the lowest average Al_2O_3 content at ~1.57 wt %. It also has the lowest TiO_2 and K_2O contents at ~0.87 wt % and 0.82 wt %, respectively, again ignoring anomalous sample D2T2-01W, which has a similar composition to some of the aphanitic varieties. With the exception of the discussion on trace elements below, sample D2T2-01W is discarded from the remainder of the study based on its anomalous major element content in relation to the remainder of the D2 Type 2 samples.

The D16 intrusive phase has the highest average C.I. at 1.44 (Figure 5.1; Table 5.1), which suggests a high degree of crustal contamination. In contrast, the aphanitic D2/D5 intrusive phase has an average C.I. of 0.97, and that of the relatively uncontaminated macrocrystic D2 Type 3 and D2 Type 2 intrusive phases is 0.93 and 0.88, respectively. The C.I. of each of the various intrusive phases, therefore, supports the petrographic

observations discussed in Chapter 4, i.e. samples that contain high abundances of crustal xenoliths show higher C.I.'s than that of the aphanitic samples that contain no macroscopically visible crustal xenoliths (Figure 5.1).

The major element concentrations of the NWC samples correlate relatively well with the Kimberley data from le Roex *et al.* (2003; Figure 5.2). The most notable exceptions are the elevated SiO_2 and Al_2O_3 concentrations of the D16 samples, the higher K_2O contents of the D5 and D18 samples and the increased MgO contents of the D2 Type 2 samples. Also notable are the lower FeO* contents of the majority of the D5, Type 5 and D16 samples.

5.2 Trace Elements

5.2.1 D2 Type 3 intrusive phase

Trace element variations between the D2 Type 3 samples are relatively minor (Figure 5.3). The high field strength elements (HFSE) (Zr 339-360 ppm; Nb 172-202 ppm; Th 14.8-17.7 ppm; Ta 7.1-8.4 ppm) and large ion lithophile elements (LILE) (Rb 77-115 ppm; Sr 1044-2053 ppm; Pb 6.9-10.6 ppm) show a broad positive correlation with the light rare earth elements (LREE) (La 142-167 ppm). Ni, Co and Cr correlate positively with Mg# (Ni 1065-1259 ppm; Co 73.6-78.3 ppm; Cr 1703-1851 ppm; Figure 5.4).

REE concentrations, normalized to chondrite (Figure 5.5), vary within a restricted range, with La abundances in the range 597-703 times chondrite and Lu ~2.65-3.65 times chondrite. Samples D2T3-03W and -04W are very similar in trace element composition and are more depleted in nearly all REE relative to the remaining three samples, progressively more so in HREE. The light REE of all samples are strongly enriched relative to the heavy REE (La/Yb_n = 153 – 185).

When normalized to primitive mantle abundances, all the D2 Type 3 samples have distinct negative K, Hf and Ti anomalies (Figure 5.6). Samples D2T3-02W and -05W show a slight relative depletion in Pb and Sr. Sample D2T3-04W is also slightly depleted in Pb. All the D2 Type 3 samples, except for sample D2T3-02W, show a slight relative enrichment in P. Samples D2T3-03W and -04W are slightly depleted in HREE relative to the remaining samples. In general, the differences in REE between the various samples are insignificant.

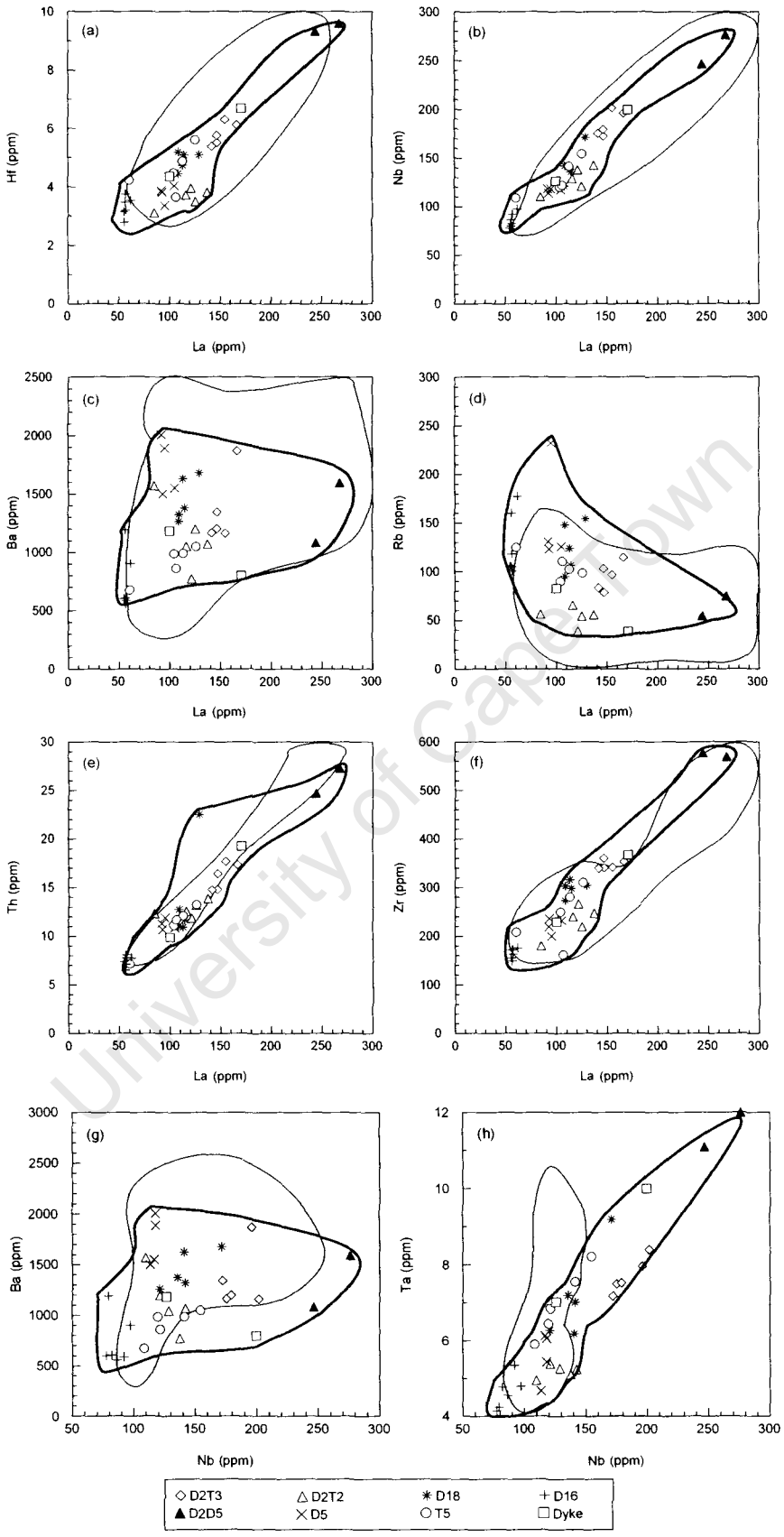

Figure 5.3. Selected incompatible trace element variation diagrams for the NWC kimberlite facies. Shaded areas indicate range of Kimberley data from le Roex *et al.* (2003).

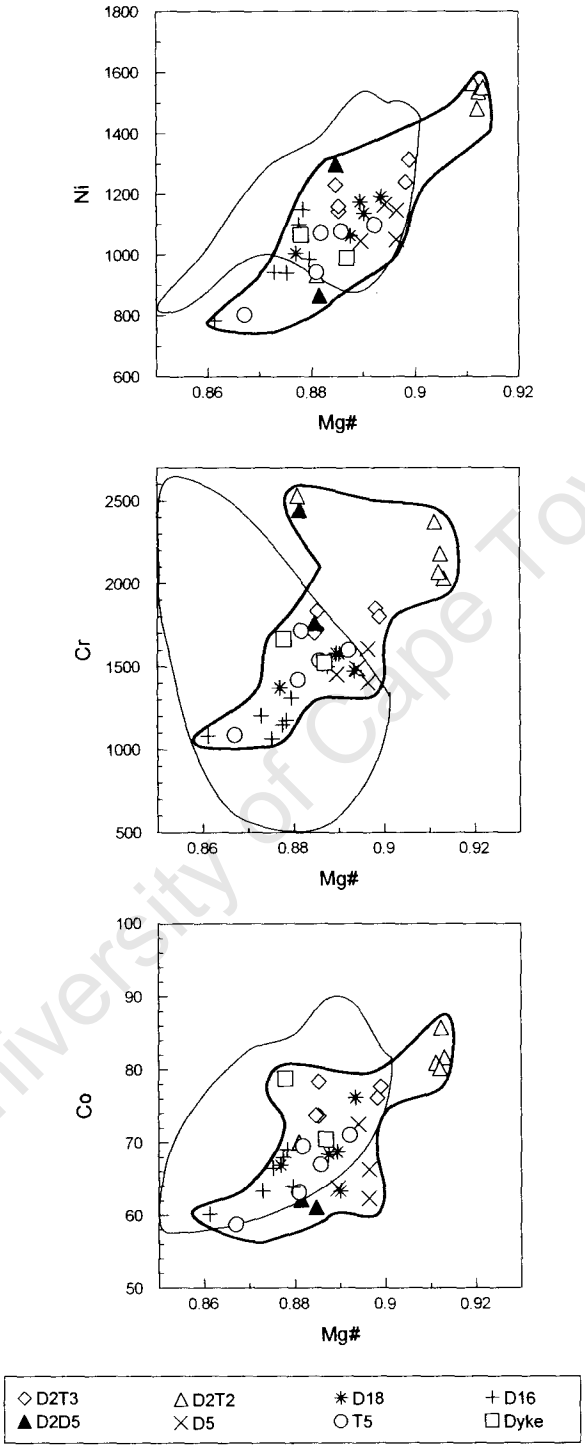

Figure 5.4. Selected compatible trace element variations of the NWC kimberlite intrusive phases in relation to Mg#. Shaded areas indicate range of Kimberley data from le Roex *et al.* (2003).

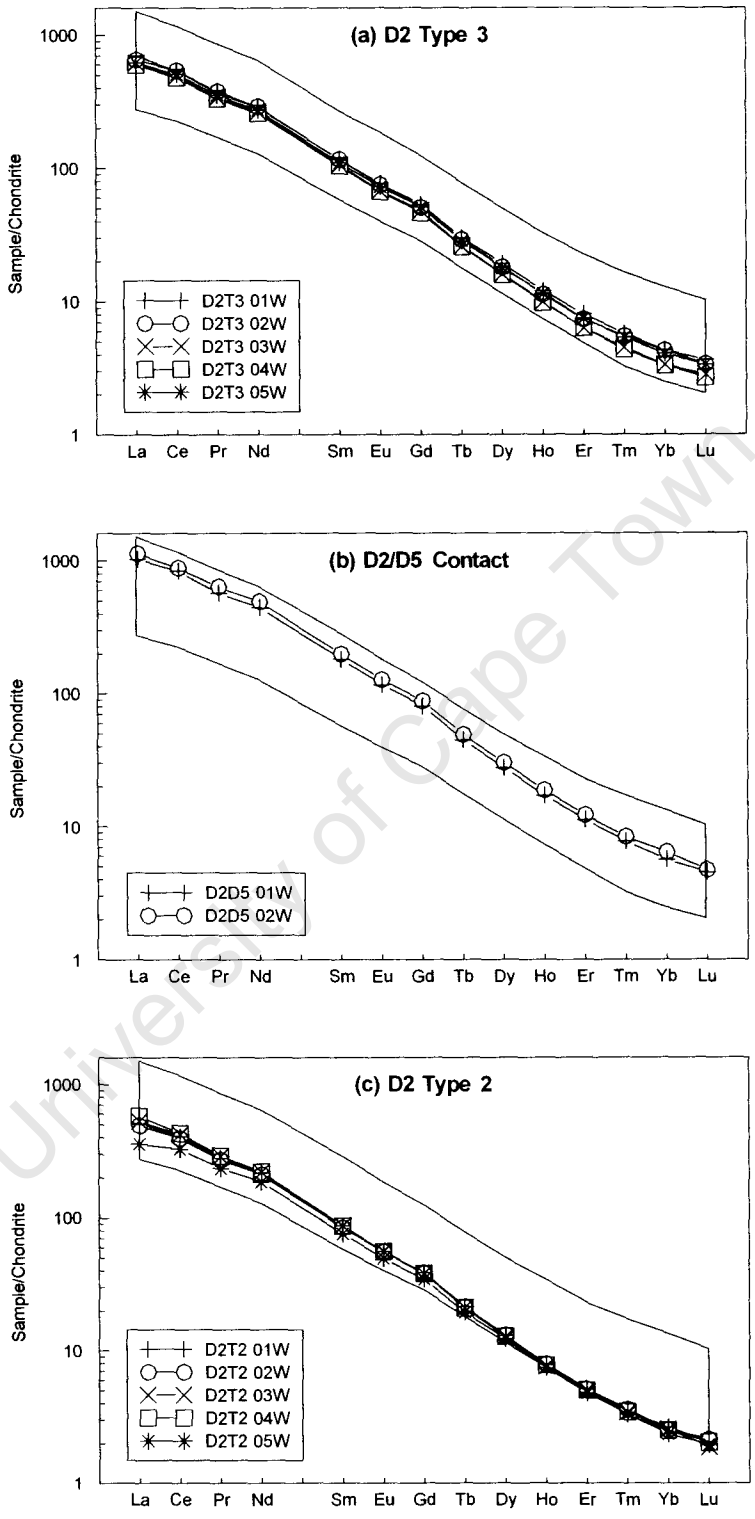

Figure 5.5. Chondrite-normalised trace element patterns of (a) D2 Type 3, (b) D2/D5 and (c) D2 Type 2. Normalizing values from Sun & McDonough (1989). Shaded areas indicate range of Kimberley data from le Roex *et al.* (2003).

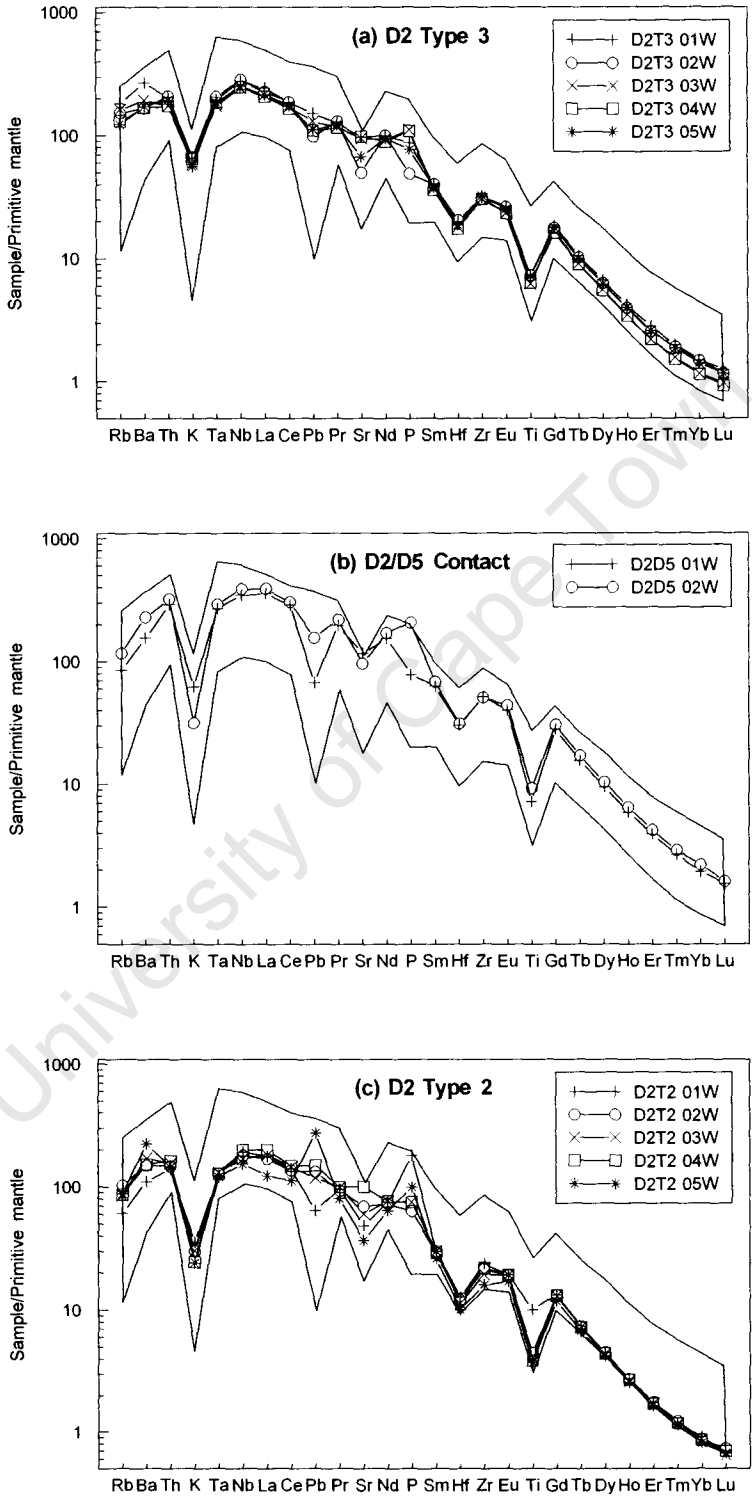

Figure 5.6. Primitive mantle-normalised trace element patterns of (a) D2 Type 3, (b) D2/D5 contact and (c) D2 Type 2. Normalizing values from Sun & McDonough (1989). Shaded areas indicate range of Kimberley data from le Roex *et al.* (2003).

5.2.2 D2/D5 intrusive phase

The aphanitic D2/D5 samples show relatively strong enrichment in the majority of trace elements (Figure 5.3) with the exception of Ba (1080-1592 ppm) and Rb (54.2-74.2 ppm). Sample D2D5-01W show slightly lower incompatible element abundances in comparison with sample D2D5-02W, except for Zr (Figure 5.3). The two samples show a relatively high variance in Ni and Cr contents with sample D2D5-01W being more enriched in Ni (1297 ppm vs. 866 ppm) and sample D2D5-02W containing more Cr (2444 ppm vs. 1762 ppm) (Figure 5.4). The two samples have similar Co contents with sample D2D5-01W having 61.0 wt % and sample D2D5-02W having 62.1 wt %.

REE abundances in the two analysed samples are very similar (Table 5.1), and they have sub-parallel chondrite normalized REE patterns (Figure 5.5 (b)) with an average La/Sm_n of 5.68 and an average La/Ybn of 180.

With the exception of Pb and P, primitive mantle normalized patterns are very similar; sample D2D5-01W has a negative Pb anomaly, whereas sample D2D5-02W has a positive P anomaly and a slightly greater negative K anomaly (Figure 5.6 (b)).

5.2.3 D2 Type 2 intrusive phase

The trace element contents of the macrocrystic D2 Type 2 samples are slightly more variable than that of the D2 Type 3 samples (Figure 5.3), with Zr varying between 179 ppm and 266 ppm and Ba between 774 ppm and 1568 ppm. Sr is highly variable with a minimum of 778 ppm (sample D2T2-05W) and a maximum of 2112 ppm (sample D2T2-04W). In contrast, Nb and Th are less variable (Nb = 110 – 142 ppm; Th = 11.8 – 13.8 ppm) and show a positive correlation with La (Figure 5.3). The Ni content of sample D2T2-01W is low (933 ppm) in comparison with the remaining four samples, which range between 1479 and 1563 ppm. The same is applicable to Co; whereas the Cr content of the same sample is high (2529 ppm) relative to the remaining four samples (2029-2372 ppm). Ni and Co correlate positively with Mg#, and Cr is scattered (Figure 5.4).

The REE contents of the D2 Type 2 kimberlite normalised to chondrite are illustrated in Figure 5.5 (c), and show sub-parallel patterns. Sample D2T2-04W is most enriched in La (137 ppm) and show the highest incompatible trace element ratios with La/Sm_n being 6.69 and La/Yb_n being 233, whereas sample D2T2-05W has the lowest La content (85 ppm) and show the lowest incompatible element ratios (La/Sm_n = 4.72; La/Yb_n = 153). All D2 Type 2 samples have a Lu content of approximately 0.05 ppm.

Figure 5.6 (c) shows the primitive mantle-normalised trace element patterns of the D2 Type 2 kimberlite. All of the samples illustrated show negative K, Hf and Ti anomalies, although sample D2T2-01W has a very subdued Ti anomaly. Sample D2T2-01W shows positive P and negative Pb anomalies; whereas sample D2T2-05W shows a positive Pb anomaly. The samples show variable Sr contents with all samples except D2T2-04W, showing a negative Sr anomaly (Figure 5.6 (c)).

5.2.4 D5 intrusive phase

The incompatible trace element variations of the D5 intrusive phase are relatively minor. The incompatible trace elements Zr, Hf and Th correlate positively with La (Zr = 199 - 236 ppm; Hf = 3.36 – 4.03 ppm; Th = 10.7 – 11.9 ppm; Figure 5.3). Ni and Cr show positive correlations with Mg#, whereas Co is scattered (Ni 1045 - 1165 ppm; Cr 1404 - 1606 ppm; Co 62.3 - 72.5 ppm; Figure 5.4).

The REE of the D5 kimberlite show sub-parallel patterns when normalised to chondrite (Figure 5.7 (a)). The light REE are strongly enriched relative to the heavy REE (La/Yb_n = 115 - 151), although less so than the intrusive phases discussed above. The La/Sm_n ratio varies between 5.22 (D5-05W) and 6.15 (D5-03W).

All D5 samples show sharp negative Ti and Hf anomalies and minor negative K anomalies when normalised to primitive mantle (Figure 5.8 (a)). The latter is unusual in comparison with the sharp negative K anomalies shown by the D2 Type 2 and 3, and D2/D5 samples. All samples show positive P and Pb anomalies, although samples D5-03W and D5-04W show more subdued P anomalies and sample D5-05W show a more subdued Pb anomaly. Sr is variable with samples D5-02W and D5-04W showing slight negative anomalies and the remaining samples slight positive anomalies. Rb and Ba are slightly elevated and scattered.

5.2.5 D18 intrusive phase

The incompatible trace element contents of the D18 intrusive phase show relatively little variation (Figure 5.3), with the exception of the Nb contents of sample D18-03W (171 ppm) that is slightly higher than that of the remaining D18 samples (121-142 ppm). Th in the same sample is approximately double that of the remaining samples (22.5 ppm vs. 10.9-12.8 ppm). The Ce/Pb ratio of sample D18-01W is very high (58.2) in relation to that of the

remaining samples (19.8 – 25.2). Ni and Co correlate positively with Mg#, whereas Cr is scattered (Ni 1005-1192 ppm; Co 63.3-76.1 ppm; Cr 1373-1580 ppm; Figure 5.4).

The D18 samples show sub-parallel patterns when normalised to chondrite (Figure 5.7 (b)). La/Sm_n ranges from 5.21 to 5.83 with sample D18-04W showing the highest ratio. La/Yb_n varies between 90.8 and 138 indicating that the light REE are strongly enriched relative to the heavy REE although less so than the D5 samples discussed above.

When normalised to primitive mantle the D18 samples show strong depletion in Ti and Hf and except for sample D18-01W, all samples show a slight positive Pb anomaly (Figure 5.8 (b)). Sr and P are scattered and sample D18-01W shows a slight negative P anomaly. Sample D18-01W shows a stronger negative depletion in K relative to the remaining samples.

5.2.6 Type 5 intrusive phase

The trace element contents of the Type 5 samples are relatively well constrained, with the exception of sample T5-02W (Figure 5.3). This sample shows a notable depletion in LREE (La 60 ppm; Ta 5.89 ppm) relative to the remaining Type 5 samples (La 104-126 ppm; Ta 6.43-8.20 ppm). The HFSE Nb and Th (108 ppm and 7.1 ppm respectively) of the same sample are also notably lower in relation to the remaining Type 5 samples (Nb 120-154 ppm; Th 11.1-13.2 ppm). Ba, Nb, Th and Zr show good positive correlations with La. Ba/Nb ranges from 6.2 to 8.2 and Nb/Ta ranges from 17.7 to 18.8. Ni (801 ppm), Co (58.7 ppm) and Cr (1086 ppm) contents of sample T5-02W are slightly lower relative to that of the remaining Type 5 samples (Ni 944-1098 ppm; Co 63.2-71.0 ppm; Cr 1419-1716 ppm) and correlate positively with Mg# (Figure 5.4).

Chondrite-normalised patterns of the Type 5 kimberlite samples plot sub-parallel to each other except for sample T5-02W which is clearly depleted in LREE relative to the other Type 5 samples (Figure 5.7 (c)). Sample T5-02W has a La/Yb_n ratio of 57.8, whereas that of the remaining samples varies between 99.4 and 154.

When normalised to primitive mantle nearly all the Type 5 samples show negative K, Pb, Sr, Hf and Ti anomalies (Figure 5.8 (c)). Sample T5-02W does not show this depletion in K and Pb and also shows a slightly different LREE pattern (similar to D16 below) from the remaining Type 5 samples. Pb and Zr are slightly scattered and sample T5-05W shows a negative Zr anomaly.

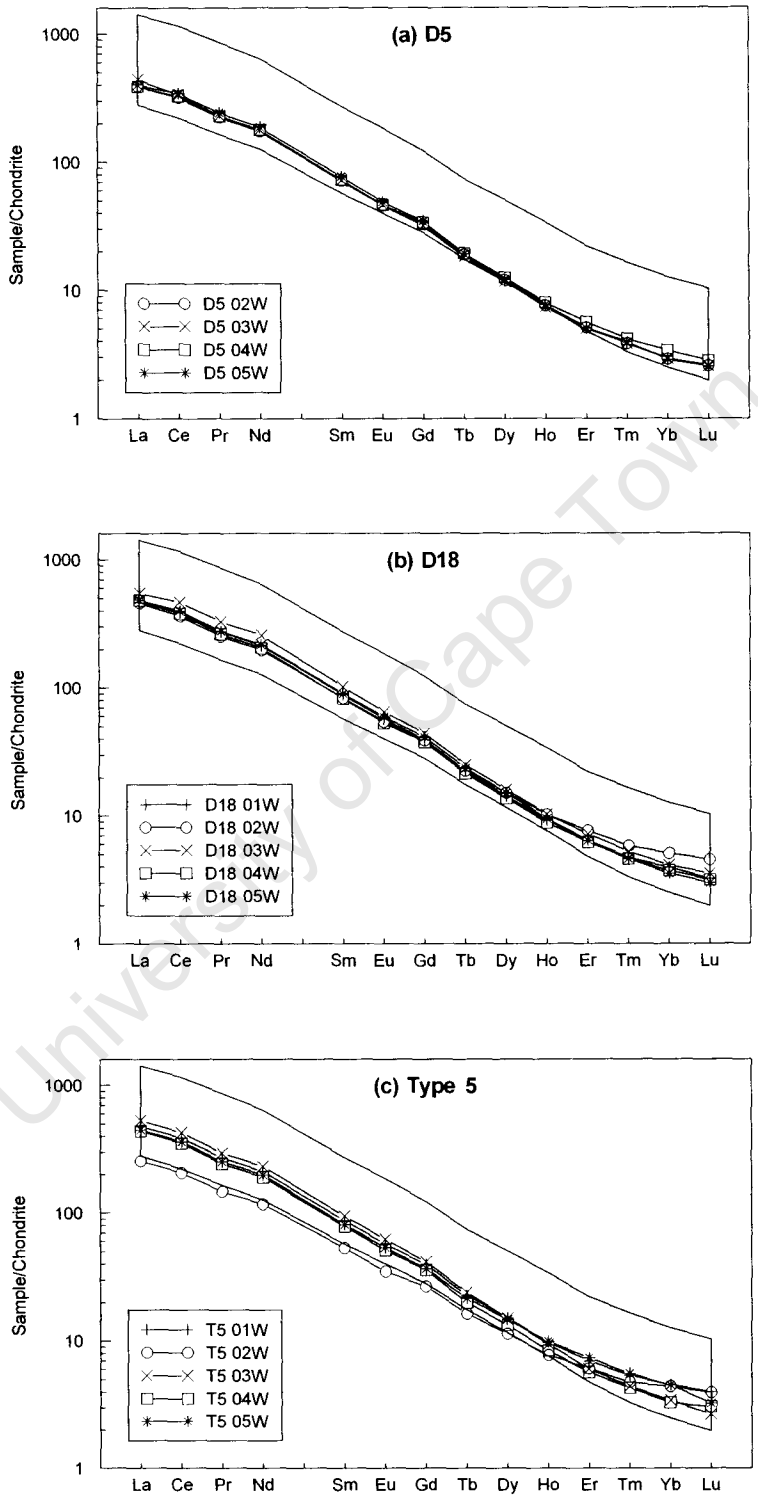

Figure 5.7. Chondrite-normalised trace element patterns of (a) D5, (b) D18 and (c) T5. Normalizing values from Sun & McDonough (1989). Shaded areas indicate range of Kimberley data from le Roex *et al.* (2003).

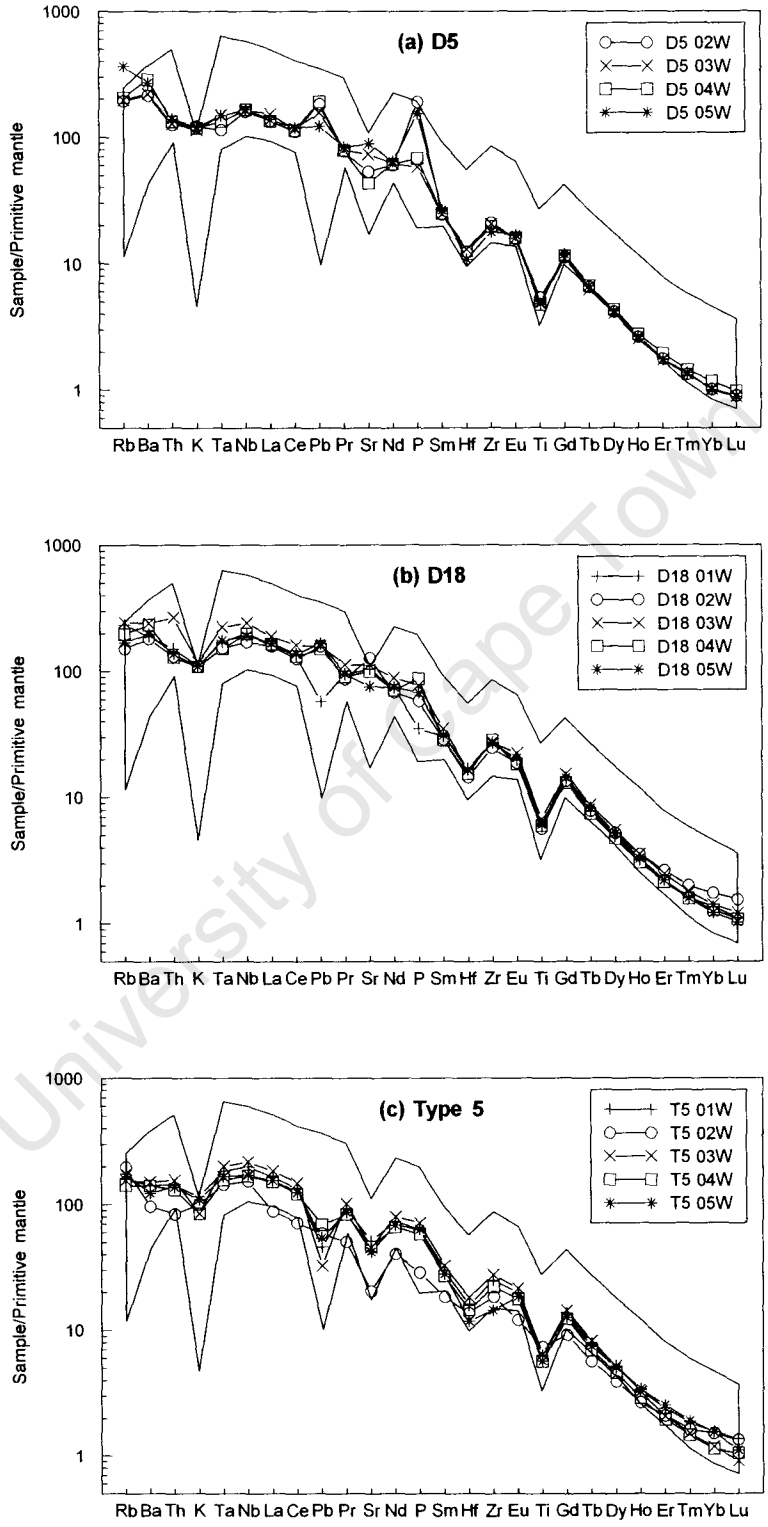

Figure 5.8. Primitive mantle-normalised trace element patterns of (a) D5, (b) D18 and (c) T5. Normalizing values from Sun & McDonough (1989). Shaded areas indicate range of Kimberley data from le Roex *et al.* (2003).

5.2.7 D16 intrusive phase

The Ba and Rb contents of samples D16-03W (Ba 901 ppm; Rb 177 ppm) and D16-05W (Ba 1190 ppm; Rb 160 ppm) are notably higher than that of the remaining D16 samples (Ba 555-606 ppm; Rb 100-118 ppm) (Figure 5.3). Sample D16-03W also has a very low Sr content (394 ppm), whereas that of sample D16-05W is very high (1176 ppm). The remaining four D16 samples show little variation with regards to their Sr content, which ranges between 502 and 521 ppm. The Ba/Nb ratio of the D16 samples varies between 6.38 (D16-03W) and 15.0 (D16-05W) and the Zr/Nb ratio between 1.72 (D16-04W) and 2.15 (D16-05W). Ni, Co and Cr are relatively well constrained (Ni 783-1148 ppm; Co 60.1-68.9 ppm; Cr 1064-1310 ppm; Figure 5.4).

When normalised to chondrite, the D16 sample patterns are sub-parallel (Figure 5.8 (a)). La/Sm_n ratios range from 4.6 (D16-02W) to 5.1 (D16-06W) and La/Yb_n from 48.4 (D16-06W) to 62.7 (D16-04W).

The D16 samples show sub-parallel primitive mantle normalised patterns and all samples show negative Ti and Hf anomalies (Figure 5.10 (a)). P is variable and shows a slightly positive anomaly for all D16 samples except for D16-03W. Pb is also variable with samples D16-01W and -02W showing negative Pb anomalies and the remaining samples positive Pb anomalies. Except for sample D16-05W, all samples show a negative Sr anomaly. Rb and Ba are slightly more elevated in samples D16-03W and -05W. Sample D16-03W shows a slightly elevated K in comparison with the remaining D16 samples, which show a slight depletion in K.

5.2.8 Dyke in D16 intrusive phase

The incompatible trace elements of the two samples collected from the dyke show a relatively large variation (Figure 5.3). Sample D16D-01W shows similar Ba/Nb ratios to the aphanitic samples, whereas sample D16D-02W has a ratio closer to the macrocrystic D2 Type 2 and 3 samples. The Ni, Co and Cr contents of these two samples show notably smaller variations with sample D16D-01W being slightly more enriched in all three elements relative to sample D16D-02W (Figure 5.4).

The two dyke samples show sub-parallel chondrite-normalised patterns with sample D16D-01W being the most enriched in all REE relative to sample D16D-02W (Figure 5.8 (b)). There is a slight convergence of the patterns towards HREE with La/Yb_n being 139 for sample D16D-01W and 117 for sample D16D-02W.

When normalised to primitive mantle both samples show strong negative K, Hf and Ti anomalies (Figure 5.10 (b)). Sample D16D-01W show relatively strong Pb and Sr anomalies, whereas sample D16D-02W shows a slight positive Pb anomaly and a relatively strong positive P anomaly.

As noted in Chapter 4, sample D16D-02W has an altered appearance possibly caused by secondary carbonate. This alteration has an influence on its major and trace elements, which is notably dissimilar to that of sample D16D-01W as discussed above. It is therefore discarded from the remainder of the study.

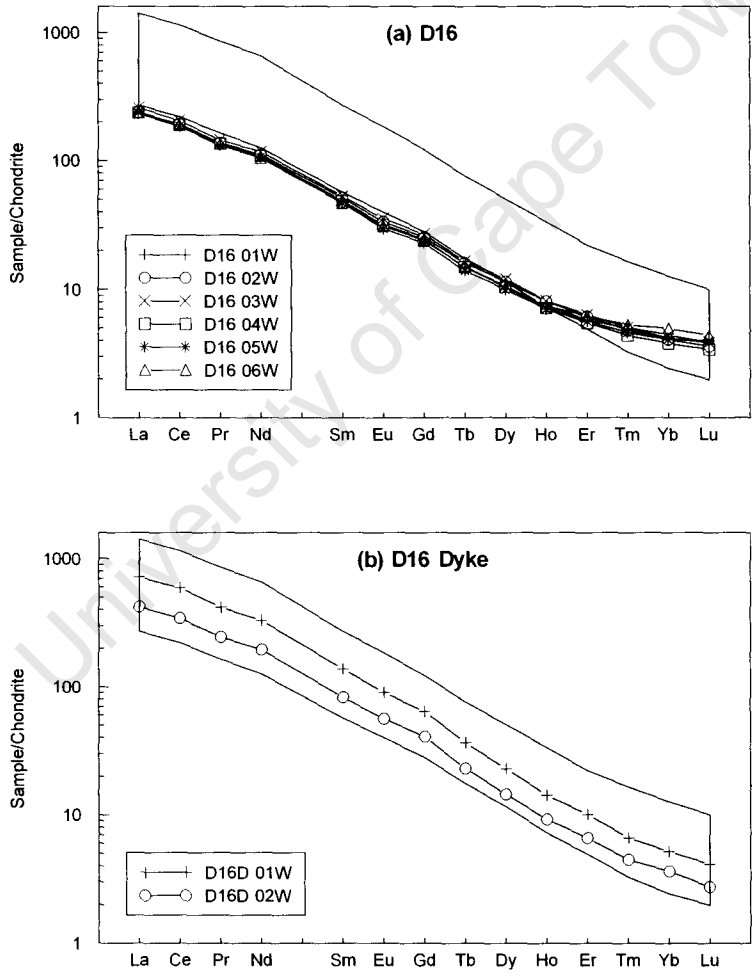

Figure 5.9. Chondrite-normalised trace element patterns of (a) D16 and (b) Dyke. Normalizing values from Sun & McDonough (1989). Shaded areas indicate range of Kimberley data from le Roex *et al.* (2003).

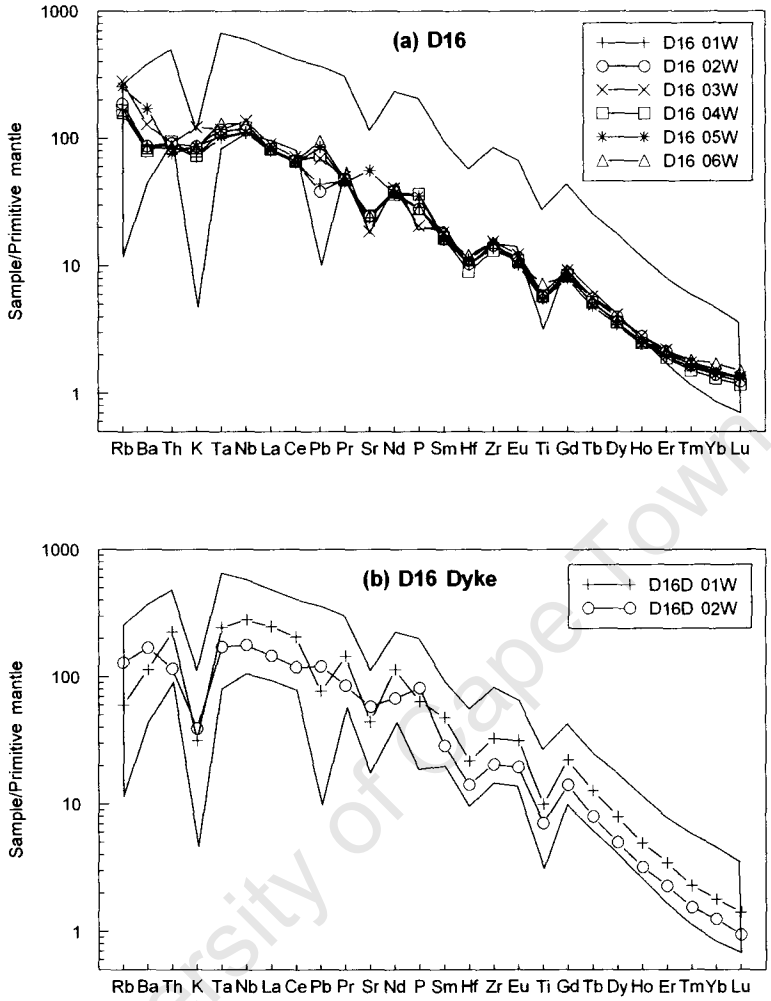

Figure 5.10. Primitive mantle-normalised trace element patterns of (a) D16 and (b) Dyke. Normalizing values from Sun & McDonough (1989). Shaded areas indicate range of Kimberley data from le Roex *et al.* (2003).

5.2.9 Summary: Trace Elements

Similar to their major element compositions, the incompatible trace elements of the different intrusive phases tend to cluster (Figure 5.3) indicating relatively clear geochemical differences between the intrusive phases. The aphanitic D2/D5 samples have the lowest average Ba/Nb ratio at 5.1 and the D5 intrusive phase the highest at 14.9. The D2 Type 2 samples show the highest average Nb/Ta ratio at 24.6 and the Type 5 samples the lowest at 18.4. There is a relatively good correlation between the trace elements of the samples in this study and that of the Kimberley samples, with the exception of the La and Nb contents of the D16 samples (Figure 5.3).

The D2 Type 2 samples show the highest average Ni content, whereas the D16 samples show the lowest average Ni content (Figure 5.4). The same trend is shown by Cr and Co. The Mg# of the NWC samples fall within a similar range to that of the Kimberley samples, with the exception of the higher Mg# of the D2 Type 2 samples (Figure 5.4). Samples from this study are similar with respect to Ni and Co as compared to the Kimberley samples, but are displaced to higher Mg#'s at a given Ni or Co content (Figure 5.4). Cr is positively correlated with Mg# for the NWC samples, but shows a negative correlation for the Kimberley samples (Figure 5.4).

The chondrite-normalised patterns of all the intrusive phases plot sub-parallel to each other and except for the D16 intrusive phase, plot within the Kimberley range of data (Figures 5.5, 5.7 & 5.9). The D16 intrusive phase show the lowest average La/Sm_n ratio at 4.9, whereas the D2 Type 2 samples show the highest average at 5.8. The D2 Type 2 also show the highest average La/Yb_n ratio (197) indicating that their light REE are the strongest enriched relative to their heavy REE in comparison with the remaining intrusive phases in this study. The D16 intrusive phase shows the lowest average La/Yb_n ratio at 57.

Primitive mantle-normalised patterns for the majority of samples in this study are sub-parallel and show strong negative K, Hf and Ti anomalies. These anomalies are more subdued in samples that show increased crustal dilution, e.g. the D5, D18, Type 5 and D16 samples. The Pb, Sr and P contents are variable not only between the different intrusive phases but also between samples within a given intrusive phase. The data correlate relatively well with the Kimberley data and only some of the REE of the more diluted intrusive phases show lower primitive mantle normalized values (Figures 5.6, 5.8 & 5.10).

6 PETROGENESIS

6.1 Introduction

Although the earliest studies of kimberlites date back in excess of a hundred years, there is still some uncertainty regarding the location and composition of the source of kimberlite magmas. The hybrid nature and secondary modification of the original magma by open system processes has complicated such investigations (e.g. le Roex *et al.*, 2003). Open system processes include mantle xenolith assimilation, crustal contamination and late stage alteration. Petrogenetic processes such as partial melting and crystal fractionation and accumulation have also been poorly understood. The influence of these processes on the major and trace element composition of kimberlite magmas have been addressed in a number of recent petrogenetic studies, e.g. Price *et al.* (2000); le Roex *et al.* (2003); Coe (2004); Harris *et al.* (2004); Becker & le Roex (2006). These authors and references therein, have shown that it is possible to correct for such processes to a certain extent, and thereby derive a close-to-primary kimberlite magma composition.

The Dutoitspan kimberlite comprises multiple intrusions, a few of which are the focus of this study. Samples from seven of these intrusions, i.e. D2 Type 2, D2 Type 3, D2/D5, D5, D18, D16 and Dyke, will be evaluated in a similar way to the studies mentioned above (Section 6.2 and 6.3). The focus will however be to determine, if possible, (i) whether the various intrusive types originate from the same primary magma, or (ii) whether different intrusive phases result from the injection of geochemically distinct primary magmas.

6.2 Open System Modification of Primary Kimberlite Magma

6.2.1 Late Stage Alteration

According to Barrett & Berg (1975), the slight but uniform serpentinisation of a kimberlite represents the first phase of serpentinisation, which could reflect autometasomatism by deuteric fluids. The latter is the result of the concentration of the volatile content of a kimberlite magma into residual fluids during solidification. A second, more extensive, phase of serpentinisation is attributed to high temperature groundwater that permeates through the kimberlite after solidification (e.g. Berg & Allsopp, 1972). Alteration by both deuteric fluids and groundwater may cause the leaching of more mobile elements such as MgO and K_2O from kimberlite and result in lower Mg# (e.g. Tompkins *et al.*, 1999). Mobile elements such as Ba, Rb and K

show no correlation with more immobile elements like La, Zr and Nb in the Dutoitspan samples, and their variations are interpreted to reflect alteration (le Roex *et al.*, 2003; Figure 6.1).

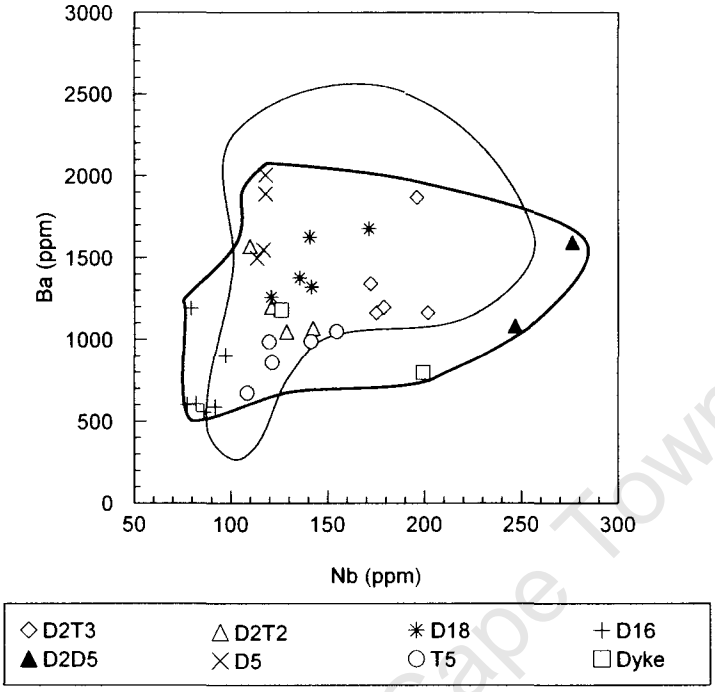

Figure 6.1. Ba vs. Nb in the Dutoitspan kimberlites. The lack of correlation between these two, and other, incompatible trace elements is interpreted to reflect alteration. Shaded area indicates range of Kimberley data from le Roex *et al.* (2003).

The alteration suggested by the behaviour of the mobile trace elements of the Dutoitspan samples is exhibited by, among others, the partial or complete serpentinisation of olivine macrocrysts and phenocrysts, as well as the presence of cryptocrystalline serpentine and calcite (e.g. Coe, 2004; Becker and le Roex, 2006). The calcite and serpentine occur in irregularly shaped pools that segregated to various degrees from the groundmass (Skinner & Clement, 1979; Clement & Reid, 1989). Calcite also rarely occurs as veins in some samples. Segregations are most notable in the Type 5 samples, whereas the serpentinisation of olivine macrocrysts and phenocrysts is most severe in the D5, D18, Type 5 and D16 samples. These samples will be treated with caution hereafter.

Another approach to evaluating the extent of alteration in kimberlite samples is that of Tompkins *et al.* (1999) who regarded kimberlite samples with a CaO content >15 wt % as carbonated kimberlite. Carbonated kimberlite generally also shows a low Mg#. Based on this observation, a single sample from the Dutoitspan sample suite can be classified as carbonated kimberlite, i.e. sample D2D5-02W collected from the contact zone between the D2 Type 3 and the D5 intrusive phase. However,

care should be taken when following this approach as it is debatable whether the carbonate present in a particular sample is primary or secondary (e.g. Kirkley *et al.*, 1989).

Sweeney *et al.* (1999) suggested that alteration would increase the loss-on-ignition (LOI) of the whole rock by the formation of hydrated phases, e.g. serpentine, and proposed that altered material can be recognised by LOI >15 %. However, no correlation could be found between the LOI and amount of serpentine in the various samples of this study and none of the samples showed LOI values >15 %.

In summary, the study of the occurrence of serpentine and calcite, as well as the behaviour of mobile trace elements in relation to immobile trace elements, is the preferred method for the determination of the extent of alteration of the Dutoitspan kimberlites. Samples classified as altered by this method will be treated with caution hereafter.

6.2.2 Crustal Contamination

During kimberlite emplacement, material from the surrounding country rocks are dislodged and included in the kimberlite magma before solidification. Country rock fragments observed during petrographic analyses of the Dutoitspan samples include shale, dolerite, amphibolite-schist and granite-gneiss. These rocks all have higher SiO_2 and Pb, and lower MgO in relation to kimberlite and, as noted by le Roex *et al.* (2003), the melting temperature of crustal material, such as shale, is low (melting begins at 100°C) and therefore these fragments may be assimilated by the kimberlite magma. Although an attempt was made to remove the visible crustal material from the analysed Dutoitspan samples, the influence of crustal assimilation on the geochemistry of certain samples is still evident, i.e. the high SiO_2 and low MgO content (Figure 6.2) and the positive Pb anomalies (e.g. Figure 6.3) of samples predominantly from the D5, D18, Type 5 and D16 intrusive phases (samples: D5-01W – D5-05W, D18-01W – D18-05W, T5-01W – T5-05W, D16-01W – D16-06W).

As discussed in Chapter 5, Clement (1982) introduced the contamination index (C.I.) in an attempt to calculate the extent of crustal contamination and weathering of kimberlite magmas. According to Clement, a kimberlite sample with a C.I. higher than 1.5 can be considered as contaminated and a C.I. of ~1.0 indicates negligible contamination. The C.I. of each of the samples in this study was calculated and is listed in Table 5.1. Two samples from the D16 intrusive phase (samples D16-01W

and D16-06W) showed C.I. values >1.5 and are considered to be crustally contaminated. These two samples are excluded from further discussion.

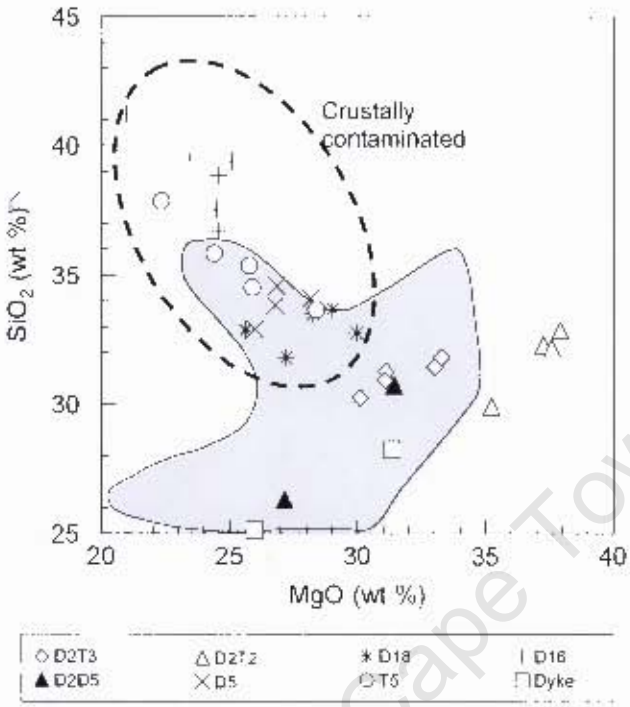

Figure 6.2. SiO_2 vs. MgO in the Dutoitspan kimberlites. Note that high SiO_2 and low MgO show an influence of crustal contamination. Shaded area indicates range of Kimberley data from le Roex *et al.* (2003).

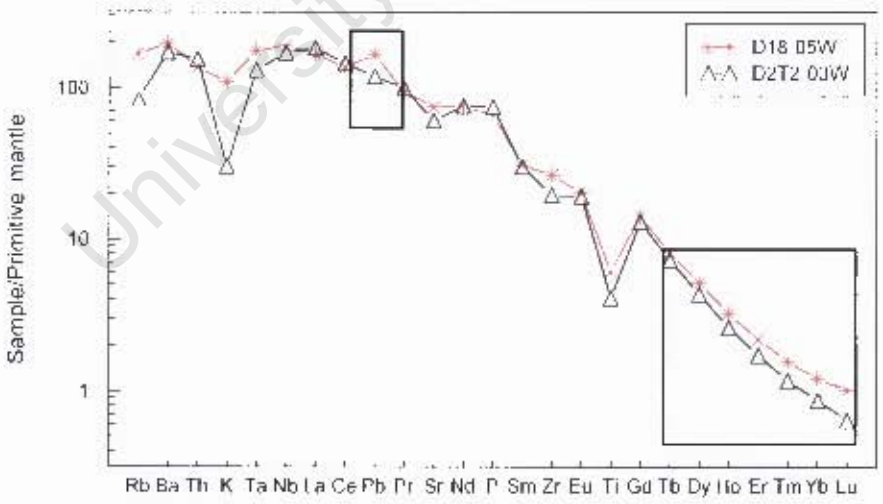

Figure 6.3. Primitive mantle-normalised trace element patterns of a crustally contaminated Dutoitspan sample, D18-05W, and a sample lacking significant influence by crustal contamination, D2T2-03W. Note the positive Pb anomaly and elevated HREE of the D18 sample in relation to the D2 Type 2 sample. Normalizing values from Sun & McDonough (1989).

Le Roex *et al.* (2003) have shown that, in addition to the effect on major elements, the accidental inclusion of crustal xenoliths in the kimberlite magma during emplacement may also affect its REE composition. The elevated HREE contents of

crustal rocks, relative to kimberlite, causes the elevation of HREE contents in crustally contaminated kimberlite magmas, with consequently lower Gd/Yb ratios in comparison with uncontaminated samples (Figure 6.4; also note elevated HREE of e.g. a D18 sample in relation to a D2 Type 2 sample in Figure 6.3). This contamination can also result in relative enrichment in Pb, and consequent positive Pb anomalies on a primitive mantle normalised diagram (le Roex *et al.*, 2003) (Figure 6.3). The following samples, in addition to those already discarded, are excluded from the remainder of this study in view of their raised HREE and Pb anomaly: all D16 samples, all D18 samples except for sample D18-01W, all D5 samples, all Type 5 samples and sample D2T2-05W.

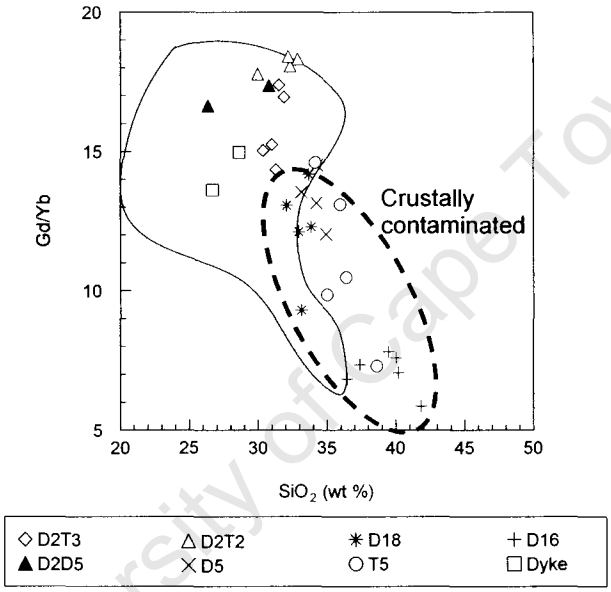

Figure 6.4. Gd/Yb vs. SiO_2 in the Dutoitspan kimberlites. Note that high SiO_2 and low Gd/Yb ratios show an influence of crustal contamination. Shaded area indicates range of Kimberley data from le Roex *et al.* (2003).

6.2.3 Peridotite entrainment

The heterogeneity of the upper mantle is illustrated in the variety of mantle xenoliths sampled by kimberlite, which include amphibole-bearing and mica-rich types, megacrysts, garnet-pyroxenites, eclogites and peridotites and dunites (e.g. Gurney and Harte, 1980). Peridotites, typically lherzolite and harzburgite that contain some garnet and chromite-rich spinel, are the most common and abundant (Gurney and Harte, 1980). Evidence of the entrainment of peridotite by kimberlite magmas can be found in the nature or texture of their macrocrysts, which is generally dominated by deformed anhedral olivine macrocrysts (Clement, 1982; Shee, 1985). The presence of phlogopite, peridotitic garnet and Cr-diopside in kimberlite samples, support the derivation of olivine macrocrysts from peridotite as they too are components of peridotite (e.g. le Roex *et al.*, 2003). Shee (1985)

suggested that orthopyroxenes are completely resorbed by the silica-poor kimberlite magma and therefore is absent as a macrocryst phase. Macrocrystic kimberlite is therefore commonly accepted to be a partial cumulate of mantle-derived minerals rather than a true liquid composition (le Roex *et al.*, 2003).

In his study of the hypabyssal facies of the Wesselton kimberlite pipe, Shee (1985) demonstrated that macrocrystic kimberlite could be corrected for mantle contamination to some extent. He firstly established the compositions of the macrocrysts and secondly subtracted by mass balance an amount equivalent to the modal abundance of the macrocrysts from the kimberlite whole rock analysis. By following this process, whole rock compositions very similar to the average aphanitic Wesselton kimberlite was achieved.

Following Becker & le Roex (2006), it will be assumed in this study that all olivine macrocrysts from the Dutoitspan macrocrystic kimberlite samples (see Table 6.1 for a list of uncontaminated Dutoitspan samples), which contain ~10-25 % olivine macrocrysts, derive from disaggregated garnet lherzolite. As noted above, kimberlites sample a number of other mantle xenoliths in addition to the common and abundant lherzolite. However, a simplified correction procedure is all that can be reasonably undertaken at the level of this study.

Table 6.1 Selected samples from the Dutoitspan intrusive phases that will be used in the modelling process. The chemical compositions of these samples have not been influenced by crustal contamination and/or alteration.

D2 Type 3 - Macrocrystic	D2/D5 - Aphanitic	D2 Type 2 - Macrocrystic	D18 - Macrocrystic	Dyke - Macrocrystic
D2T3-01W	D2D5-01W	D2T2-02W	D18-01W	D16D-01W
D2T3-02W	D2D5-02W	D2T2-03W		
D2T3-03W		D2T2-04W		
D2T3-04W				
D2T3-05W				

The need to take differences in densities between lherzolite and kimberlite and their macrocrystic components into account during the macrocryst correction procedure, should be recognised and is discussed here. The density of Fo_{94} is approximately 3.2 g/cm^3 and that of aphanitic Dutoitspan kimberlite is approximately 3.1 g/cm^3. At high temperature, the density of kimberlite is relatively low (~2.2 g/cm^3) due to the presence of volatiles, where the partial molar volume of H_2O and its change with temperature affects the density of kimberlite very strikingly. Under these conditions the olivine and peridotite has a significantly higher density in comparison with the kimberlite magma. At room temperature, these differences are not as noticeable, and since the measured Dutoitspan kimberlite densities at room temperature are

not that different to olivine or peridotite at room temperature, the density difference can be ignored for mass balance calculations. This holds true since the wt % of each oxide as analysed are also relative to the bulk composition at room temperature and not at 1200°C. Working with cation proportions is more correct, but the differences are negligible given all the assumptions noted earlier in this section.

An average garnet lherzolite from the Kimberley area consists of ~68% olivine, ~23 % orthopyroxene, ~3 % clinopyroxene, ~5 % garnet and <1 % phlogopite (see Table 6.2 for average major and trace element composition), as determined from the Bultfontein and Jagersfontein samples of Grégoire *et al.* (2003), and is indicated in Figure 6.5. It then follows that ~15-35 % garnet lherzolite has been entrained and disaggregated. The effect of the entrainment on the D2 Type 3, D2 Type 2, D2/D5, D18 and Dyke samples is illustrated in Figure 6.5. By proportionally subtracting the estimated entrained garnet lherzolite from each of the samples, a close-to-primary magma composition was calculated for selected Dutoitspan intrusive phases (Table 6.2).

D2 Type 2 primary magma

The D2 Type 2 samples contain approximately 22 % olivine macrocrysts and form a tight cluster, which are distinct from the remaining Dutoitspan samples that form a linear trend towards the average garnet lherzolite (Figure 6.5). Following the correction for ~32 % garnet lherzolite entrainment, as inferred from the modal abundance of olivine, the average Ni (1376 ppm) and MgO (36.2 wt %) content and Mg-number (0.899) of the D2 Type 2 samples (Table 6.2) are significantly higher compared to the corresponding averages of the other intrusive phases listed in Table 6.2 (also see illustration of high Ni and Co content of D2 Type 2 samples in Figure 5.3) and the close-to-primary Group 1 kimberlites from Becker & le Roex (2006) (~22-28 wt % MgO; 660-1190 ppm Ni; Mg-number 0.82-0.87). This may illustrate the weakness with this approach, resulting from: (1) macrocrysts being unevenly distributed in the rock and material crushed for chemical analysis may be more macrocryst-rich than shown by thin section; (2) flow differentiation favouring enrichment of olivine in the kimberlite sample such that the applied correction procedure using peridotite, under-corrected for MgO and Ni. Alternately, the D2 Type 2 kimberlite may represent a different magma from a different source region composition.

Table 6.2 Average close-to-primary major and trace element compositions of selected Dutoitspan intrusive phases following a macrocryst correction procedure. The estimated modal proportions of olivine macrocrysts and calculated proportion of peridotite entrained are also given. Average Kimberley lherzolite composition calculated from Grégoire et al. (2003).

Sample #	Average lherzolite	D2 Type 3 - Macrocrystic	D2/D5 - Aphanitic	D2 Type 2 - Macrocrystic	D18 - Macrocrystic	Dyke - Macrocrystic
% Olivine	68	15.6	6.5	21.7	15	17
% Peridotite		22.9	9.6	31.9	22	25
Major Elements (wt %)						
SiO_2	43.5	27.8	27.0	27.7	30.5	24.9
TiO_2	0.059	3.54	2.92	2.41	4.78	3.4
Al_2O_3	1.51	1.47	1.84	0.61	1.23	2.5
Fe_2O_3	6.32	9.63	9.03	9.12	8.75	11.8
MnO	0.107	0.164	0.170	0.158	0.134	0.2
MgO	41.7	29.2	28.1	36.2	27.4	30.0
CaO	1.06	12.0	14.9	11.5	8.88	15.7
Na_2O	0.171	0.599	0.624	0.510	0.656	0.6
K_2O	0.133	2.43	1.54	1.20	4.32	1.3
P_2O_5	0.031	2.49	3.56	2.28	0.980	1.9
Cr_2O_3	0.361	0.233	0.307	0.307	0.178	0.2
NiO	0.264	0.124	0.123	0.168	0.122	0.1
L.O.I.	4.70	10.3	9.84	7.85	12.0	7.3
Total	100	100	100	100	100	100
Mg#	0.937	0.872	0.875	0.899	0.876	0.851
Trace Elements (ppm)						
Sc	8.46	11.2	17.7	10.5	9.96	17.7
V	17.2	129	189	102	99.9	84.6
Cr**	1112	1989	2233	2712	1578	1850
Co	90.6	71.5	58.5	78.9	72.0	74.8
Ni**	1919	1007	977	1376	987	781
Cu	5.75	80.8	178	60.5	26.9	77.6
Rb	5.19	121	71.5	83.5	188	49.0
Sr	38.6	2226	2460	2356	2784	1230
Y	1.26	18.8	27.3	15.1	16.0	25.1
Zr**	7.95	450	634	342	386	485
Nb**	3.37	240	291	191	181	265
Ba	35.9	1727	1495	1604	1684	1051
La	3.02	196	284	184	139	227
Ce	6.39	405	582	370	302	481
Pr	0.745	43.5	63.7	39.2	33.1	52.7
Nd	2.79	166	243	148	127	205
Sm	0.444	21.9	32.3	19.1	17.2	28.0
Eu	0.126	5.39	7.86	4.68	4.18	6.95
Gd	0.335	13.3	19.2	11.3	10.2	17.4
Tb	0.047	1.35	1.95	1.13	1.06	1.81
Dy	0.240	5.71	8.13	4.67	4.56	7.68
Ho	0.045	0.791	1.12	0.623	0.652	1.06
Er	0.118	1.49	2.14	1.17	1.32	2.17
Tm	0.017	0.163	0.226	0.123	0.148	0.219
Yb	0.113	0.816	1.12	0.575	0.822	1.14
Lu	0.019	0.099	0.128	0.066	0.099	0.132
Hf	0.176	7.52	10.5	5.32	6.61	8.86
Ta	0.182	10.0	12.8	7.71	8.94	13.25
Pb	0.415	10.9	9.00	13.8	5.11	7.12
Th	0.363	21.0	28.8	19.2	16.3	25.5
U	0.091	5.90	7.14	5.30	4.45	5.80
Zr/Nb	2.36	1.88	2.20	1.79	2.14	1.83
La/Nb	0.897	0.820	0.980	0.970	0.769	0.856
Ba/Nb	10.7	7.26	5.06	8.49	9.32	3.97
Nb/Ta	18.6	24.0	22.7	24.7	20.2	20.0
Ce/Pb	15.4	37.9	77.5	27.1	59.2	67.5
La/Smn*	4.39	5.79	5.68	6.23	5.22	5.22
La/Ybn*	19.1	173	182	230	121	143

LOI: loss on ignition; Mg#: atomic $Mg/(Mg+Fe^{2+})$ with $Fe_2O_3/FeO=0.15$; * - normalised to chondrite; ** - trace elements analysed by XRF, all other trace elements analysed by ICP-MS

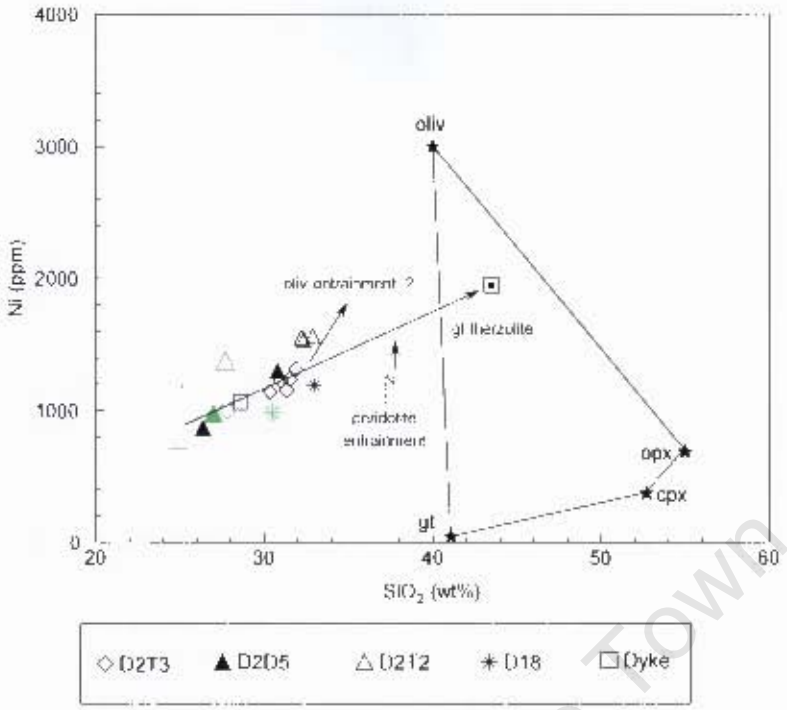

Figure 6.5. Ni vs SiO_2 in the Dutoitspan kimberlites. Black symbols - sample compositions before macrocryst correction; green symbols – close-to-primary magma compositions. The marked garnet lherzolite is an average Bultfontein and Jagersfontein lherzolite determined from Grégoire *et al.* (2003) (see text). Representative compositions of garnet, clinopyroxene, orthopyroxene and olivine are also from Grégoire *et al.* (2003).

D2 Type 3 primary magma

The D2 Type 3 samples define a slight linear trend towards garnet lherzolite (Figure 6.5). It was estimated from the petrographic analysis of these samples that they contain an average modal proportion of ~16 % olivine. It then follows that ~23 % garnet lherzolite has been entrained and disaggregated by this intrusive phase. The corrected average composition of the D2 Type 3 (Table 6.2) compare well with the close-to-primary Group 1 kimberlite magma calculated by Becker & le Roex (2006), i.e. ~29 wt % vs. ~22-28 wt % MgO; 28 wt % vs. ~21-30 wt % SiO_2; ~1007 ppm vs. 660-1190 ppm Ni; Mg-number ~0.87 vs. 0.82-0.87.

Dyke primary magma

Following the elimination of samples due to the effects of crustal contamination as discussed earlier in this chapter, a single sample from each of the D18 and Dyke intrusive phases remained and are shown in Figure 6.5. Together with the D2 Type 3 samples, the Dyke sample defines a linear trend towards garnet lherzolite. A modal abundance of 24 % olivine was estimated from the thin section of this sample, which suggests that 35 % garnet lherzolite was entrained and disaggregated by this intrusive phase. With the exception of the relatively low Ni

(600 ppm vs. 660-1190 ppm) and SiO_2 (20.1 wt % vs. ~21-30 wt %), the corrected sample composition of the Dyke sample fall well within the close-to-primary Group 1 kimberlite magma of Becker & le Roex (2006) (Table 6.3).

The relatively low Ni (600 ppm) and SiO_2 (20.1 wt %) of the corrected Dyke composition (Table 6.2) suggests that the amount of olivine may have been overestimated in this particular sample and that some of the olivine macrocrysts do not originate from peridotite and are rather high P phenocrysts. It was also noted in Chapter 4 (Section 4.8) that macroscopically the dyke is similar in appearance to the macrocrystic D2 Type 3 intrusive phase in places but had an aphanitic or micro-porphyritic appearance (i.e. lacked olivine macrocrysts) in other areas. An average olivine content of ~17 % (average of 10 % olivine macrocrysts in eliminated sample D16Dyke-02P and 24 % olivine macrocrysts in sample D16Dyke-01P; Appendix A) would perhaps be a better estimate for the average Dyke sample, which implies that only 24 % garnet lherzolite was entrained on average and disaggregated by this intrusive phase. Correcting for 24 % garnet lherzolite would increase the Ni content to 781 ppm, SiO_2 to 24.9 wt % and Mg# to 0.85, which compares better with the close-to-primary Group 1 kimberlite magma of Becker & le Roex (2006).

D18 primary magma

A modal abundance of 15 % olivine was estimated from the thin section of sample D18-01P, which suggests that 22 % garnet lherzolite was entrained and disaggregated into the D18 intrusive phase. With the exception of a slightly high Mg# (0.876 vs. 0.82-0.87; Becker & le Roex, 2006), the corrected sample composition of the Dyke sample falls well within the close-to-primary Group 1 kimberlite magma of Becker & le Roex (2006) (Table 6.3).

D2/D5 primary magma

As discussed in Chapter 5, the two D2/D5 samples are quite different in major element compositions but similar in incompatible trace element compositions. Figure 6.5 also shows that sample D2D5-02W is least affected by lherzolite entrainment of all Dutoitspan samples in this study, including sample D2D5-01W. By calculating an average composition for the D2/D5 intrusive phase from these two samples and subsequently correcting for 9.6 % peridotite entrainment (as estimated from an average olivine macrocryst content of 6.5 %), a close-to-primary D2/D5 kimberlite magma (~27 wt % SiO_2; ~28 wt % MgO; Mg number ~0.87; ~1.8 wt % Al_2O_3; ~2.9 wt % TiO_2; ~1.5 wt % K_2O; ~15 wt % CaO) is derived. This is very similar in composition to that of the close-to-primary Group 1 kimberlite magma of

Becker & le Roex (2006), the close-to-primary Uintjiesberg kimberlite magma of Harris *et al.* (2004) and the close-to-primary Kimberley kimberlite magma of le Roex *et al.* (2003) (Table 6.2 and 6.3). Al_2O_3 is however slightly lower in comparison with these studies. K_2O falls well within the range given by Becker & le Roex (2006) (Table 6.3).

Table 6.3. Comparison of selected major elements of primary magmas from various related studies. All values, with the exception of Mg# are given as weight %.

	This study	Becker & le Roex (2006)	Harris *et al.* (2004)	Le Roex *et al.* (2003)
SiO_2	~25-31	~21-30	~25	~26-27
MgO	~27-36	~22-28	~26	~26-27
CaO	~9-16	~10-17	~15	~12
K_2O	~1.2-4.3	~0.2-1.7	~1.1	~1.0-2.0
Al_2O_3	~0.6-2.5	~2.2-3.7	~2.3	~2.2
Mg#	~0.85-0.90	~0.82-0.87	~0.85	~0.86

A single or multiple primary magma(s)?

Becker & le Roex (2006) and other workers have shown that, by correcting for the entrainment of lherzolite based on the modal percentage of olivine macrocrysts in each sample, a sub-parallel upwards displacement of the REE patterns is caused. The corrections described above show a similar effect on the samples from this study, although not illustrated here. The resulting chondrite normalised REE patterns of each of the calculated Dutoitspan primary magmas are illustrated in Figure 6.6 and the following observations were made:

- The aphanitic D2/D5 contact zone primary magma plots largely sub-parallel to that of the D2 Type 3 primary magma. However, the incompatible element ratios of the two intrusive phases are somewhat different, i.e. Zr/Nb of 1.88 vs. 2.20, La/Sm_n of 5.79 vs. 5.68, Nb/Ta of 24.0 vs. 22.7, for D2 Type 3 and D2/D5 respectively. The sub-parallel patterns may therefore be as a result of incorrect peridotite correction due to the possibility that some of the olivine macrocrysts do not originate from peridotite and are rather high P phenocrysts.

- The D2 Type 2 intrusive phase composition has lower relative HREE abundances than the other calculated magmas. The incompatible trace element ratios are slightly different from that of the D2 Type 3, i.e. Zr/Nb of

1.79 vs. 1.88, La/Sm_n of 6.23 vs. 5.79, Nb/Ta of 24.7 vs. 24.0, for D2 Type 2 and D2 Type 3 respectively. This is consistent with different degrees of partial melting (Section 6.3.2).

- Both the Dyke and specifically the D18 calculated primary magmas show HREE enrichment relative to the remainder of the calculated primary magmas (Figure 6.6). This may indicate an influence by crustal contamination as discussed in Section 6.2.2, or differences in degrees of partial melting (see Section 6.3.2).

Based on the observations above, the Dutoitspan intrusive phases may originate from slightly different primary magmas formed by slightly different degrees of partial melting or may be related to slight differences in source region composition at similar degrees of partial melting.

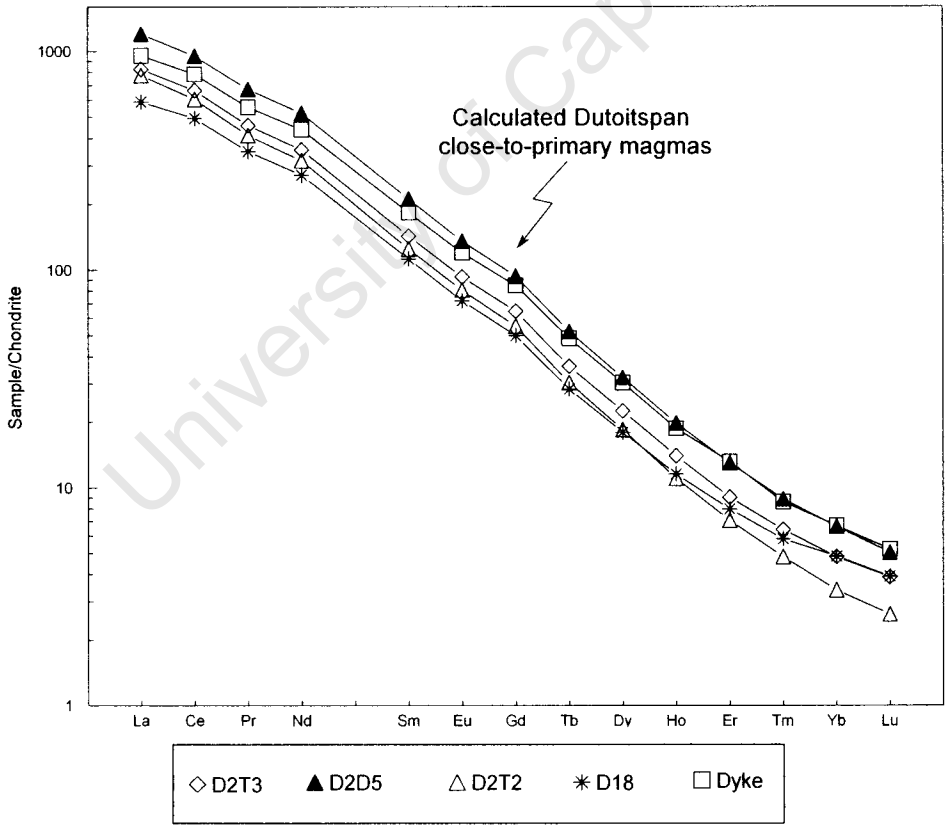

Figure 6.6. Chondrite normalised REE variation of the calculated Dutoitspan close-to-primary magmas. While the Dyke and D2/D5 have similar HREE abundances, they differ in LREE. The D18 has a significantly different REE slope, as does D2 Type 2. Chondrite values are from Sun and McDonough (1989).

6.3 Petrogenetic Modification of Primary Kimberlite Magma

6.3.1 Crystal Fractionation

Whereas peridotite entrainment results in raised Ni and Co contents in kimberlite magmas, olivine fractionation causes a depletion of these elements in the magma. Le Roex *et al.* (2003) have shown that the most evolved Kimberley kimberlites, i.e. aphanitic kimberlites, are examples of magmas that have undergone crystal fractionation processes and characteristically show lower Mg-numbers, lower Ni content, etc. in relation to the macrocrystic samples from the same area. Olivine fractionation thus has an opposite effect on kimberlite magma compositions to that of peridotite entrainment.

The majority of samples in this study plot on a trend towards the average Kimberley lherzolite calculated from Grégoire *et al.* (2003) (see Section 6.2.3 above; Figure 6.5), and the lack of aphanitic Dutoitspan samples precludes a detailed evaluation of the effect of crystal fractionation.

6.3.2 Partial Melting

A number of experimental studies have been undertaken over the past three decades with regard to kimberlitic melts (Wyllie, 1987; Eggler, 1987; Dalton & Presnall, 1998a; Wyllie & Lee, 1999), showing that low degrees of partial melting of a carbonated garnet lherzolite at ~3-8GPa can produce melts similar in composition to that of kimberlite magmas. Dalton & Presnall (1998a) have also shown that by varying the degree of partial melting from ~0.3 % to ~1.0 % a continuum between carbonatite and kimberlite melts exists. The aim of this section is to investigate the role of partial melting in the formation of the Dutoitspan kimberlite magmas and to derive possible compositions of their source regions.

Le Roex *et al.* (2003) recognised two groups of kimberlites in the Kimberley cluster based on their chondrite-normalised patterns: those with sub-parallel patterns and those with diverging LREE patterns. It was shown that peridotite entrainment causes a relatively uniform depletion in all REE (also see Section 6.2.3. above) and therefore results in sub-parallel chondrite-normalised patterns. In contrast, it was shown that by changing the degree of partial melting, diverging LREE patterns are attained with residual garnet acting as a buffer on HREE. The Dutoitspan primary magma chondrite-normalised REE patterns range from sub-parallel to diverging (Section 6.2.3, Figure 6.6). It was therefore proposed in Section 6.2.3 that the Dutoitspan intrusive phases originate from slightly different primary magmas with

different degrees of partial melting or differences in the amount of residual garnet. These observations are investigated further below.

Following le Roex *et al.* (2003) and Becker & le Roex (2006), a process of semi-quantitative modelling was followed to derive possible source compositions of the close-to-primary Dutoitspan kimberlite magmas. The source compositions are calculated by applying the equations for non-modal batch melting (Shaw, 1970) and partition coefficients as shown in Table 6.4. A residual mineralogy similar to that used by le Roex *et al.* (2003) (Table 6.5) in the study of the Kimberley kimberlites is used since it included the Dutoitspan kimberlite, as opposed to that used by Becker and le Roex (2006) for a broader region of Group 1 kimberlites. A fixed degree (F = 1 %) of partial melting was assumed.

Table 6.4. Partition coefficients for incompatible elements used in partial melting modelling from a compilation in Späth *et al.* (2001).

	Rb	Ba	Th	U	K	Ta	Nb	La	Ce	Pb	Pr	Sr	Nd	P
Oliv	0.001	0.001	0.001	0.001	0.001	0.001	0.001	0.001	0.001	0.001	0.001	0.001	0.001	0.001
Opx	0.001	0.001	0.001	0.001	0.001	0.001	0.001	0.001	0.001	0.001	0.001	0.001	0.001	0.001
Cpx	0.001	0.001	0.001	0.001	0.01	0.01	0.01	0.05	0.08	0.08	0.1	0.12	0.14	0.1
Gt	0.001	0.001	0.001	0.001	0.001	0.001	0.001	0.01	0.021	0.021	0.054	0.001	0.087	0.05

	Sm	Hf	Zr	Eu	Ti	Gd	Tb	Dy	Ho	Er	Tm	Yb	Lu
Oliv	0.001	0.001	0.001	0.001	0.001	0.001	0.001	0.001	0.001	0.001	0.001	0.001	0.001
Opx	0.001	0.01	0.01	0.01	0.01	0.016	0.019	0.022	0.022	0.03	0.03	0.1	0.1
Cpx	0.14	0.2	0.2	0.15	0.17	0.2	0.25	0.3	0.3	0.28	0.29	0.3	0.3
Gt	0.13	0.1	0.1	0.2	0.1	0.3	0.6	0.9	1.4	2	3	4	6

* Note: Oliv = olivine, Opx = orthopyroxene, Cpx = clinopyroxene, Gt = garnet

Table 6.5. Residual modal proportions and melt modes of peridotitic minerals (after le Roex *et al.*, 2003) used to model the source region of the Dutoitspan kimberlite.

Phase	Modal proportion (vol. %)	Melting proportion
Oliv	0.63	0.05
Opx	0.23	0.05
Cpx	0.12	0.5
Gt	0.02	0.4

The chondrite normalised REE content of the calculated source region of the Dutoitspan close-to-primary magmas (1 % partial melt) is illustrated in Figure 6.7. In general, the calculated source compositions are depleted in HREE relative to LREE (Lu ~0.43 – 0.97 x chondrite; La ~10.1 – 20.6 x chondrite). The source compositions of the Dyke and D2/D5 intrusive phases show similar abundances of LREE relative to chondrite, but diverging HREE patterns. The higher HREE abundances of the Dyke relative to the D2/D5 source, suggests a higher

abundance of residual garnet in the composition of the Dyke source. The chondrite normalised source composition of the D2 Type 3 kimberlite plots sub-parallel to that of the Dyke and show a uniform depletion in all REE relative to that of the Dyke source composition. The D2 Type 2 source shows similar LREE abundances to that of the D2 Type 3 intrusive phase but notably lower HREE abundances relative to chondrite. This suggests that the D2 Type 2 source contains less residual garnet in relation to the D2 Type 3 source. Finally, the D18 source shows similar chondrite normalised HREE abundances but is depleted in LREE relative to the D2 Type 3 source, suggesting lower degrees of partial melting than the D2 Type 3 source. The Dutoitspan source compositions fall well within the Kaapvaal craton garnet lherzolite field from Grégoire *et al.* (2003) and in the upper portion of the Group I kimberlite range of Becker & le Roex (2006).

The primitive mantle normalised trace element compositions of the suggested primary magmas and their calculated source compositions are illustrated in Figure 6.8. Here the most notable feature of the calculated source is the negative anomalies of Rb, K, Sr, Hf and Ti. As noted in section 6.3.1., a number of recent studies of kimberlite petrogenesis (e.g. Becker & le Roex, 2006; le Roex *et al.*, 2003; Harris *et al.*, 2004) have argued in detail that these anomalies are features intrinsic to the source of Group 1 kimberlite magmas. Based on the similarities between the samples in this study and the above mentioned, the arguments are suggested to be applicable to the Dutoitspan primary kimberlite magmas and their calculated source compositions.

In summary, differences in the Dutoitspan close-to-primary magmas can be attributed to slight differences in source compositions at similar degrees of partial melting or different degrees of partial melting of the same source composition.

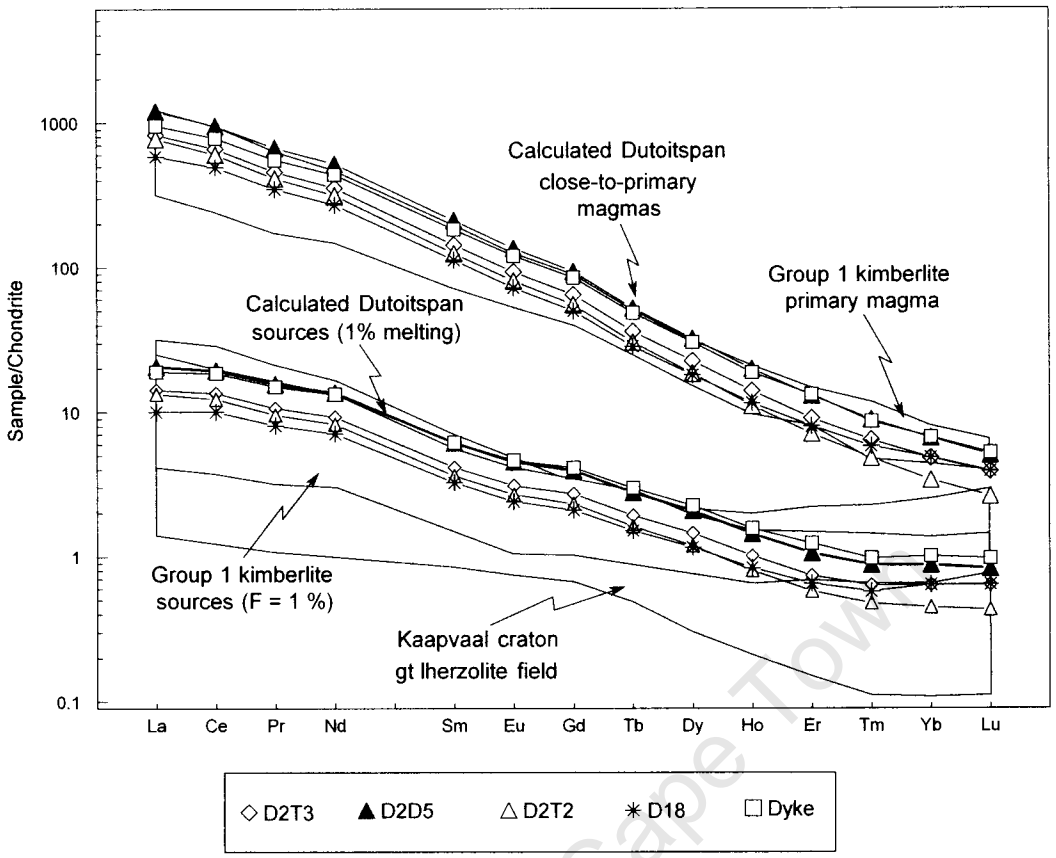

Figure 6.7. Chondrite normalised REE variation of the calculated Dutoitspan kimberlite source compositions assuming F = 1 % and a residual source region mineralogy of ol:opx:cpx:gt = 0.63:0.23:0.12:0.02. The Dutoitspan primary magmas and the Group I kimberlite primary magma and source ranges (Becker & le Roex, 2006) are shown for comparison. Chondrite values are from Sun and McDonough (1989) and the field of Kaapvaal garnet lherzolites is from Grégoire *et al.* (2003).

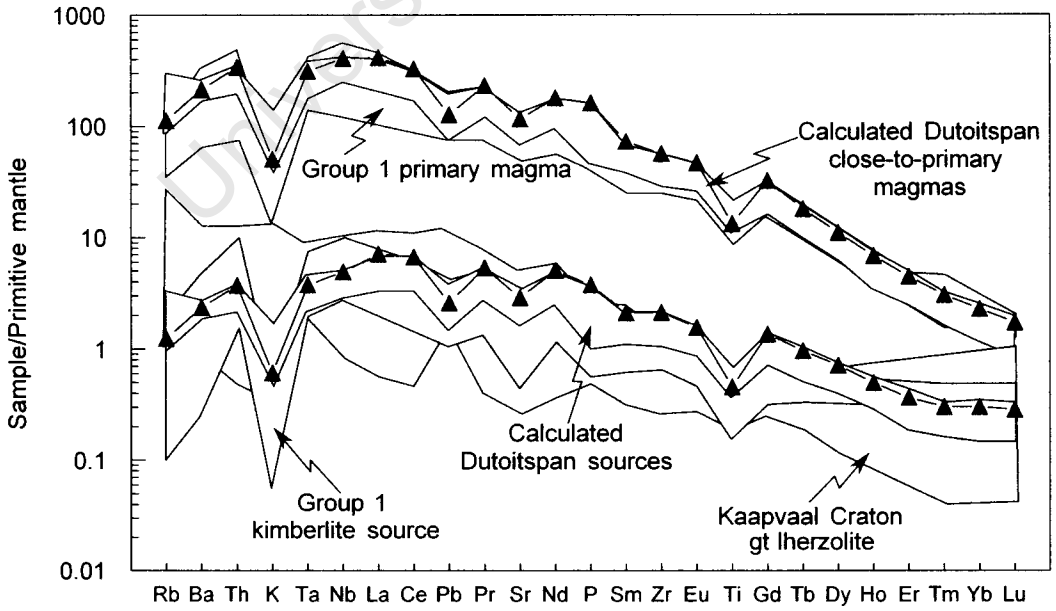

Figure 6.8. Predicted primitive mantle normalised patterns of the source composition range of the Dutoitspan close-to-primary magmas (colourless fields; D2/D5 shown as an example), calculated by forward modelling from close-to-primary kimberlite magmas with F=1 % and residual source region mineralogy as in Figure 6.7. Group I kimberlite primary magma range and calculated source composition range from Becker and le Roex (2006) are shown for comparison. Chondrite values are from Sun and McDonough (1989) and the field of Kaapvaal garnet lherzolites is from Grégoire *et al.* (2003).

6.3.3 Source Region Evolution: A Brief Discussion

Tainton and McKenzie (1994), le Roex *et al.* (2003), Harris *et al.* (2004), Coe (2004) and Becker & le Roex (2006) have all argued for a two-stage evolutionary model of the source region of kimberlites. This model comprises an initial depletion event (suggested by the low HREE and high Mg# and Ni content of the inferred primary magmas), followed by a metasomatic enrichment event. Additionally, these authors have argued that for the depleted signature to be preserved, the kimberlite source must be located in the lithospheric mantle. The Group 1 kimberlites have also been shown by these authors to have incompatible trace element ratios similar to the South Atlantic ocean island basalts (OIB), suggesting derivation of the metasomatising fluids/melts from a sub-continental lithospheric source, possibly a mantle plume.

The depletion of HREE relative to primitive mantle abundances in the calculated source of the inferred primary Dutoitspan magmas (assuming 1 % partial melting and 2 volume % residual garnet) of 0.15 to 0.33 times primitive mantle (Figure 6.8) and the enrichment in highly incompatible trace elements of ~1 to 6 times primitive mantle abundances, are requisites for a metasomatised source (le Roex *et al.*, 2003). The low HREE abundances, and the high Mg-number (Mg# ~0.85 – 0.90) and high Ni content (~781 - 1376ppm) of the inferred primary magma, suggest that the source was depleted prior to metasomatic enrichment. It is thus probably located within the refractory sub-lithospheric mantle (e.g. le Roex *et al.*, 2003). The latter argument is based on the view that the convecting asthenosphere is unlikely to preserve the depleted signature for an extensive period of time (Tainton and McKenzie, 1994; le Roex *et al.*, 2003).

The Dutoitspan primary magmas are strongly enriched in LREE and incompatible trace elements, and have incompatible trace element ratios (e.g. La/Nb = 0.769 – 0.980, Ce/Pb = 27.1 – 77.5, Ba/Nb = 3.97 – 9.32) that correlate well with those of the South Atlantic ocean island basalts (OIB) and the Group 1 kimberlites from Becker and le Roex (2006) (Figure 6.9). Although isotope studies were not undertaken in this study, Becker and le Roex (2006) and Smith (1983) have shown that Group 1 kimberlites in general and the Kimberley kimberlites in particular, have unradiogenic Sr and radiogenic Nd isotope ratios, similar to Depleted Mantle and OIB, and that their sources therefore likely contain an asthenospheric component. Consequently, based on the similarities between the Dutoitspan kimberlite primary magmas and that of the Kimberley kimberlites (le Roex *et al.*, 2003) and Group 1 kimberlites in general (Becker and le Roex, 2006), it is proposed that metasomatic fluids originating from an upwelling mantle plume (and currently located in the South Atlantic – e.g. le Roex, 1986) have

metasomatised the depleted mantle keel beneath Kimberley and led to enrichment in incompatible trace elements and volatile phases. Subsequent melting of the originally depleted, but subsequently re-enriched SCLM in the presence of H_2O and CO_2 (eg. Dalton and Presnall, 1998a), led to the formation of the Dutoitspan kimberlite.

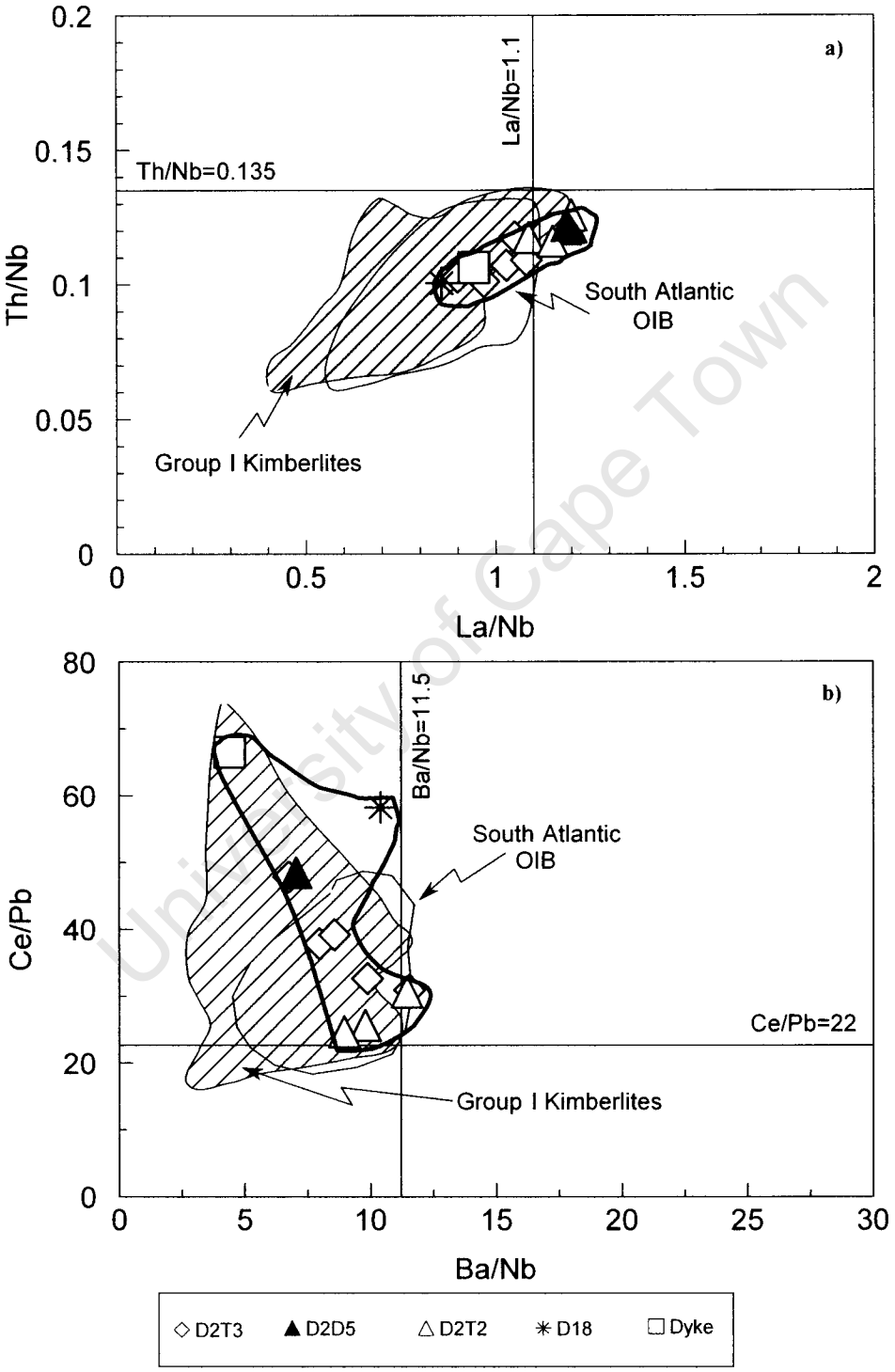

Figure 6.9. Variation of selected incompatible trace element ratios of the Dutoitspan kimberlitic intrusive phases after Becker & le Roex (2006). Field of South Atlantic ocean island basalts is from compilations of PetDB (www.petdb.ldeo.columbia.edu) after Becker & le Roex (2006). The diagonally shaded fields represent Group I kimberlite data from Becker & le Roex (2006).

7 SUMMARY AND CONCLUSIONS

7.1 Introduction

The Dutoitspan Group 1 kimberlite pipe forms part of the well-known cluster of pipes located in and around the city of Kimberley, South Africa. This cluster of pipes, which includes the De Beers, Kimberley, Wesselton and Bultfontein pipes, represents the type locality of kimberlite. A bulk sampling project of an area known as the Northwest Corner (NWC) on 760 m Level of the underground mine afforded the author an opportunity to study and sample eight distinctive intrusive phases, i.e. D2 Type 2, D2 Type 3, D2/D5, D5, D18, Type 5, D16 and the D16 dyke. The sampling tunnel was mapped in detail and samples were collected for petrographic and whole rock chemical analysis to firstly assess whether the various phases that are macroscopically distinct, also have different microscopic and geochemical compositions. Secondly, the aim of the study was to derive a close-to-primary kimberlite magma composition for the Dutoitspan kimberlite by evaluating and isolating the effects of late stage alteration, crustal contamination, peridotite entrainment and crystal fractionation. Subsequently, semi-quantitative models were developed to characterise the geochemistry of the source region and to assess the effect of variable degrees of melting and residual mineralogy on inferred source compositions. Finally, the evolution of the Dutoitspan kimberlite source region is investigated in relation to depletion and enrichment events, and its physical location.

7.2 Petrography

The various intrusive phases encountered during the NWC bulk sampling project have been described in detail based on macro- and microscopic observations of each of the thirty-five samples collected during this study. These descriptions are summarised below:

- *D2 Type 3* - macrocrystic opaque- and monticellite-rich hypabyssal kimberlite;
- *D2/D5* – aphanitic opaque- and monticellite-rich hypabyssal kimberlite;
- *D5* – macrocrystic monticellite- and phlogopite-rich hypabyssal kimberlite;
- *D2 Type 2* – macrocrystic altered monticellite kimberlite of the hypabyssal type;
- *D18* – macrocrystic diopside-bearing phlogopite-rich hypabyssal kimberlite;
- *Type 5* – segregationary textured phlogopite-bearing hypabyssal kimberlite;

- *D16* – macrocrystic diopside-bearing hypabyssal kimberlite;
- *D16 Dyke* – varies from an aphanitic to a macrocrystic hypabyssal kimberlite.

Olivine is the dominant macrocryst phase in the majority of samples but varies in modal proportions between 3 % and 40 % and in alteration from unaltered to highly serpentinised. Other macrocryst phases include opaque oxides and phlogopite. Olivine is also the dominant phenocryst phase and varies between 10 % and 30 % in abundance. Similar to the olivine macrocrysts, the phenocrysts are variably altered. The groundmass is often dominated by monticellite (maximum abundance: 30%). Opaque oxides, serpentine and carbonate are also major groundmass phases. Perovskite is relatively common in the majority of samples and amounts on average to 3 modal %. Accessory groundmass minerals include apatite, diopside and chlorite. A number of samples, specifically from the D5, D18, Type 5 and D16 intrusive phases, have an altered appearance with portions of their groundmass replaced by clay minerals. Crustal xenoliths are also more abundant in these samples. The xenoliths vary from highly altered in the D2 Type 2 and 3 intrusive phases to largely unaltered in the D16 intrusive phase and range in abundance from 3 to 45 vol. %.

7.3 Whole Rock Geochemistry

Major and trace element compositions of the various intrusive phases tend to cluster, indicating relatively clear geochemical differences between the intrusive phases. Across the various intrusive phases, compositions are variable (major elements: 21.0-37.9 wt % MgO, 26.3-41.2 wt % SiO_2, Mg# 0.86-0.91, 0.81–2.00 wt % TiO_2, 1.36-6.61 wt % Al_2O_3, 3.85-16.9 wt % CaO, 7.0-9.1 wt % FeO*, 0.73–3.65 wt % K_2O; trace element ratios: Zr/Nb 1.33 – 2.34, Nb/Ta 18.4 - 24.6). In terms of REE abundances, La/Sm_n ratios are restricted (4.9 - 5.8), but La/Yb_n ratios vary considerably (57 – 197) and indicate that all samples are highly enriched in LREE relative to HREE. The average whole rock composition of each intrusive phase is summarised in Table 7.1.

The whole rock compositions of the D16, D18, Type 5 and D5 intrusive phases are significantly influenced by crustal contamination, i.e. negatively correlated SiO_2 and MgO, a broadly positive correlation between P_2O_5 and MgO, high K_2O, and low FeO*. The D16 intrusive phase has the highest average C.I. (contamination index; >1.4), the highest average SiO_2 and the lowest average MgO abundances. In contrast, the aphanitic D2/D5 and the relatively uncontaminated macrocrystic D2 Type 3, D2 Type 2 and Dyke intrusive phases show a much lower C.I. (<1.0) and major element

compositions and correlations opposite to that of the crustally contaminated intrusive phases.

Table 7.1 Selected average major and trace element contents of analysed Dutoitspan intrusive phases.

	D2 Type 3	D2/D5	D2 Type 2	D5	D18	Type 5	D16	Dyke
Major Elements (wt %)								
SiO_2	31.1	28.5	30.9	33.9	32.9	35.5	38.9	26.7
TiO_2	2.70	2.61	1.79	4.66	4.29	4.53	6.00	2.32
Al_2O_3	1.47	1.78	1.13	1.06	1.30	1.34	1.29	1.78
Fe_2O_3	8.76	8.71	8.14	7.17	7.96	7.62	7.70	8.63
MgO	31.7	29.3	35.3	26.9	28.0	25.3	23.8	28.7
CaO	9.3	13.23	9.7	6.88	7.64	6.03	4.76	10.2
Na_2O	0.490	0.572	0.442	0.824	0.833	1.10	1.54	0.38
K_2O	1.87	1.41	0.87	3.56	3.32	2.92	2.60	1.02
Mg#	0.890	0.883	0.906	0.894	0.887	0.881	0.87	0.88
C.I.	0.934	0.964	0.880	1.05	1.01	1.22	1.45	0.941
Trace Elements (ppm)								
Cr**	1783	2103	2235	1487	1502	1472	1164	1595
Co	75.9	61.6	79.7	66.2	68.7	65.9	65.1	74.6
Ni**	1216	1082	1412	1102	1114	999	983	1027
Rb	95	64.4	53.9	153	125	105	128	60.1
Zr**	347	573	230	221	299	241	163	297
Nb**	185	262	128	117	142	129	85.7	163
Ba	1346	1336	1130	1735	1452	910	740	988
La	151	256	117	96.3	115	102	57.1	135
Hf	5.81	9.45	3.61	3.77	4.91	4.57	3.31	5.52
Th	16.2	25.9	12.7	11.2	13.8	11.1	7.42	14.5
Zr/Nb	1.88	2.20	1.79	1.90	2.12	1.86	1.91	1.82
Nb/Ta	24.0	22.7	24.6	21.1	20.0	18.5	18.5	19.0
La/Sm_n*	5.78	5.68	5.85	5.56	5.47	5.42	4.89	5.16
La/Yb_n*	167	180	197	135	122	110	57.2	128

LOI: loss on ignition; Mg#: atomic $Mg/(Mg+Fe^{2+})$ with $Fe_2O_3/FeO=0.15$; * - normalised to chondrite; ** - trace elements analysed by XRF, all other trace elements analysed by ICP-MS

The relatively high Mg-number and Ni, Co and Cr content of the D2 Type 2 are the result of the significant influence of olivine concentration. Primitive mantle-normalised patterns for the majority of samples in this study show strong negative K, Hf and Ti anomalies. These anomalies are more subdued in samples that show increased crustal dilution, eg. the D5, D18, Type 5 and D16 samples. The Pb, Sr and P contents are variable not only between the different intrusive phases but also between samples within a given intrusive phase. A positive Pb anomaly is common for the crustally contaminated intrusive phase samples. The patterns correlate relatively well with the Kimberley data (le Roex *et al.*, 2003).

As mentioned above, crustal contamination and late stage alteration had a significant effect on the major and trace element contents of some of the Dutoitspan intrusive phases. Approximately 60 % of the samples were therefore eliminated from the study based on the degree to which their whole rock compositions were affected by alteration or contamination. These include all samples from the Type 5, D5 and D16 intrusive phases and, with the exception of a single sample, all D18 samples.

The majority of Dutoitspan samples have been affected by mantle xenolith entrainment, i.e. increased MgO, SiO_2 and Ni abundances and dilution of REE and other incompatible trace element abundances. In contrast, no evidence of the effects of crystal fractionation was found. Following Becker & le Roex (2006), the intrusive phase compositions were corrected for peridotite entrainment by using an average Kimberley garnet lherzolite comprising ~68 % olivine, ~23 % orthopyroxene, ~3 % clinopyroxene, ~5 % garnet and <1 % phlogopite. The Dutoitspan samples, which contain 10 % - 25 % olivine macrocrysts, are therefore calculated to have entrained ~15 % - 35 % garnet lherzolite.

By correcting for peridotite entrainment, an average close-to-primary magma was calculated for each of the intrusive phases: D2 Type 3, D2 Type 2, D2/D5, D18 and the Dyke. The major element compositions of these close-to-primary magmas show a restricted but significant range: ~25-31 wt % SiO_2, ~27-36 wt % MgO, ~9-16 wt % CaO, ~1.2-4.3 wt % K_2O, ~0.6-2.6 wt % Al_2O_3 and Mg# ~0.85-0.90 with ~781-1376 ppm Ni and ~139-284 ppm La. These compositions fall well within the major element ranges of the Group 1 kimberlites of Becker and le Roex (2006), le Roex *et al.* (2003) and Harris *et al.* (2004).

7.4 Source Region Evolution

The calculated source compositions of the Dutoitspan close-to-primary magmas are depleted in HREE by factors of 0.43 to 0.97 relative to chondrite, and are enriched in LREE by factors of 10 to 21 relative to chondrite. The primitive mantle normalised REE content of the calculated source show, similar to the primary magmas, negative Rb, K, Sr, Hf and Ti anomalies that have been transferred from the source to the primary magma in the absence of any residual phases that may fractionate these elements. Following the arguments of e.g. Becker *et al.* (2006), le Roex *et al.* (2003) and Harris *et al.* (2004), these anomalies are assumed to be features intrinsic to the source of Group 1 kimberlite magmas. The calculated source region compositions of the Dutoitspan kimberlite intrusive phases fall within the field of Kaapvaal garnet lherzolite compositions from Grégoire *et al.* (2003).

The low HREE abundances, and the high Mg-# and high Ni content of the inferred primary magmas suggest derivation of the Dutoitspan primary magmas from a refractory source that had experienced a prior depletion event prior to metasomatic enrichment of the source. The incompatible element ratios of the Dutoitspan primary magmas and the isotope ratios of the Kimberley Group 1 kimberlites correlate well with

those of the South Atlantic ocean island basalts (OIB). It is therefore suggested that metasomatic fluids originating from an upwelling mantle plume that is located in the South Atlantic (e.g. le Roex, 1986) have metasomatised the depleted mantle keel beneath Kimberley and led to enrichment in incompatible trace elements and volatile phases. The primary magmas giving rise to the Dutoitspan kimberlite, formed by the melting of the originally depleted, but subsequently re-enriched SCLM in the presence of H_2O and CO_2 (e.g. Dalton and Presnall, 1998a).

8 ACKNOWLEDGEMENTS

I would like to thank my supervisor, Anton le Roex, for his expert guidance, support and patience.

My mentor, Jock Robey, is sincerely thanked for having enough faith in me to initiate the project and for being a great source of inspiration and enthusiasm. Special thanks to Johann Stiefenhofer for his reviews and support and patience, not only with the thesis but also at the office. Many thanks are due to Edson Machado and to other members of staff at Kimberley Mines, where my career in kimberlite geology started. The Survey Department of Kimberley Mines is thanked for their assistance with locality plans and survey data.

De Beers Group Services (Pty.) Ltd. is thanked for the funding of the project and financial support. Special thanks are due to present and past line managers for allowing me to take the much needed study leave.

Megan Coetzee and Nancy Coe are thanked for their assistance in an initially unknown environment. Thank you also to support staff at the University of Cape Town, especially Ernest Stout and Fayrooza Rawoort for their help with sample preparation and analyses.

My sincere gratitude to my parents for their love, support and encouragement. Thank you also to my brother and friends for your support and encouragement.

Last, but not least, thank you to Anton Opperman for his unconditional love, support and understanding.

9 REFERENCES

Allsopp, H. L. & Barrett, D. R. (1975). Rb-Sr age determinations on South African kimberlite pipes. *Physics and Chemistry of the Earth* **9**, 605-617.

Allsopp, H. L., Nicolaysen, L. O. & Hahn-Weinheimer, P. (1969). Rb/K ratios and Sr-isotopic compositions of minerals in eclogitic and peridotitic rocks. *Earth and Planetary Science Letters*, **5**, 23-44.

Anderson, D. L. (1984). Kimberlite and the evolution of the mantle. In: Kornprobst, J. (Ed) *Kimberlites and Related Rocks: Kimberlites 1*. Elsevier, Amsterdam, 395-403.

Bailey, D. K. (1993). Petrogenetic implications of the timing of alkaline, carbonatite and kimberlitic igneous activity in Africa. *South African Journal of Geology* **96**, 67-74.

Barrett, D. R. & Berg, G. W. (1975). Complementary petrographic and strontium-isotope ratio studies of South African kimberlite. *Physics and Chemistry of the Earth* **9**, 619-635.

Beard, A. D., Downes, H., Hegner, E., Sablukov, S. M., Vetrin, V. R. & Balogh, K. (1998). Mineralogy and geochemistry of Devonian ultramafic minor intrusions of the southern Kola Peninsula, Russia: Implications for the petrogenesis of kimberlites and melilitites. *Contributions to Mineralogy and Petrology* **130**, 288-303.

Beattie, P., Ford, C. & Russell, D. (1991). Partition coefficients for olivine-melt and orthopyroxene-melt systems. *Contributions to Mineralogy and Petrology* **109**, 212-224.

Becker, M. & le Roex, A.P. (2006). Geochemistry of South African On- and Off-craton, Group I and Group II: Petrogenesis and Source Region Evolution. *Journal of Petrology* **47**, 673-703.

Bell, D. R., Schmitz, M. D. & Janney, P. E. (2003). Mesozoic thermal evolution of the southern African mantle lithosphere. *Lithos* **71**, 273-288.

Berg, G. W. & Allsopp, H. L. (1972). Low $^{87}Sr/^{86}Sr$ ratios in fresh South African kimberlites. *Earth and Planetary Science Letters* **16**, 27-30.

Birch, G. F. (1981). The Karbonat Bombe: A precise, rapid and cheap instrument for determining calcium carbonate in sediments and rocks. *Transactions of the Geological Society of South Africa* **84**, 199-203.

Boyd, F. R. (1973). A pyroxene geotherm. *Geochimica et Cosmochimica Acta* **37**, 2533-2546.

Boyd, F. R. & Mertzman, S. A. (1987). Composition and structure of the Kaapvaal lithosphere, southern Africa. In: Mysen, B. O. (Ed) *Magmatic Processes: Physicochemical Principles*. Geochemical Society Special Publication, Pennsylvania, **1**, 13-24.

Brey, G. P. & Ryabchikov, I. D. (1994). Carbon dioxide in strongly silica undersaturated melts and origin of kimberlite magmas. *Neues Jahrbuch für Mineralogie Monatshefte* **10**, 449-463.

Canil, D. (2004). Mildly incompatible elements in peridotites and the origins of mantle lithosphere. *Lithos,* **77**, 375-393.

Canil, D. & Scarfe, C. M. (1990). Phase relations in peridotite + CO_2 systems to 12 GPa: Implications for the origin of kimberlite and carbonate stability in the Earth's upper mantle. *Journal of Geophysical Research* **95**, B10, 15805-15816.

Chazey III, W. J., Neal, C. R., Jain, J. C. & Kinman, W. S. (2003). A reappraisal of Rb, Y, Zr, Pb and Th value in geochemical reference material BHVO-1. *Geostandards Newsletter* **27**, 181-192.

Clement, C. R. & Skinner, E. M. W. (1979). A textural-genetic classification of kimberlitic rocks. *Kimberlite Symposium II*, Abstracts, 18-21.

Clement, C. R. (1982). *A comparative geological study of some major kimberlite pipes in the Northern Cape and Orange Free State*. Unpubl. PhD, University of Cape Town, 432pp.

Clement, C. R., Skinner, E. M. W. & Scott Smith, B. H. (1984). Kimberlite redefined. *Journal of Geology* **92**, 223-228.

Clement, C. R. & Skinner, E. M. W. (1985). A textural-genetic classification of kimberlites. *Transactions of the Geological Society of South Africa* **88**, 403-409.

Coe, N. J. (2004). *Petrogenesis of the Swartruggens and Star kimberlite dyke swarms, South Africa.* Unpubl. MSc, University of Cape Town, 146pp.

Coetzee, M. (2005). *Geochemistry of selected South African group I, group II and transitional kimberlites located on and off the Kaapvaal craton.* Unpubl. MSc, University of Cape Town, 161pp.

Crough, S. T., Morgan, W. J. & Hargraves, R. B. (1980). Kimberlites: Their relation to mantle hotspots. *Earth and Planetary Science Letters* **50**, 260-274.

Dalton, J. A. & Presnall, D. C. (1998a). The continuum of primary carbonatitic - kimberlitic melt compositions in equilibrium with lherzolite: Data from the system CaO-MgO-Al_2O_3-SiO_2-CO_2 at 6GPa. *Journal of Petrology* **39**, 1953-1964.

Dalton, J. A. & Presnall, D. C. (1998b). Carbonatitic melts along the solidus of model lherzolite in the system CaO-MgO-Al_2O_3-SiO_2-CO_2 from 3-7GPa. *Contributions to Mineralogy and Petrology* **131**, 123-135.

Dawson, J. B. (1971). Advances in kimberlite geology. *Earth Sciences Review* **7**, 187-214.

Dawson, J. B. & Hawthorne, J. B. (1973). Magmatic sedimentation and carbonatitic differentiation in kimberlite sills at Benfontein, South Africa. *Journal of Geological Society, London,* **129**, 61-85.

Dawson, J. B. (1980). *Kimberlites and their xenoliths.* Springer-Verlag, Berlin, 252pp.

Dawson, J. B. (2004). A fertile harzburgite-garnet lherzolite transition: possible inferences for the roles of strain and metasomatism in upper mantle peridotites. *Lithos*, **77**, 553-569.

de Wit, M. J., Roering, C., Hart, R. J., Armstrong, R. A., de Ronde, C. E. J., Green, R. W. E., Tredoux, M., Peberdy, E. & Hart, R. A. (1992). Formation of an Archean continent. *Nature* **357**, 553-562.

Douglass, J. & Schilling, J.-G. (1999). Plume-ridge interactions of the Discovery and Shona mantle plumes with the southern Mid-Atlantic Ridge (40^0-55^0S). *Journal of Geophysical Research* **104**, B2, 2941-2962.

Dowall, D. P., Pearson, D. G., Nowell, G. M., Kjarsgaard, B. A., Armstrong, J. & Horstwood, M. S. A. (2003). Comparative geochemistry of kimberlites from the Lac de Gras Field, NWT - An integrated isotopic and elemental study. *VIIIth International Kimberlite Conference*, Extended Abstracts.

Eccles, D. R., Heaman, L. M., Luth, R. W. & Creaser, R. A. (2004). Petrogenesis of the Late Cretaceous northern Alberta kimberlite province. *Lithos*, **76**, 435-459.

Edgar, A. D. & Charbonneau, H. E. (1993). Melting experiments on a SiO_2-poor, CaO-rich aphanitic kimberlite from 5-10GPa and their bearing on sources of kimberlite magmas. *American Mineralogist* **78**, 132-142.

Eggler, D. H. (1987). Solubility of major and trace elements in mantle metasomatic fluids: Experimental constraints. In: Menzies, M. A. & Hawkesworth, C. J. (Eds) *Mantle Metasomatism,* Academic Press, London, 21-41.

Eggler, D. H. & Wendlandt, R. F. (1979). Experimental studies on the relationship between kimberlite magmas and partial melting of peridotite. In: Boyd, F. R. & Meyer, H. O. A. (Eds) *Kimberlites, diatremes and diamonds: Their geology, petrology and geochemistry*, American Geophysical Union, Washington D.C., **1**, 300-330.

Erlank, A. J., Waters, F. J., Hawkesworth, C. J., Haggerty, S. E., Allsopp, H. L., Rickard, R. S. & Menzies, M. A. (1987). Evidence for mantle metasomatism in peridotite nodules from the Kimberley pipes, South Africa. In: Menzies, M. A. & Hawkesworth, C. J. (Eds) *Mantle Metasomatism,* Academic Press, London, 221-311.

Field, M., Gibson, J. G., Wilkes, T. A., Gababotse, J. & Khutjwe, P. (1997). The geology of the Orapa A/K1 kimberlite Botswana: further insight into the emplacement of kimberlite pipes. *Russian Geology and Geophysics,* **38**, 24-39.

Field, M. & Scott Smith, B. H. (1999). Contrasting geology and near-surface emplacement of kimberlite pipes in southern African and Canada. In: Gurney, J. J., Gurney, J. L., Pascoe, M. D. & Richardson, S. R. (Eds) *Proceedings of the VIIth International Kimberlite Conference*, Red Roof Design, Cape Town, **1**, 214-237.

Finnerty, A. A. & Boyd, F. R. (1987). Thermobarometry for garnet peridotite xenoliths: a basis for mantle stratigraphy. In: Nixon, P. H. (Ed) *Mantle Xenoliths*, John Wiley & Sons, New York, 381-402.

Foley, S. (1992). Petrological characterisation of the source components of potassic magmas: Geochemical and experimental constraints. *Lithos* **28**, 187-204.

Fraser, K. J., Hawkesworth, C. J., Erlank, A. J., Mitchell, R. H. & Scott-Smith, B. H. (1985-1986). Sr, Nd and Pb isotope and minor element geochemistry of lamproites and kimberlites. *Earth and Planetary Science Letters* **76**, 57-70.

Freund, F. (1984). Volume instabilities in the mantle as a possible source for kimberlite formation. In: Kornprobst, J. (Ed) *Kimberlites and Related Rocks: Kimberlites 1.* Elsevier, Amsterdam, 405-415.

Girnis, A. V., Brey, G. P. & Ryabchikov, I. D. (1995). Origin of group IA kimberlites: Fluid saturated melting experiments at 45-55kBar. *Earth and Planetary Science Letters* **134**, 283-296.

Govindaraju, K. (1994). Compilation of working values and sample description for 383 Geostandards. *Geostandards Newsletter*, **18**, 158pp.

Green, P. F. (1985). Comparison of zeta calibration baselines for fission track dating of apatite, zircon and sphene. Isotope Geoscience 58, 1–22.

Green, T. H. (1995). Significance of Nb/Ta as an indicator of geochemical processes in the crust-mantle system. *Chemical Geology* **120**, 347-359.

Greenough, J. D. (1988). Minor phases in the Earth's mantle: Evidence from trace and minor element patterns in primitive alkaline magmas. *Chemical Geology* **69**, 177-192.

Grégoire M., Bell, D. R. & le Roex, A. P. (2003). Garnet lherzolites from the Kaapvaal craton (South Africa): Trace element evidence for a metasomatic history. *Journal of Petrology* **44**, 629-657.

Griffin, W. L., Graham, S., O'Reilly, S. Y. & Pearson, N. J. (2004). Lithosphere evolution beneath the Kaapvaal Craton: Re-Os systematics of sulfides in mantle-derived peridotites. *Chemical Geology* **208**, 89-118.

Griffin, W. L., O'Reilly, S. Y., Natapov, L. M. & Ryan, C. G. (2003). The evolution of lithospheric mantle beneath the Kalahari Craton and its magmas. *Lithos,* **71**, 215-241.

Gudfinnsson, G. H. & Presnall, D. C. (2003). Continuous gradations among primary kimberlitic, carbonatitic, melilititic, and komatiitic melts in equilibrium with garnet lherzolite at 3-8GPa. *VIIIth International Kimberlite Conference*, Extended Abstracts.

Gurney, J. J. & Harte, B. (1980). Chemical variations in upper mantle nodules from southern African kimberlites. *Phil. Trans. R. Soc. Lond.* **A 297**, 273-303.

Haggerty, S. E. (1987). Metasomatic mineral titanates in upper mantle xenoliths. In: Nixon, P.H. (Ed) *Mantle Xenoliths,* John Wiley & Sons, New York, 671-690.

Haggerty, S. E. (1994). Superkimberlites: A geodynamic window to the Earth's core. *Earth and Planetary Science Letters* **122**, 57-69.

Hallam, C. D. (1967). Map of Northwest Corner. *Unpubl. Kimberley Mines, De Beers Consolidated Mines Ltd.*

Hanson, G. N. & Langmuir, C. H. (1978). Modelling of major elements in mantle-melt systems using trace element approaches. *Geochimica et Cosmochimica Acta* **42**, 725-741.

Harlow, G. E. & Davies, R. (2004). Status report on the stability of K-rich phases at mantle conditions. *Lithos* **77**, 647-653.

Harris, M., le Roex, A. P. & Class, C. (2004). Geochemistry of the Uintjiesberg kimberlite, South Africa: Petrogenesis of an off-craton, group I, kimberlite. *Lithos* **74**, 149-165.

Hart, S. R. & Brooks, C. (1977). The geochemistry and evolution of Early Precambrian mantle. *Contributions to Mineralogy and Petrology* **61**, 109-128.

Konzett, J., Armstrong, R. A., Sweeney, R. J. & Compston, W. (1998). The timing of MARID metasomatism in the Kaapvaal mantle: An ion probe study of zircons from MARID xenoliths. *Earth and Planetary Science Letters* **160**, 133-145.

Kopylova, M. G., Matveev, S. & Raudsepp, M. (2007). Searching for parental kimberlite melt. *Geochimica et Cosmochimica Acta* **71**, 3616-3629.

Kramers, J. D., Smith, C. B., Lock, N. P., Harmon, R. S. & Boyd, F. R. (1981). Can kimberlites be generated from an ordinary mantle? *Nature* **291**, 53-56.

La Tourette, T., Hervig, R. L. & Holloway, J. R. (1995). Trace element partitioning between amphibole, phlogopite, and basanite melt. *Earth and Planetary Science Letters* **135**, 13-30.

Lee, C.-T. & Rudnick, R. L. (1999). Compositionally stratified cratonic lithosphere: petrology and geochemistry of peridotite xenoliths from the Labait Volcano, Tanzania. In: Gurney, J. J., Gurney, J. L., Pascoe, M. D., Richardson, S. H. (Eds) *Proceedings of the VIIth International Kimberlite Conference*, Red Roof Design, Cape Town, **2**, 872-887.

le Roex, A. P. (1986). Geochemical correlation between southern African kimberlites and South Atlantic hotspots. *Nature* **324**, 243-245.

le Roex, A. P., Bell, D. R. & Davis, P. (2003). Petrogenesis of group I kimberlites from Kimberley, South Africa: evidence from bulk-rock geochemistry. *Journal of Petrology* **44**, 2261-2286.

le Roex, A. P., Dick, H. J. B. & Fisher, R. L. (1989). Petrology and geochemistry of MORB from 25^{0}E to 46^{0}E along the Southwest Indian Ridge: Evidence for contrasting styles of mantle enrichment. *Journal of Petrology* **30**, 947-986.

le Roex, A. P. & Lanyon, R. (1998). Isotope and trace element geochemistry of Cretaceous Damaraland lamprophyres and carbonatites, northwestern Namibia: Evidence for plume-lithosphere interactions. *Journal of Petrology* **39**, 1117-1146.

le Roex, A. P., Erlank, A. J. & Needham, H. D. (1981). Geochemical and mineralogical evidence for the occurrence of at least three distinctmagma types in the 'Famous' region. *Contributions to Mineralogy and Petrology* **77**, 24-37.

le Roux, P. J., le Roex, A. P., Schilling, J.-G., Shimizu, N., Perkins, W. W. & Pearce, N. J. G. (2002). Mantle heterogeneity beneath the southern Mid-Atlantic Ridge: trace element evidence for contamination of ambient lithospheric mantle. *Earth and Planetary Science Letters* **203**, 479-498.

Lewis, H. C. (1887). On a diamondiferous peridotite and the genesis of the diamond. *Geol. Mag.*, **3**, 22-24.

Lorenz, V. (1975). Formation of phreatomagmatic maar-diatreme volcanoes and its relevance to kimberlite diatremes. *Physics and Chemistry of the Earth* **9**, 17-27.

MacGregor, I. A. (1999). Petrologic and thermal structure of the upper mantle beneath South Africa in the Cretaceous. In: Gurney, J. J., Gurney, J. L., Pascoe, M. D., Richardson, S. H. (Eds) *Proceedings of the VIIth International Kimberlite Conference*, Red Roof Design, Cape Town, **2**, 872-887.

Maaloe, S. & Aoki, K. (1977). The major element composition of the upper mantle estimated from the composition of lherzolites. *Contributions to Mineralogy and Petrology* **63**, 161-173.

Mathias, M., Siebert, J. C. & Rickwood, P. C. (1970). Some aspects of the mineralogy and petrology of ultramafic xenoliths in kimberlite. *Contributions to Mineralogy and Petrology* **26**, 75-123.

McCandless, T. E. (1999). Kimberlites: Mantle expressions of deep-seated subduction. In: Gurney, J. J., Gurney, J. L., Pascoe, M. D., Richardson, S. H. (Eds) *Proceedings of the VIIth International Kimberlite Conference*, Red Roof Design, Cape Town, **2**, 545-549.

McDade, P., Blundy, J. D. & Wood, B. J. (2003). Trace element partitioning between mantle wedge peridotite and hydrous MgO-ric melt. *American Mineralogist*, **88**, 1825-1831.

McDonough, W. F. (1990). Constraints on the composition of the continental lithospheric mantle. *Earth and Planetary Science Letters* **101**, 1-18.

McKenna, N. (2001). *A study of the diamonds, diamond inclusion minerals and other mantle minerals from the Swartruggens kimberlite, South Africa*. Unpubl. MSc, University of Cape Town, 152pp.

McKenzie, D. & O'Nions, R. K. (1983). Mantle reservoirs and ocean island basalts. *Nature* **301**, 229-231.

Meibom, A. & Anderson, D. L. (2003). The statistical upper mantle assemblage. Earth and Planetary Science Letters, **217**, 123-139.

Menzies, M. A., Rogers, N., Tindle, A. & Hawkesworth, C. J. (1987). Metasomatic and enrichment processes in lithospheric peridotites, an effect of asthenosphere – lithosphere interaction. In: Menzies, M. A. & Hawkesworth, C. J. (Eds) *Mantle Metasomatism*, Academic Press, London, 365-313-361.

Mitchell, R. H. (1979). The alleged kimberlite-carbonatite relationship: additional contrary mineralogical evidence. *Am. Jour. Sci.* **279**, 570-589.

Mitchell, R. H. (1986). *Kimberlites: Mineralogy, geochemistry, and petrology*. Plenum Press, New York, 442pp.

Mitchell, R.H. (1994). Suggestions for revisions to the terminology of kimberlites and lamprophyres from a genetic viewpoint. In Proc. Fifth Int. Kimberlite Conf. **1**. Kimberlites and Related Rocks and Mantle Xenoliths (H.O.A. Meyer & O.H. Leonardos, eds.). *Companhia de Pesquisa de Recursos Minerais (Brasilia), Spec. Publ.* **1/A**, 15-26.

Mitchell R. H. (1995). *Kimberlites, orangeites, and related rocks*. Plenum Press, New York, 406pp.

Mitchell, R. H. (2004). Experimental studies at 5-12GPa of the Ondermatjie hypabyssal kimberlite. *Lithos* **76**, 551-564.

Mitchell, R. H. (2006). Potassic magmas derived from metasomatized lithospheric mantle: nomenclature and relevance to exploration for diamond-bearing rocks. *Journal Geological Society of India,* **67**, 317-327.

Mitchell, R. H. & Crocket, J. H. (1971). The isotopic composition of Sr in some South African kimberlites. *Contributions to Mineralogy and Petrology* **30**, 277-290.

Moore, R. O. & Gurney, J. J. (1985). Pyroxene solid solution in garnets included in diamond. *Nature* **318**, 553-555.

Naidoo, P., Stiefenhofer, J., Field, M. & Dobbe, R. (2004). Recent advances in the geology of Koffiefontein Mine, Free State Province, South Africa. *Lithos* **76**, 161-182.

Nelson, D. R., Chivas, A. R., Chappell, B. W. & McCullogh, M. T. (1988). Geochemical and isotopic systematics of carbonatites and implications for the evolution of ocean-island sources. *Geochimica et Cosmochimica Acta* **52**, 1-17.

Nisbet, E. G., Cheadle, M. J., Arndt, N. T. & Bickle, M. J. (1993). Constraining the potential temperature of the Archean mantle: A review of evidence from komatiites. *Lithos* **30**, 291-307.

Nowell, G. M., Pearson, D. G., Kempton, P. D., Noble, S. R. & Smith, C. B. (1999). Origins of kimberlites: A Hf isotope perspective. In: Gurney, J. J., Gurney, J. L., Pascoe, M. D., Richardson, S. H. (Eds) *Proceedings of the VIIth International Kimberlite Conference*, Red Roof Design, Cape Town, **2**, 616-624.

Nowell, G. M., Pearson, D. G., Bell, D. R., Carlson, R. W., Smith, C. B., Kempton, P. D. & Noble, S. R. (2004). Hf isotope systematics of kimberlites and their megacrysts: New constraints on their source regions. *Journal of Petrology* **45**, 1583-1612.

O'Brien, H. E. & Tyni, M. (1999). Mineralogy and geochemistry of kimberlites and related rocks from Finland. In: Gurney, J. J., Gurney, J. L., Pascoe, M. D., Richardson, S. H. (Eds) *Proceedings of the VIIth International Kimberlite Conference*, Red Roof Design, Cape Town, **2**, 625-636.

O'Connor, J. M. & le Roex, A. P. (1992). South Atlantic hot spot-plume systems: 1. Distribution of volcanism in time and space. *Earth and Planetary Science Letters,* **113**, 343-364.

O'Nions, R. K. & Pankhurst, R. J. (1974). Petrogenetic significance of isotope and trace element variations in volcanic rocks from the mid-Atlantic. *Journal of Petrology* **15**, 603-634.

Pearson, D. G., Rogers, N. W., Irving, A. J., Smith, C. B. & Hawkesworth, C. J. (1995). Source regions of kimberlites and lamproites: Constraints from Re-Os isotopes. *VIth International Kimberlite Conference*, Extended Abstracts, 430-432.

Pearson, D. G. & Nowell, G. M. (2002). The continental lithospheric mantle: characteristics and significance as a mantle reservoir. *Philosophical Transactions of the Royal Society of London* **A360**, 2383-2410.

Pearson, D. G., Nowell, G. M., Dowall, D. P., Kjarsgaard, B. A., Kopylova, M. G. & Armstrong, J. A. (2003). The relative roles of lithosphere and convecting mantle in kimberlites from the Slave Province, NWT: Constraints from Re-Os isotopes and olivine population studies. *VIIIth International Kimberlite Conference*, Extended Abstracts.

Phillips, D., Harris, J. W. & Viljoen, K. S. (2004). Mineral chemistry and thermobarometry of inclusions for De Beers pool diamonds, Kimberley, South Africa. *Lithos* **77**, 155-179.

Potts, P. J. (1987) *A handbook of silicate rock analysis*. Blackie Academic and Professional, Glasgow, 622pp.

Pretorius, W. & Barton, J.M., JR. (2003). Petrology and geochemistry of crustal and upper mantle xenoliths from the Venetia Diamond Mine – evidence for Archean crustal growth and subduction. *South African Journal of Geology*, **106**, 213-230.

Price, S. E., Russell, J. K. & Kopylova, M. G. (2000). Primitive magma from the Jericho pipe, N.W.T., Canada: Constraints on primary kimberlite melt chemistry. *Journal of Petrology* **41**, 789-808.

Rampone, E., Romairone, A. & Hofmann, A. W. (2004). Contrasting bulk and mineral chemistry in depleted mantle peridotites: evidence for reactive porous flow. *Earth and Planetary Science Letters*, **218**, 491-506.

Read, G., Grutter, H., Winter, S., Luckman, N., Gaunt, F. & Thomsen, F. (2004). Stratigraphic relations, kimberlite emplacement and lithospheric thermal evolution, Quiricó Basin, Minas Gerais State, Brazil. *Lithos*, **77**, 803-818.

Ringwood, A. E., Kesson, S. E., Hibberson, W. & Ware, N. (1992). Origin of kimberlites and related magmas. *Earth and Planetary Science Letters* **113**, 521-538.

Rogers, N. W., Hawkesworth, C. J. & Palacz, Z. A. (1992). Phlogopite in the generation of olivine melilitites from Namaqualand, South Africa and implications for element fractionation processes in the upper mantle. *Lithos* **28**, 347-365.

Rudnick, R. L., McDonough, W. F. & Chappell, B. W. (1993). Carbonatite metasomatism in the northern Tanzanian mantle: petrographic and geochemical characteristics. *Earth and Planetary Science Letters* **114**, 463-475.

Rudnick, R. L. & Fountain, D. M. (1995). Nature and composition of the continental crust: A lower crustal perspective. *Reviews of Geophysics* **33**, 267-309.

Sato, H. (1977). Nickel content of basaltic magmas: Identification of primary magmas and a measure of the degree of olivine fractionation. *Lithos* **10**, 113-120.

Sato, K., Katsura, T. & Ito, E. (1997). Phase relations in natural phlogopite with and without enstatite up to 8GPa: Implication for mantle metasomatism. *Earth and Planetary Science Letters* **146**, 511-526.

Scott, B. H. (1979). Petrogenesis of kimberlites and potassic lamprophyres from central West Greenland. In: Boyd, F. R. & Meyer, H. O. A. (Eds) *Kimberlites, diatremes and diamonds: Their geology, petrology and geochemistry*, American Geophysical Union, Washington D.C., **1**, 190-205.

Schérsten, A., Elliott, T., Hawkesworth, C. & Norman, M. (2004). Tungsten isotope evidence that mantle plumes contain no contribution from the Earth's core. *Nature* **427**, 234-237.

Schmidt, K. H., Bottazzi, P., Vannucci, R. & Mengel, K. (1999). Trace element partitioning between phlogopite, clinopyroxene and leucite lamproite melt. *Earth and Planetary Science Letters* **168**, 287-299.

Schmitz, M. D., Bowring, S. A., de Wit, M.J. & Gartz, V. (2004). Subduction and terrane collision stabilize the western Kaapvaal craton tectosphere 2.9 billion years ago. *Earth and Planetary Science Letters* **222**, 363-376.

Schulze, D. J. (1995). Low-Ca garnet harzburgites from Kimberley, South Africa: abundance and bearing on the structure and evolution of the lithosphere. *Journal of Geophysical Research*, **100**, 12 513-12 526.

Sharp, W. E. (1974). A plate tectonic origin for diamond-bearing kimberlites. *Earth and Planetary Science Letters* **21**, 351-354.

Shaw, D. M. (1970). Trace element fractionation during anatexis. *Geochimica et Cosmochimica Acta* **34**, 237-243.

Shee, S. R. (1985). *The petrogenesis of the Wesselton Mine kimberlites, Kimberley, Cape Province, R.S.A.* Unpubl. PhD, University of Cape Town, 220pp.

Simon, N. S. C., Irvine, G. J., Davies, G. R., Pearson, D. G. & Carlson, R. W. (2003). The origin of garnet and clinopyroxene in "depleted" Kaapvaal peridotites. *Lithos* **71**, 289-322.

Simonetti, A., Bell, K. & Shrady, C. (1997). Trace- and rare-earth-element geochemistry of the June 1993 natrocarbonatite lavas, Oldoinyo Lengai (Tanzania): Implications for the origin of carbonatite magmas. *Journal of Volcanology and Geothermal Research* **75**, 89-106.

Skinner, E. M. W. (1989). Contrasting group I and group II kimberlite petrology: Towards a genetic model for kimberlites. In: Ross, J. (Ed) *Kimberlites and Related Rocks: Their composition, occurrence, origin and emplacement*, Geological Society of Australia Special Publication, Perth, **14**, 528-544.

Skinner, E. M. W. & Clement, C. R. (1977). Mineralogical classification of South African kimberlites. *IInd International Kimberlite Conference*, Abstracts, Unpaginated.

Skinner, E. M. W. & Marsh, J. S. (2004). Distinct kimberlite classes with contrasting eruption processes. *Lithos* **76**, 183-200.

Smith, C. B. (1983). Pb, Sr, and Nd isotopic evidence for sources of southern African Cretaceous kimberlites. *Nature* **304**, 51-54.

Smith, C. B., Allsopp, H. L., Kramers, J. D., Hutchinson, G. & Roddick, J. C. (1985a). Emplacement ages of Jurassic-Cretaceous South African kimberlites by the Rb-Sr method on phlogopite and whole rock samples. *Transactions of the Geological Society of South Africa* **88**, 249-266.

Smith, C. B., Gurney, J. J., Skinner, E. M. W., Clement, C. R. & Ebrahim, N. (1985b). Geochemical character of Southern African kimberlites: A new approach based on isotopic constraints. *Transactions of the Geological Society of South Africa* **88**, 267-280.

Snowden, D. V. (1981). Mineralogy and petrology of two kimberlites at Dutoitspan Mine, Kimberley. *Unpubl. MSc, Rhodes University*, 113pp.

Solov'eva, L. V., Gornova, M. A., Egorov, K. N. & Smirnova, E. V. (2004). REE and HFSE distribution in rocks and minerals from granular peridotite xenoltihs in the Udachnaya Kimberlite Pipe. *Doklady Earth Sciences*, **395A**, 456-460.

Sparks, R. S. J., Baker, L., Brown, R. J., Field, M., Schumacher, J., Stripp, G. & Walters, A. (2006). Dynamical constraints on kimberlite volcanism. *Journal of Volcanology and Geothermal Research*, **155**, 18-48.

Späth, A., le Roex, A. P. & Opiyo-Akech, N. (2001). Plume-lithosphere interaction and the origin of continental rift-related alkaline volcanism - the Chyulu Hills Volcanic Province, Southern Kenya. *Journal of Petrology* **42**, 765-787.

Storey, B. C. (1995). The role of mantle plumes in continental breakup: Case histories from Gondwanaland. *Nature* **377**, 301-308.

Sun, S.-s. & McDonough, W. F. (1989). Chemical and isotopic systematics of oceanic basalts: implications for mantle composition and processes. In: Saunders, A. D. & Norry, M. J. (Eds) *Magmatism in the ocean basins*, Blackwell Scientific Publications, Oxford, 313-345.

Sweeney, R. J., Green, D. H. & Sie, S. H. (1992). Trace and minor element partitioning between garnet and amphibole and carbonatitic melt. *Earth and Planetary Science Letters* **113**, 1-14.

Sweeney, R. J. & Winter, F. (1999). Kimberlites as high-pressure melts: The determination of segregation depth from major element geochemistry. In: Gurney, J. J., Gurney, J. L., Pascoe, M. D., Richardson, S. H. (Eds) *Proceedings of the VIIth International Kimberlite Conference*, Red Roof Design, Cape Town, **2**, 846-851.

Tainton, K. M. & McKenzie, D. (1994). The generation of kimberlites, lamproites and their source rocks. *Journal of Petrology* **35**, 787-817.

Tankard, A. J., Jackson, M. P. A., Erikson, K. A., Hobday, D. K., Hunter, D. R. & Minter, W. E. L. (1982). *Crustal evolution of southern Africa: 3.8 billion years of earth history*. Springer-Verlag, New York, 523pp.

Taylor, W. R., Tompkins, L. A. & Haggerty, S. E. (1994). Comparative geochemistry of West African kimberlites: Evidence for a micaceous kimberlite end-member of sublithospheric origin. *Geochimica et Cosmochimica Acta* **58**, 4017-4037.

Tompkins, L. A., Meyer, S. P., Han, Z., Hu, S., Armstrong, R. & Taylor, W. R. (1999). Petrology and geochemistry of kimberlites from Shandong and Liaoning Provinces, China. In: Gurney, J. J., Gurney, J. L., Pascoe, M. D., Richardson, S. H. (Eds) *Proceedings of the VIIth International Kimberlite Conference*, Red Roof Design, Cape Town, **2**, 872-887.

Trofimov, V. S. (1978). Role of intermediate magma chambers in the formation of kimberlites and diamonds. *International Geology Review*, **22**, 490-496.

van Achterberg, E., Griffin, W. L. & Stiefenhofer, J. (2001). Metasomatism in mantle xenoliths from the Letlhakane kimberlites: estimation of element fluxes. *Contributions to Mineralogy & Petrology* **141**, 397-414.

Viljoen, K. S., Dobbe, R., Smit, B., Thomassot, E. & Cartigny, P. (2004). Petrology and geochemistry of a diamondiferous lherzolite from the Premier diamond mine, South Africa. *Lithos*, **77**, 539-552.

Viljoen, K. S., Phillips, D., Harris, J. W. & Robinson, D. N. (1999). Mineral inclusions in diamonds from the Venetia kimberlites, Northern Province, South Africa. In: Gurney, J. J., Gurney, J. L., Pascoe, M. D., Richardson, S. H. (Eds) *Proceedings of the VIIth International Kimberlite Conference*, Red Roof Design, Cape Town, **2**, 888-895.

Wagner, P. A. (1914). *The diamond fields of southern Africa*. The Transvaal Lieder, Johannesburg, 346pp.

Walker, R. J., Carlson, R. W., Shirey, S. B. & Boyd, F. R. (1989). Os, Sr, Nd and Pb isotope systematics of southern African peridotite xenoliths: Implications for the chemical evolution of subcontinental mantle. *Geochimica et Cosmochimica Acta* **53**, 1583-1595.

Walter, M. J. (1998). Melting of garnet peridotite and the origin of komatiite and depleted lithosphere. *Journal of Petrology* **39**, 29-60.

Wass, S. Y. & Rogers, N. W. (1980). Mantle metasomatism - precursor to continental alkaline volcanism. *Geochimica et Cosmochimica Acta* **44**, 1811-1823.

Waters, F. G. & Erlank, A. J. (1988). Assessment of the vertical extent and distribution of mantle metasomatism below Kimberley, South Africa. In: Menzies, M. A. & Cox, K. G. (Eds) *Oceanic and continental lithosphere: similarities and differences*, Clarendon Press, Oxford, 185-204.

Weaver, B. L. (1991). The origin of ocean island basalt end-member compositions: Trace element and isotopic constraints. *Earth and Planetary Science Letters* **104**, 381-397.

Wedepohl, K. H. & Muramatsu, Y. (1975). The chemical composition of kimberlites compared with the average composition of three basaltic magma types. In: Boyd, F. R. & Meyer, H. O. A. (Eds) *Kimberlites, diatremes and diamonds: Their geology, petrology and geochemistry*, American Geophysical Union, Washington D.C., **1**, 300-312.

Wendlandt, R. F. (1999). An experimental and theoretical analysis of partial melting in the system KAlSiO4-CaO-MgO-SiO2-CO2 and applications to the genesis of potassic magmas, carbonatites and kimberlites. In: Gurney, J. J., Gurney, J. L., Pascoe, M. D., Richardson, S. H. (Eds) *Proceedings of the VIIth International Kimberlite Conference*, Red Roof Design, Cape Town, **2**, 359-369.

Williams, H. M., Turner, S. P., Pearce, J. A., Kelley, S. P. & Harris, N. B. W. (2004). Nature and source regions for post-collisional, potassic magmas in southern and northern Tibet from geochemical variation and inverse trace element modelling. *Journal of Petrology* **45**, 555-607.

Willis, J. P. (1999). *Instrumental Parameters and data Quality for Routine Major and Trace Element Determinations by WDXRFS*. Cape Town: University of Cape Town.

Woolley, A. R., Bergman, S. C., Edgar, A. D., Le Bas, M. J., Mitchell, R. H., Rock, N. M. S. and Scott Smith, B. H. (1996). Classification of lamprophyres, lamproites, kimberlites, and the kalsilitic, melilitic, and leucitic rocks. *The Canadian Mineralogist* **34**, 175-186.

Wyllie, P. J. (1980). The origin of kimberlite. *Journal of Geophysical Research* **85**, B12, 6902-6910.

Wyllie, P. J. (1987). Discussion of recent papers on carbonated peridotite, bearing on mantle metasomatism and magmatism. *Earth and Planetary Science Letters* **82**, 391-397.

Wyllie, P. J. & Lee, W.-J. (1999). Kimberlites, carbonatites, peridotites and silicate-carbonate liquid immiscibility explained in parts of the system CaO-(Na_2O + K_2O)-(MgO + FeO)-(SiO_2 + Al_2O_3)-CO_2. In: Gurney, J.J., Gurney, J.L., Pascoe, M.D., & Richardson, S.H. (eds) *Proceedings of the VIIth International Kimberlite Conference*. Cape Town: Red Roof Design, 923-932.

Yutkina, E. V., Kononova, O. A., Bogatikov, A. P., Ovchinnikova, G. V. & Levsky, L. K. (2004). Kimberlites of Eastern Priazov'e (Ukraine) and geochemical characteristics of their sources. *Petrology*, **12**, 134-148.

Yutkina, E. V., Kononova, O. A., Kozar, N. A. & Knyaz'kov, A. P. (2003). Sr-Nd and geochemical compositions of the Eastern Azov Region, their age, and nature of the lithospheric source. *Doklady Earth Sciences*, **391**, 751-754.

APPENDIX A.

DETAILED PETROGRAPHIC ANALYSIS OF THE DUTOITSPAN INTRUSIVE KIMBERLITE PHASES

The various intrusive phases of the Dutoitspan kimberlite pipe are described below based on macro- and microscopic observations made during this study. Summaries of the sizes and abundances of the mineral constituents of the various samples are tabulated at the end of each section. Modal abundances were determined by visual estimation. This method is preferred over point counting based on the variability of the macrocrystic composition of kimberlites over a few centimetres (e.g. le Roex *et al.*, 2003). The textural-genetic classification system of Clement and Skinner (1985) is used to describe and classify the various samples (see discussion in Chapter 4).

A.1 D2 Type 3 (NWCD2T3-01P – 05P)

Macroscopic description:

Macroscopically the D2 Type 3 is a dark-grey, hard kimberlite with fresh to slightly altered olivine macrocrysts. It contains approximately 10-15% thermally altered, sub angular xenoliths which are possibly crustal in origin. It is magmatic in texture and massive in structure.

Microscopic descriptions (Plate A.1; Table A.1):

NWCD2T3-01P

This is a macrocrystic kimberlite that contains abundant olivine macro- and phenocrysts. The predominantly fresh macrocrysts are sub rounded and, in some cases, slightly elongated. They show undulose extinction and are therefore interpreted as xenocrysts from mantle peridotite xenoliths sampled by the kimberlite. The occurrence of recrystallised varieties suggests the presence of sheared peridotite xenoliths. One olivine and diopside fragment suggests that lherzolite mantle xenoliths were sampled. An olivine and spinel fragment also occurs. The phenocrysts in the size range 0.2 to 0.3 mm have been altered completely to serpentine, whilst fresh cores are preserved in the larger ones. Rare twins have been observed. Opaque oxides, predominantly spinel and possibly some ilmenite, are highly abundant in the matrix, and occur as necklaces around xenoliths and olivines. A few atoll spinels were observed. The bulk of the spinels however occur as aggregates, while others are euhedral to subhedral. Pools of carbonate and phlogopite laths are ubiquitous in the

matrix. Clay, chlorite and serpentine also occur in the matrix which has an orange-brown colour in some areas. Anhedral perovskite is abundant and forms necklaces around many of the olivines. Fresh monticellite is the major groundmass mineral. Euhedral to subhedral apatite, that poikilitically encloses earlier formed monticellite and spinel, is present in rare amounts in the matrix. The xenoliths are completely altered to clay, carbonate and opaque oxides. They are sub angular to sub rounded.

NWCD2T3-02P

This sample is very similar in appearance to the one described above. Variations in size distribution and abundance of the mineral constituents are given in Table A.1.

NWCD2T3-03P

Although very similar to the samples described above, serpentine and clay seems more abundant in NWCD2T3-03P and commonly occur in pools. Carbonate is less abundant in this sample compared to the two above. One of the xenoliths which has been completely carbonatised, seems to have a reaction halo surrounding it.

NWCD2T3-04P

Carbonate is notably more abundant than in any of the samples described above, and occurs both as veins and in pools. The olivine macrocrysts seem to have undergone slightly different alteration compared to the samples above – they seem slightly greenish in appearance, and their edges, as well as the large cracks towards their centres, are serpentinised. Another dissimilarity is that the smaller xenoliths are altered to carbonate and opaque oxides, while some of the larger ones are altered to carbonate and clay.

NWCD2T3-05P

This sample differs from NWCD2T3-01P and NWCD2T3-02P only in that the edges of some of the olivine macrocrysts have been altered to Fe-hydroxide, and a few altered phlogopite macrocrysts occur.

Summary

Based on petrographic observations the D2 Type 3 can be classified as a macrocrystic opaque- and monticellite-rich hypabyssal kimberlite.

Table A.1. Summary of sizes (mm) and abundances (%) of mineral constituents of D2 Type 3 samples.

	NWCD2T3-01P			NWCD2T3-02P			NWCD2T3-03P			NWCD2T3-04P			NWCD2T3-05P		
	Max (mm)	Avg (mm)	%	Max (mm)	Avg (mm)	%	Max (mm)	Avg (mm)	%	Max (mm)	Avg (mm)	%	Max (mm)	Avg (mm)	%
Ol macro	5.00	2.50	10	5.50	2.50	15	3.40	2.20	15	5.60	2.20	23	6.00	2.00	15
Ol pheno	1.50	0.80	30	1.40	0.60	25	2.00	0.50	20	1.40	0.50	15	2.40	0.70	25
Oxides	0.10	0.01	10	0.05	0.01	10	0.05	0.02	10	0.20	0.015	10	0.16	0.015	10
Phl	0.25	0.10	5	0.23	0.05	6	0.25	0.05	5	0.125	0.05	2	0.15	0.05	5
Pvk	0.09	0.05	2	0.10	0.05	3	0.12	0.05	2	0.14	0.06	3	0.09	0.04	2
Mont	-	0.015	21	-	0.02	19	-	0.02	20	-	0.02	10	-	0.02	20
Chl	-	-	3	-	-	3	-	-	-	-	-	-	-	-	-
Clay	-	-	2	-	-	3	-	-	5	-	-	5	-	-	3
Serp	-	-	1	-	-	2	-	-	5	-	-	10	-	-	5
Carb	-	-	6	-	-	5	-	-	3	-	-	15	-	-	5
Cpx	-	-	3	-	-	2	-	-	-	-	-	-	-	-	-
Apt	0.30	0.20	2	0.25	0.075	2	0.075	0.035	2			2		0.05	3
CRX	5.40	1.00	5	3.40	0.80	5	5.00	2.00	10	3.40	0.50	5	1.40	0.50	5

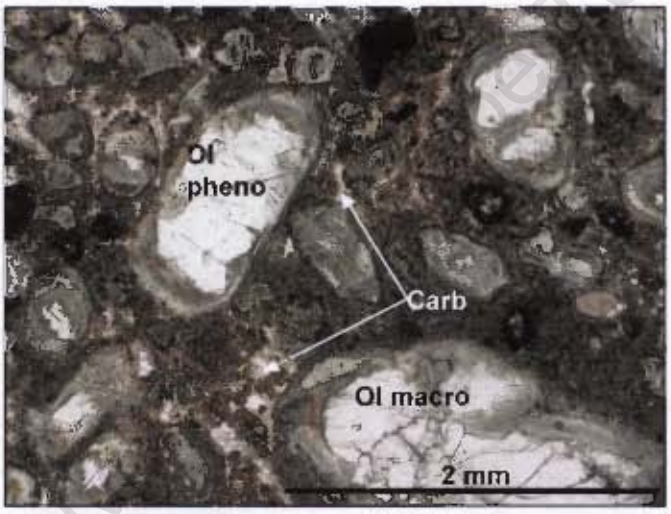

Plate A.1. Representative photomicrograph of D2 Type 3, which contains abundant olivine macro- and phenocrysts (Ol macro, Ol pheno). Pools of carbonate (carb) are ubiquitous in this monticellite- and spinel-rich matrix.

A.2 D2 Type 3 – D5 Contact zone (NWCD2D5-01P – 02P)

Macroscopic description:

The contact zone between the D2 Type 3 and the D5 contains alternating flow bands of black microporphyritic kimberlite and macrocrystic kimberlite which contain only very rare completely altered xenoliths. This is a very hard, magmatic, inequigranular kimberlite.

Microscopic descriptions (Table A.2):

NWCD2D5-01P

The thin section of NWCD2D5-01P is comprised of three areas due to flow banding. The centre area can be classified as a microporphyritic kimberlite. It contains very small olivine phenocrysts and approximately double the amount of oxides than the rest of the thin section (Plate A.2b).

The flow bands on either side of the microporphyritic portion contain on average larger olivine phenocrysts as well as a few olivine macrocrysts (Plate A.2a). All the olivines are fresh although some have slightly altered rims.

Perovskite is ubiquitous in the matrix and a large ilmenite macrocryst occurs. Abundant elongated crystals of apatite were observed in one of the flow bands on the side. Laths of phlogopite and abundant monticellite occur in the groundmass. The matrix comprises predominantly of serpentine and to a lesser extent carbonate. Furthermore both occur in pools and the carbonate occasionally as veins. Rare completely altered xenoliths make up the remainder of the thin section.

NWCD2D5-02P

The thin section of NWCD2D5-02P is similar in appearance to the flow bands occurring on the sides of the thin section discussed above.

Summary

Petrographically the contact zone can be classified as a microporphyritic opaque- and monticellite-rich hypabyssal kimberlite.

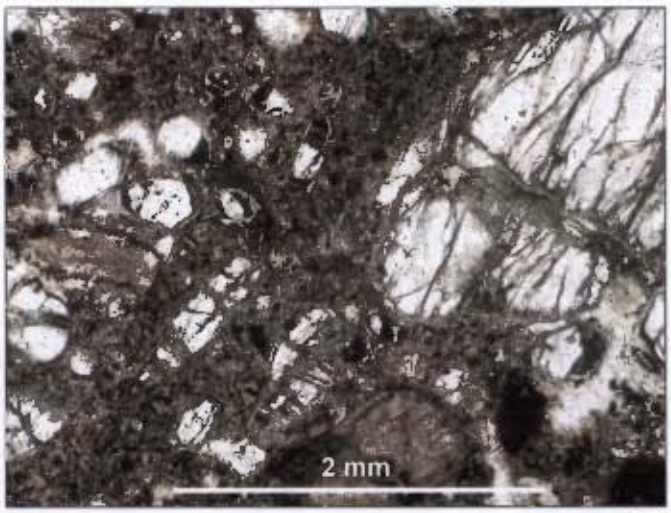

Plate A.2a. Photomicrograph of the macrocrystic flow band of sample NWCD2D5-01P, which is similar in appearance to the D2 Type 3.

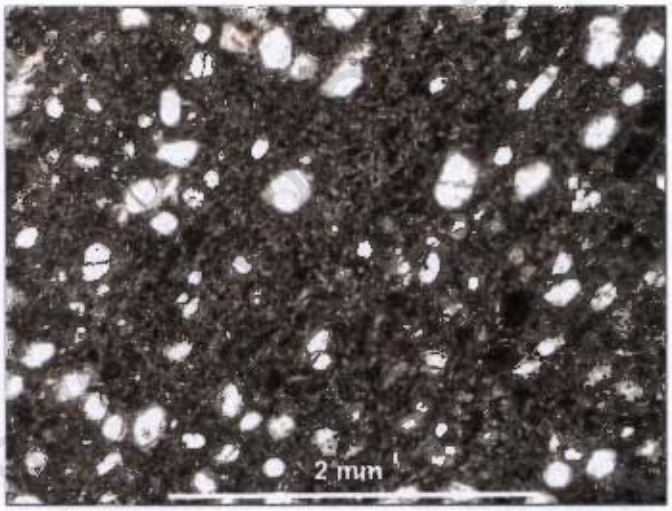

Plate A.2b. Photomicrograph of the aphanitic flow band of sample NWCD2D5-01P. Note the lack of olivine macrocrysts.

Table A.2. Summary of sizes (mm) and abundances (%) of mineral constituents of D2 Type 3 – D5 Contact zone samples.

	NWCD2D5-01P			NWCD2D5-02P		
	Max (mm)	Avg (mm)	%	Max (mm)	Avg (mm)	%
Ol macro	4.00	1.20	3	3.60	2.20	10
Ol pheno	0.80	0.40	25	1.20	0.40	15
Oxides	0.16	0.02	15	0.24	0.02	15
Phl macro	2.20	0.80	2	-	-	-
Phl	-	0.10	3	-	0.10	2
Pvk	0.18	0.08	3	0.12	0.05	2
Mont	-	0.02	28	-	0.02	30
Chl	-	-	-	-	-	-
Clay	-	-	-	-	-	-
Serp	-	-	5	-	-	5
Carb	-	-	10	-	-	5
Cpx		-	-	-	-	-
Apt	-	0.10	1	-	0.10	1
CRX	2.80	1.00	5	1.20	0.60	5

A.3 D5 (NWCD5-01P – 05P)

Macroscopic description:

The D5 has a dark, slightly pinkish to brownish grey colour and contains thermally or metasomatically altered xenoliths. Many of these xenoliths have a pinkish brown rim and some (possibly shale) are completely pinkish brown in colour. Others (possibly basement granite) have a greenish colour. The rock is competent but highly altered with moderate textural preservation. It is inequigranular and magmatic in texture.

Microscopic descriptions (Table A.3):

NWCD5-01P

The matrix of this rock is orange-brown in colour (Plate A.3). It contains abundant fairly fresh olivine macrocrysts with serpentinised rims. Similar to the D2 Type 3, they show undulose extinction and are therefore interpreted as xenocrysts from mantle peridotite xenoliths sampled by the kimberlite. The occurrence of recrystallised varieties suggests the presence of sheared peridotite xenoliths. The olivine phenocrysts are partly to completely serpentinised. A number of phlogopite macrocrysts that have been partly resorbed and are surrounded by secondary spinel, occur regularly throughout the matrix and are probably xenocrysts derived from MARID-type xenoliths. The matrix consists of clay (pectolite – radiating groups of acicular crystals), perovskite, laths of phlogopite phenocrysts, spinel, and apatite. Stubby prisms of diopside occur in pools in some areas of the matrix. A number of these diopsides are slightly elongated. Clay is the main base mineral phase, followed by serpentine and some carbonate.

The xenoliths have been completely altered to clay (pectolite) and carbonate with a few fresh phlogopites recognisable. They seem to be mostly surrounded by phlogopite and perovskite. A xenolith consisting almost entirely of phlogopite with some ilmenite, possibly a MARID (3.7mm), has been observed.

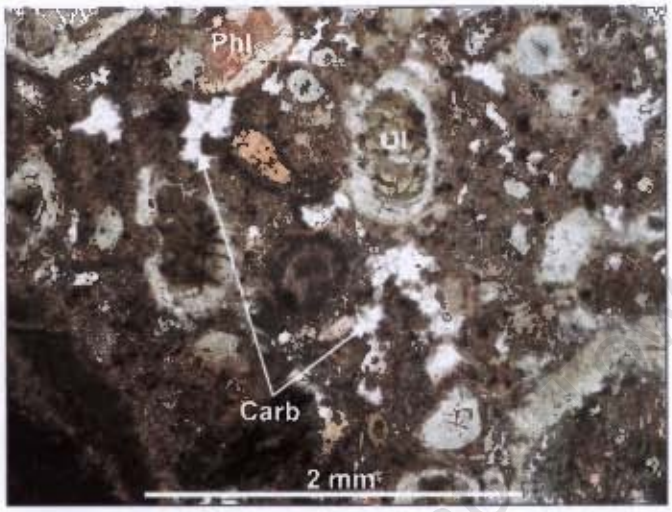

Plate A.3. Photomicrograph of sample NWCD5-01P, which is representative of the D5 facies. Olivine phenocrysts (Ol) are serpentinised to a large extent. Phlogopite macrocrysts (Phl) are common in the phlogopite-rich matrix. The abundance of carbonate appears to be higher in this view than is generally the case in the D5 facies.

NWCD5-02P

This sample is markedly more clay-rich than the sample described above. It contains slightly more carbonate but notably less serpentine.

NWCD5-03P

This sample contains less clay and monticellite but more pools of carbonate than both NWCD5-01P and 02P.

NWCD5-04P

This sample comprises less olivine macrocrysts but more carbonate than sample NWCD5-01P but is similar in all other aspects.

NWCD5-05P

Groundmass phlogopite is more abundant in this sample compared to those described above, whereas the number of xenoliths is slightly less.

Summary

Based on petrographic observations the D5 is classified as a macrocrystic monticellite- and phlogopite-rich hypabyssal kimberlite.

Table A.3. Summary of sizes (mm) and abundances (%) of mineral constituents of D5 samples.

	NWCD5-01P			NWCD5-02P			NWCD5-03P			NWCD5-04P			NWCD5-05P		
	Max (mm)	Avg (mm)	%	Max (mm)	Avg (mm)	%	Max (mm)	Avg (mm)	%	Max (mm)	Avg (mm)	%	Max (mm)	Avg (mm)	%
Ol macro	4.80	2.20	20	5.00	2.00	20	5.00	2.00	20	4.00	2.50	15	4.00	3.00	20
Ol pheno	3.60	0.60	15	1.20	0.60	15	1.00	0.60	15	1.40	0.70	15	2.2	0.7	15
Oxides	0.10	0.015	2	0.13	0.015	2	0.10	0.015	2	0.12	0.015	2	0.20	0.015	2
Phl macro	1.20	0.70	5	3.40	1.00	5	1.60	1.00	5	3.50	0.50	5	1.60	0.70	5
Phl	0.10	0.08	10	0.20	0.08	10	0.15	0.08	10	0.20	0.08	10	0.15	0.08	15
Pvk	0.16	0.06	3	0.15	0.06	3	0.12	0.06	3	0.125	0.07	3	0.10	0.07	3
Mont	-	0.02	10	-	0.02	10	-	0.005	5	-	0.005	10	-	0.005	5
Chl	-	-	-	-	-	-	-	-	-	-	-	-	-	-	-
Clay	-	-	15	-	-	20	-	-	13	-	-	15	-	-	15
Serp	-	-	5	-	-	<1	-	-	5	-	-	5	-	-	5
Carb	-	-	<1	-	-	2	-	-	5	-	-	3	-	-	1
Cpx	-	-	-	-	-	-	0.15	0.025	1	-	-	-	-	-	-
Apt	-	0.10	<1	-	-	-	0.08	0.05	1	-	0.06	<1	-	0.05	2
CRX	5.40	2.00	15	3.00	2.00	15	4.20	2.50	15	6.00	1.40	15	3.00	1.80	12

A.4 D2 Type 2 (NWCD2T2-01P – 05P)

Macroscopic description:

This is a dark grey to black macrocrystic kimberlite which seemingly contains no xenoliths. It is inequigranular and magmatic in texture. It is a very hard kimberlite with a massive structure.

Microscopic descriptions (Table A.4):

NWCD2T2-01P

The D2 Type 2 is a macrocrystic kimberlite that contains abundant anhedral to subhedral, fresh, rounded olivine macrocrysts that are sometimes partly altered to serpentine and chlorite. Similar to the D2 Type 3, a number of these macrocrysts have been recrystallised. Fresh olivine phenocrysts are also highly abundant. Some are slightly altered to serpentine. The most dominant groundmass minerals are euhedral to subhedral monticellite and spinel. The monticellite is fresh to totally altered. Many of the spinels are <0.003 mm. Perovskite occur quite commonly in matrix. Rare subangular to subrounded crustal xenoliths, which are completely altered, and fragments of garnet xenocrysts were observed as well. In many cases they are almost completely oxidised whilst some have been altered to clay. Rare phlogopite macrocrysts which have been completely resorbed were also found. Very few rounded ilmenite macrocrysts occur. The base minerals are irregular carbonate and serpentine.

In rare cases the carbonate occurs in aggregates. One possible autolith (1.3 mm) occurs in this sample. It looks similar to the surrounding kimberlite except that it contains fewer oxides and the olivines are more altered.

NWCD2T2-02P

This sample is very similar in appearance to the sample described above (Plate A.4a).

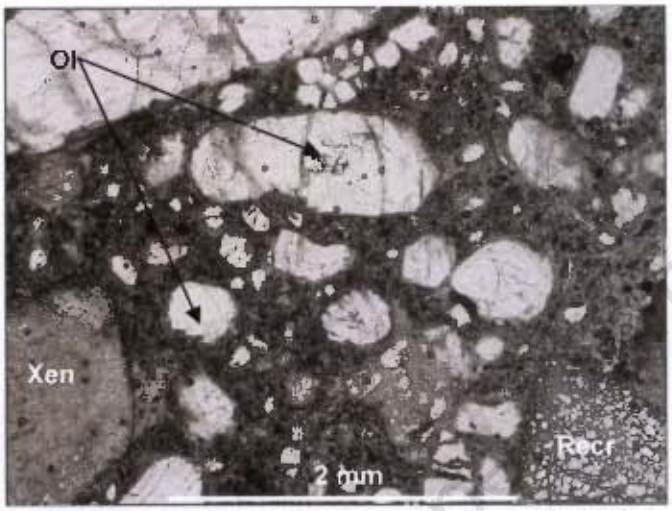

Plate A.4a. Photomicrograph of sample NWCD2T2-02P. Note the relative high abundance of olivine macro- and phenocrysts (Ol) set in a monticellite- and spinel-rich matrix. A recrystallised olivine macrocryst (Recr) is present in the bottom right corner, and one of the very rare xenoliths (Xen) in the bottom left corner.

NWCD2T2-03P

This sample is markedly more clay- and carbonate-rich than the previous two samples (Plate A.4b). Olivine phenocrysts are also more abundant in this sample, whereas the olivine macrocrysts, perovskite and opaque oxides are less abundant.

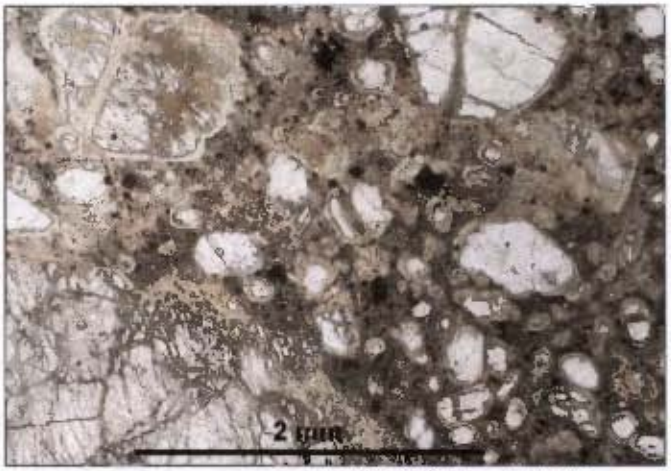

Plate A.4b. Photomicrograph of NWCD2T2-03P. This sample is markedly more clay-rich than that of NWCD2T2-02P above.

NWCD2T2-04P

This sample is similar to one described above, except that it contains slightly less olivine phenocrysts and clay, and slightly more monticellite and opaque oxides.

NWCD2T2-05P

This sample seems to be much more carbonate-rich and the olivines are slightly more altered and surrounded by a prominent concentration of oxides. The sample was collected very close to the contact with D18.

Summary

Petrographically this kimberlite is classified as a macrocrystic altered monticellite kimberlite of the hypabyssal type.

Table A.4. Summary of sizes (mm) and abundances (%) of mineral constituents of D2 Type 2 samples.

	NWCD2T2-01P			NWCD2T2-02P			NWCD2T2-03P			NWCD2T2-04P			NWCD2T2-05P		
	Max (mm)	Avg (mm)	%	Max (mm)	Avg (mm)	%	Max (mm)	Avg (mm)	%	Max (mm)	Avg (mm)	%	Max (mm)	Avg (mm)	%
Ol macro	5.20	3.00	25	5.00	3.00	25	5.60	2.80	20	5.50	3.50	20	5.00	3.00	25
Ol pheno	2.00	0.30	25	2.20	0.40	25	1.20	0.30	30	2.00	0.30	25	2.00	0.30	25
Oxides	0.20	0.02	15	0.20	0.02	15	0.20	0.02	10	0.30	0.02	13	0.30	0.02	15
Phl	0.50	0.25	2	0.50	0.20	2	0.10	0.25	1	1.00	0.10	2	0.25	0.10	2
Pvk	0.10	0.06	3	0.15	0.06	3	0.10	0.05	2	0.15	0.08	3	0.15	0.08	3
Mont	-	0.02	20	-	0.02	18	-	0.02	10	-	0.02	15	-	0.02	2
Chl	-	-	-	-	-	-	-	-	-	-	-	-	-	-	-
Clay	-	-	-	-	-	-	-	-	10	-	-	5	-	-	-
Serp	-	-	2	-	-	2	-	-	2	-	-	2	-	-	5
Carb	-	-	3	-	-	5	-	-	8	-	-	10	-	-	20
Cpx	-	-	-	-	-	-	-	-	-	-	-	-	-	-	-
Apt	-	-	-	-	-	-	-	-	-	-	-	-	-	-	-
CRX	3.00	1.00	5	3.40	1.20	5	2.40	0.80	4	3.50	1.00	5	-	0.80	3

A.5 D18 (NWCD18-01P – 05P)

Macroscopic description:

Macroscopically the D18 looks very similar to the D5 in that the xenoliths are thermally or metasomatically altered and the matrix, as well as the rims of the xenoliths, has a pinkish brown colour. Hallam (1967) has classified the D18, Type 4B and the D5, Type 4A, implying that there might be some relation between the two. The D18 is a competent rock that is inequigranular and non-fragmental in texture. Its structure is massive.

Microscopic descriptions (Table A.5):

These thin sections are similar in appearance to those of the D5 and are orange-brown to green in colour.

NWCD18-01P

This macrocrystic kimberlite breccia contains abundant anhedral to subhedral, slightly altered olivine macrocrysts. A number of these olivines have an orange colouration due to alteration. In rare instances the olivine macrocrysts have been recrystallised. Slightly altered phlogopite macrocrysts occur regularly throughout the matrix. Some of these phlogopites are kink banded. The olivine phenocrysts are euhedral to subhedral in shape and are partly to completely altered to serpentine. Euhedral to subhedral perovskite and spinel are common in the matrix and ilmenite also occurs. The matrix is very rich in groundmass phlogopite. Rare apatite and diopside were observed in thin sections made of the D18 in a previous study by the author. Carbonate is the most abundant base mineral and sometimes occurs as segregationary pools. Serpentine and clay is also common in the greenish matrix. The subrounded to subangular xenoliths are mostly completely altered to carbonate and phlogopite and seem to be of crustal origin. Only dolerites are recognisable.

NWCD18-02P

This sample is very similar in appearance to the sample described above except that it contains fewer olivine and phlogopite macrocrysts and more monticellite (Plate A.5). The olivine macrocrysts are more altered.

NWCD18-03P

This sample contains markedly more groundmass phlogopite and monticellite, and less clay, serpentine and carbonate than both samples NWCD18-01P and 02P. The majority of the olivine macrocrysts have been completely serpentinised. A relatively large amphibolite crustal xenolith (8mm) is present.

NWCD18-04P

Notably less olivine macrocrysts and more xenoliths occur in this sample compared to those described above.

NWCD18-05P

Olivine phenocrysts and opaque oxides are notably more abundant in this sample compared to the remainder of the D18 samples. The olivine macrocrysts are relatively fresh, similar to those of sample NWCD18-01P. As in the previous two samples, only amphibolite is recognised as part of the xenolith suite. This sample contains an autolith that is aphanitic in texture – its border is only defined by a rim of opaque oxides and it consists of abundant olivine phenocrysts and opaque oxides.

Summary

Petrographically the D18 is classified as a macrocrystic diopside-bearing phlogopite-rich hypabyssal kimberlite.

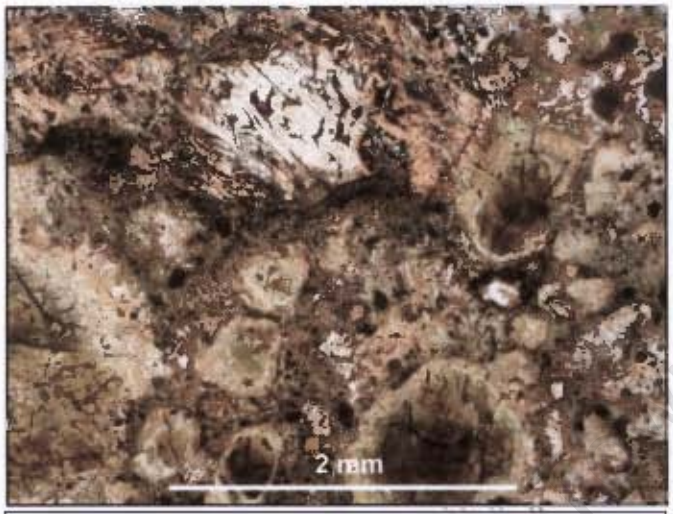

Plate A.5. Photomicrograph of sample NWCD18-02P. The olivine macro- and phenocrysts are completely altered to serpentine. A relatively large altered phlogopite macrocryst is present towards the top of this view. Similar to the D5 the matrix is phlogopite–rich.

Table A.5. Summary of sizes (mm) and abundances (%) of mineral constituents of D18 samples.

	NWCD18-01P			NWCD18-02P			NWCD18-03P			NWCD18-04P			NWCD18-05P		
	Max (mm)	Avg (mm)	%	Max (mm)	Avg (mm)	%	Max (mm)	Avg (mm)	%	Max (mm)	Avg (mm)	%	Max (mm)	Avg (mm)	%
Ol macro	4.80	2.80	15	6.30	2.50	10	4.00	2.50	15	2.60	1.50	5	4.20	2.50	10
Ol pheno	1.90	0.50	15	1.40	0.60	15	1.40	0.50	10	1.30	0.50	15	1.70	0.50	18
Oxides	0.15	0.015	2	-	0.015	2	0.04	0.015	2	0.22	0.02	2	0.10	0.03	4
Phl macro	2.50	1.20	12	3.20	2.00	5	1.50	1.00	5	4.70	1.50	15	2.80	1.50	10
Phl	-	0.04	8	-	0.20	15	-	0.20	20	-	0.20	12	-	0.20	10
Pvk	0.20	0.08	3	0.16	0.06	3	0.08	0.05	3	0.20	0.07	3	0.20	0.07	3
Mont	-	-	5	-	-	10	-	-	25	-	-	10	-	-	8
Chl	-	-	-	-	-	-	-	-	-	-	-	-	-	-	-
Clay	-	-	10	-	-	10	-	-	3	-	-	8	-	-	6
Serp	-	-	5	-	-	5	-	-	3	-	-	3	-	-	5
Carb	-	-	15	-	-	15	-	-	3	-	-	6	-	-	10
Cpx	-	-	-	-	-	-	-	-	-	-	-	-	-	-	-
Apt	-	0.05	<1	-	0.04	<1	0.20	0.04	1	-	0.05	<1	-	0.05	1
CRX	3.20	1.50	10	4.50	3.00	10	8.00	2.50	10	12.00	2.00	20	7.20	2.50	15

A.6 Type 5 (NWCT5-01P – 05P)

Macroscopic description:

This is a purplish to dark grey kimberlite breccia with partly to highly altered olivine macrocrysts which exhibit a golden colour in most instances. The xenoliths are partly to completely altered and seem to have reacted chemically with the matrix as the area surrounding these xenoliths are disrupted and usually has a lighter colour than the remainder of the matrix. One of the samples however is darker grey in colour and unlike the remaining samples is not segregationary textured in appearance.

Microscopic descriptions (Table A.6):

NWCT5-01P

This macrocrystic kimberlite breccia is segregationary-textured with abundant pools of carbonate and some serpentine. The matrix is clay rich and contains diopside as well as some apatite. Perovskite is common in the matrix and opaque oxides occur as well. The abundant olivine macro- and phenocrysts are almost completely altered to serpentine and are yellowish-green to dark yellow in colour. Rare twinned phenocrysts were observed. Slightly altered phlogopite macrocrysts are common in the matrix. Some of these are kink-banded. The xenoliths are partly to completely altered and are comprised of shale and amphibolite. A large amphibolite constitutes approximately 60% of this thin section. For comparison this amphibolite was not taken into account in modal abundance calculations in Table A.6 below.

NWCT5-02P

Notably less carbonate occur in this sample compared to the sample described above. In other aspects the two samples are very similar in appearance.

NWCT5-03P

The olivine macrocrysts in this sample are relatively fresh and have serpentinised rims. The olivine phenocrysts show reversed alteration with serpentinised cores and fresh rims. Opaque oxides, carbonate and clay are notably more abundant compared to the previous two samples. Relatively few xenoliths occur and monticellite is also less abundant.

NWCT5-04P

This sample is very similar to the one above except that it contains abundant xenoliths and the olivines are highly serpentinised.

NWCT5-05P

In this sample the olivine macrocrysts and phenocrysts are similar in abundance (Plate A.6).

Summary

Based on petrographic observations the Type 5 samples are classified as a segregationary textured phlogopite-bearing hypabyssal kimberlite.

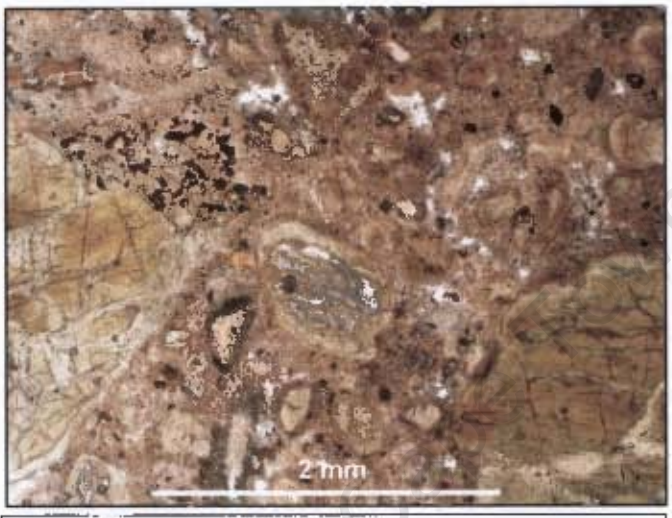

Plate A.6. Photomicrograph of sample NWCT5-05P. Note the segregationary texture of this sample, which is characteristic of the Type 5

Table A.6. Summary of sizes (mm) and abundances (%) of mineral constituents of Type 5 samples.

	NWCT5-01P			NWCT5-02P			NWCT5-03P			NWCT5-04P			NWCT5-05P		
	Max (mm)	Avg (mm)	%	Max (mm)	Avg (mm)	%	Max (mm)	Avg (mm)	%	Max (mm)	Avg (mm)	%	Max (mm)	Avg (mm)	%
Ol macro	2.00	1.40	15	2.00	1.20	8	5.50	2.00	15	5.00	2.50	10	4.20	2.00	15
Ol pheno	3.00	0.50	20	1.40	0.60	15	2.00	0.60	25	3.60	0.50	20	1.40	0.50	15
Oxides	0.05	0.01	1	0.10	0.015	1	0.10	0.015	10	0.32	0.02	6	0.50	0.02	3
Phl macro	1.00	0.5	10	1.80	0.70	5	3.80	0.70	4	2.60	0.60	3	3.20	0.50	3
Phl	-	-	3	-	-	3	-	-	3	-	-	2	-	-	5
Pvk	0.14	0.07	3	0.30	0.08	2	0.15	0.08	4	0.20	0.10	3	0.16	0.08	3
Mont	-	0.005	23	-	0.005	18	-	0.005	2	-	0.005	1	-	0.005	8
Chl	-	-	-		-	-		-	-	-	-	-	-	-	-
Clay	-	-	5	-	-	3	-	-	10	-	-	5	-	-	10
Serp			-			2		-	4	-	-	3	-	-	5
Carb	-	-	12	-	-	2	-	-	17	-	-	15	-	-	10
Cpx	-	0.01	1	-	0.01	1	-	0.01	1	-	0.03	1	-	0.03	1
Apt	0.175	0.03	2	0.2	0.03	1	-	0.03	1	-	0.03	<1	-	0.03	2
CRX	2.00	1.00	5	8.00	1.00	39	1.80	0.80	4	9.80	1.50	30	4.20	2.00	20

A.7 D16 (NWCD16-01P – 06P)

Macroscopic description:

All of the hand specimens of the D16 collected for this study look similar to those of the Type 5 except that the matrix seem to be slightly lighter grey in colour. Underground the D16 mostly lacked the purplish colour typical of the Type 5 and characteristically contained abundant angular white, carbonatised country rock fragments and many of the olivines were black in colour.

Microscopic descriptions (Table A.7):

NWCD16-01P

Microscopically the D16 looks similar to the Type 5 in that the olivines are also dark yellow in colour and its texture is segregationary to globular segregationary (Plate A.7a). Again the xenoliths are partly to completely altered. The shales show zonal alteration and are carbonatised in some instances, while the dolerites and amphibolites are relatively fresh. Spinel and perovskite do occur in the matrix but in lesser amounts than in Type 5. Microlitic diopside occur on the rims of the xenoliths and olivines as well as in the matrix. Serpentine is the main base mineral whilst carbonate is less abundant. This sample contains abundant altered xenoliths of sedimentary origin, and lesser amounts of amphibolite.

NWCD16-02P

Olivine macrocrysts are highly abundant in this sample and it contains notably less country rock xenoliths and clay than sample NWCD16-01P above.

NWCD16-03P

Opaque oxide minerals and perovskite are more abundant in this sample compared with the first two samples of the D16 discussed above. The sample contains slightly more olivine macrocrysts than phenocrysts.

NWCD16-04P

Olivine macrocrysts and phenocrysts are similar in abundance in this sample and it contains similar amounts of clay to sample NWCD16-01P. In contrast to the D16 samples discussed up to this point, rare apatite was observed in this sample.

NWCD16-05P

This sample is similar in appearance to sample NWCD16-02P, however the olivines are highly altered (Plate A.7b). Opaque minerals are slightly higher in abundance and

the microlitic diopside are coarser grained in comparison with the remainder of the D16 samples. The country rock xenoliths are highly altered.

NWCD16-06P

Similar to samples NWCD16-01P and -04P, this sample has a high clay content. A large country rock xenolith is present and the estimated mineral abundances may therefore be skewed.

Summary

The D16 samples bear characteristics of both volcaniclastic and hypabyssal kimberlite and are therefore classified as diopside-bearing transitional kimberlite.

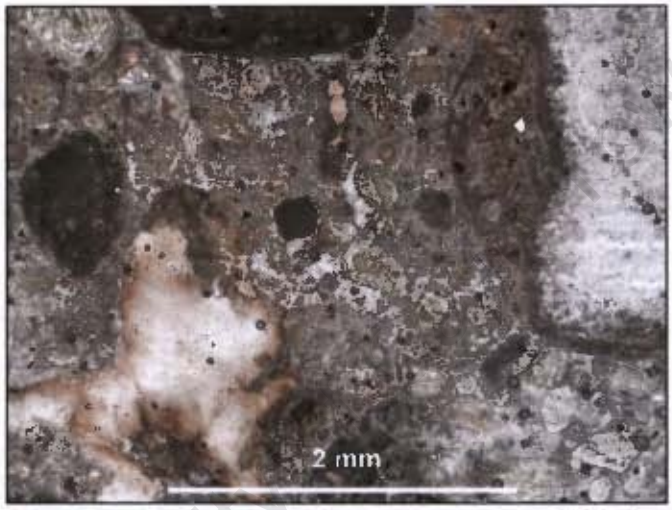

Plate A.7a. Photomicrograph of sample NWCD16-01P. The matrix of this sample consists primarily of serpentine (clear areas between clasts) and clay.

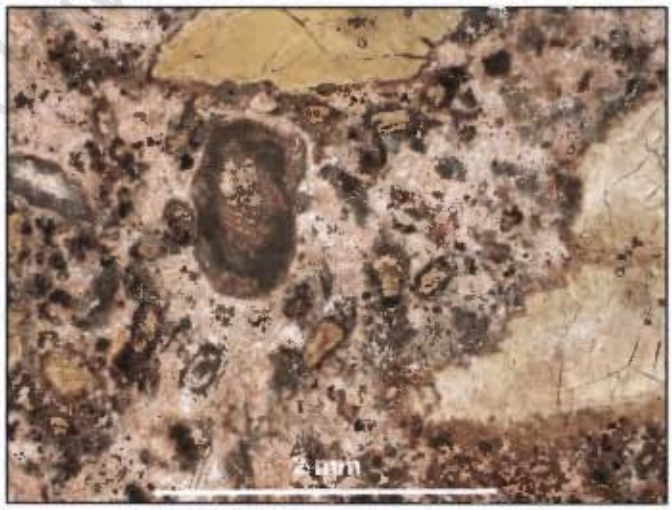

Plate A.7b. Photomicrograph of sample NWCD16-05P. The olivine macro- and phenocrysts are serpentine and clay-altered. Opaque minerals are higher in abundance in this sample relative to the other D16 samples.

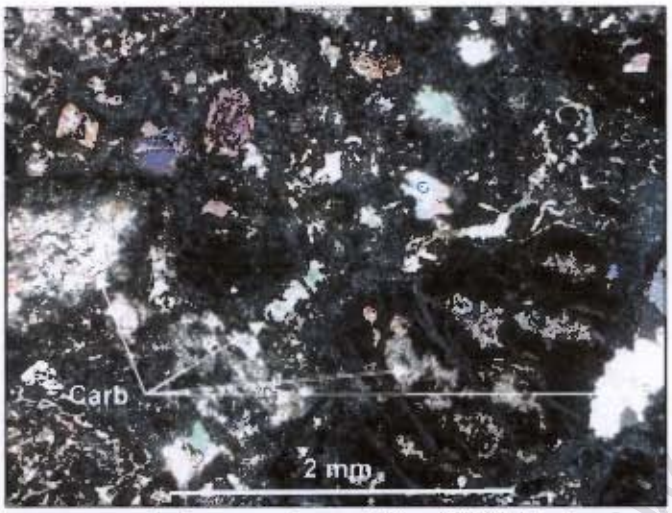

Plate A.8c. Photomicrograph of sample NWCD16DYKE-02P under crossed polars (same view as Plate A.8b). This sample has been carbonatised to a large extent (Carb) and isotropic pools of serpentine are ubiquitous as seen here

Table A.8. Summary of sizes (mm) and abundances (%) of mineral constituents of D16 Dyke samples.

	NWCD16DYKE-01P			NWCD16DYKE-02P		
	Max (mm)	Avg (mm)	%	Max (mm)	Avg (mm)	%
Ol macro	4.20	2.50	24	3.20	2.00	10
Ol pheno	1.60	0.50	30	1.00	0.40	15
Oxides	0.60	0.04	14	0.08	0.03	5
Phl	-	-	<1	1.4	-	2
Pvk	0.12	0.08	3	0.20	0.08	3
Mont	-	0.03	20	-	-	-
Chl	-	-	-	-	-	-
Clay	-	-	<1		-	-
Serp	-	-	2		-	-
Carb	-	-	4			10
Cpx	-	-	-	-	0.15	5
Apt	-	-	<1	-	-	-
CRX	1.60	1.00	3	19.00	0.50	45

APPENDIX B.

SAMPLE PREPARATION AND ANALYTICAL TECHNIQUES

B.1 Electron Microprobe Analysis

The CAMECA Camebax 4 channel electron microprobe of the Department of Geological Sciences at the University of Cape Town (UCT) was used to determine the mineral major element compositions listed in Chapter 5. A beam current of 15nA and an accelerating voltage of 15kV were used. X-ray emissions from the major elements were detected by using TLAP (Na, Mg, Si, Al), LiF (200) (Fe, Ni) and PET (Ca, Ti, K, Cr) analysing crystals. In all cases, ten second counting times were used at peak and background positions, except Ni, for which the counting time was increased to thirty seconds. Online data reduction was performed according to the PAP method.

B.2 X-Ray Fluorescence (XRF) Spectrometry

Major, minor and selected trace element concentrations were determined by using a Philips X'Unique wavelength dispersive spectrometer at the Department of Geological Sciences, UCT. Fusion discs were prepared for major element analysis and pressed powder briquettes for trace element analysis. The following sample preparation procedure was followed prior to analysis:

- The exact weight of ~2g of powdered sample placed into porcelain crucibles were recorded;
- These crucibles were left to dry overnight in an oven at ~110°C and weighed the following morning to determine the H_2O^- weight percentage present in each sample;
- To determine the lost on ignition (LOI) weight percentage in each sample, the samples were roasted at ~850°C and weighed again;
- For the preparation of fusion discs in the Pt-Au crucibles of the Claisse fluxy, 0.7g of roasted sample and 6g of a $Li_2B_4O_7$ and $LiBO_2$ flux were mixed;
- 6g of the powdered samples were pressed into briquettes using boric acid as a backing under a 10t press;
- Samples were subsequently stored in a desiccator prior to analysis.

A Mo-Sc X-ray tube was used for major element analysis. To determine the concentrations of Zn, Cu, Ni, Co, Cr and V, an Au tube was used, whereas a Rh tube was used to determine the concentrations of Nb, Zr, Y, Sr, Rb and U. Analytical errors

Table B.3.1 Average of analyses (n=6) of total procedural blanks (ppm).

	TPB
Sc	0.1264
V	0.0486
Cr	0.1626
Co	0.0074
Ni	0.0699
Cu	0.0637
Rb	0.0076
Sr	0.0651
Y	0.0045
Zr	0.1232
Nb	0.0080
Cs	0.0018
Ba	0.0625
La	0.0046
Ce	0.0090
Pr	0.0010

	TPB
Nd	0.0036
Sm	0.0006
Eu	0.0003
Gd	0.0007
Tb	0.0002
Dy	0.0009
Ho	0.0002
Er	0.0005
Tm	0.0001
Yb	0.0006
Lu	0.0002
Hf	0.0033
Ta	0.0073
Pb	0.2639
Th	0.0006
U	0.0004

Table B.3.2 Average of analyses (n=6) of the international standard BHVO-1 (ppm).

	Average	%RSD
Sc	32.3	2.8650
V	310	3.7144
Cr	275	3.1401
Co	45.6	1.8993
Ni	119	2.0466
Cu	145	2.3958
Rb	9.33	2.3755
Sr	398	2.1955
Y	24.5	1.6495
Zr	177	1.2372
Nb	18.5	1.1528
Cs	0.10	2.7021
Ba	131	1.1149
La	14.5	1.3371
Ce	37.4	1.4724
Pr	5.04	1.5460

	Average	%RSD
Nd	24.4	1.6625
Sm	5.75	1.4100
Eu	1.92	1.0440
Gd	5.94	1.2501
Tb	0.84	1.3864
Dy	5.02	1.3612
Ho	0.91	0.9100
Er	2.35	1.1197
Tm	0.30	1.3302
Yb	1.86	1.0049
Lu	0.25	1.5213
Hf	4.01	1.0870
Ta	1.10	0.8914
Pb	2.29	1.1060
Th	1.20	1.6870
U	0.42	1.9930

Certain trace elements were analysed by both XRF and ICP-MS. Although the results from the two methods compared well, the ICP-MS data was used for the majority of trace elements and only in the case of Nb, Zr, Cr and Ni were the XRF analyses preferred. The XRF results were on average 12.7%, 12.5%, 14.5% and 5.0% higher than those obtained from ICP-MS analyses for the respective elements. This difference may be ascribed to incomplete dissolution during the sample preparation for ICP-MS analyses, i.e. minerals such as ilmenite, chromite and zircon may not dissolve completely using standard HF/HNO_3 dissolution procedures, particularly in kimberlites (e.g. Potts, 1987). Comparisons of the results of the 4 elements obtained from the two methods are shown in Figure B.3.1.

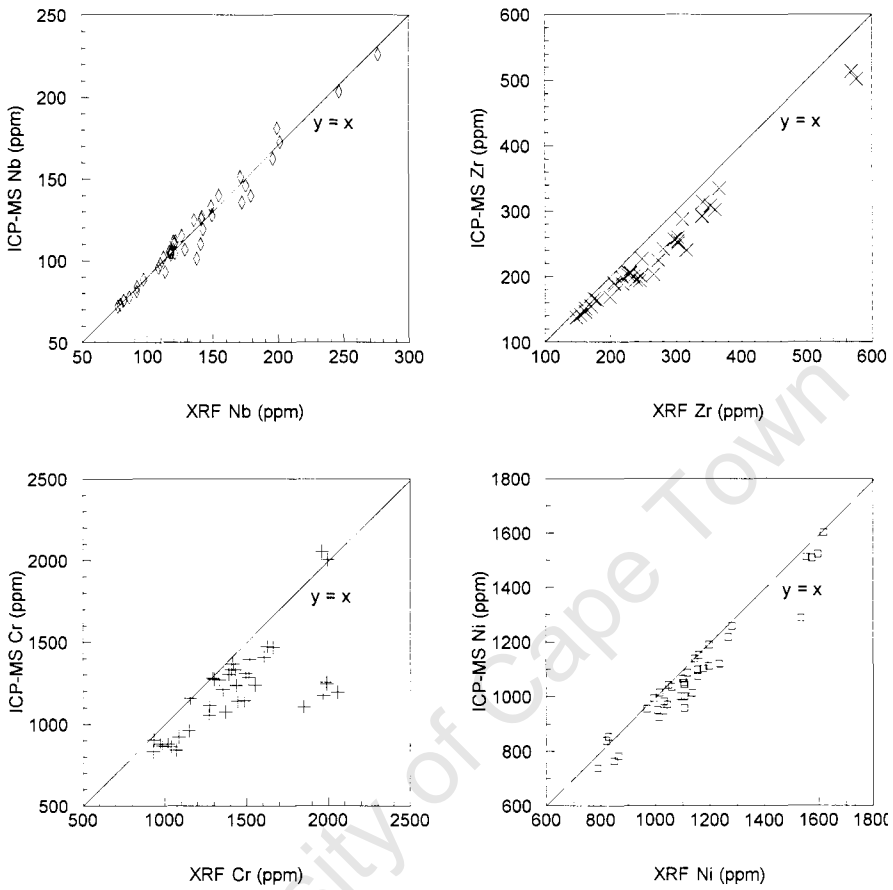

Figure B.3.1 Comparison of ICP-MS and XRF analyses of Nb, Zr, Cr and Ni.

B.4 Karbonat Bombe

CO_2 concentrations in the samples were measured by using the Karbonat Bombe (Birch, 1981). This instrument consists of a plexiglass cylinder with a screw-on lid and a manometer. A small plastic bucket is contained within the cylinder. The following procedure was followed:

- Calibration of instrument: 1g $CaCO_3$ is placed in the cylinder. The small bucket is filled with ~5ml of concentrated HCl and placed in the cylinder. The lid is screwed on tightly and the cylinder is shaken to allow the mixture of the $CaCO_3$ and the acid. A reading is taken from the manometer on completion of the reaction between the two components. The procedure is repeated for 0.5g $CaCO_3$. The results of the calibrations performed are depicted in Figure B.4.1.
- The instrument is thoroughly cleaned between analyses.

- $CaCO_3$ analysis: 3-5g of sample powder is weighed and placed into the cylinder. Concentrated HCl is added as described above and the cylinder is shaken. The manometer reading is taken and the $CaCO_3$ concentration is determined by using the calibration lines in Figure B.4.1.
- The CO_2 contents of the samples are subsequently calculated using stoichiometry.
- Standards of 1g $CaCO_3$ are analysed following the analyses of every five samples.

The precision of this technique is ~2% for samples containing >5% $CaCO_3$, and <4% for samples containing <5% $CaCO_3$.

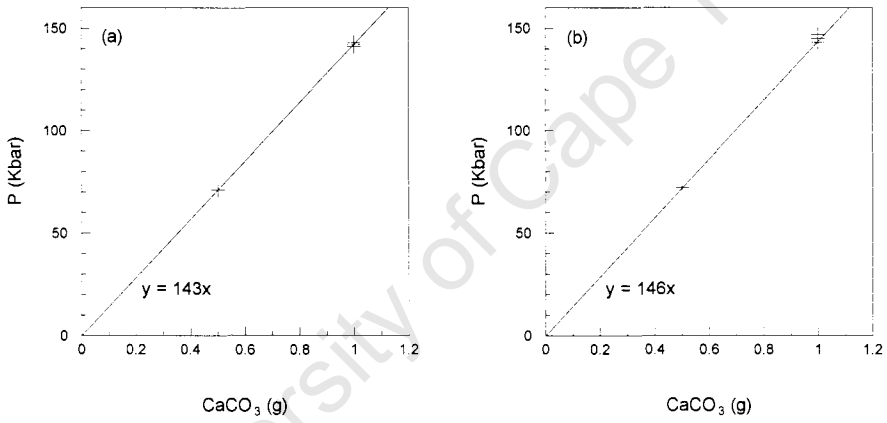

Figure B.4.1 $CaCO_3$ calibration curves for (a) D2 Type 2 & 3, D2/D5 and D5 samples and the three samples from which xenoliths were not picked; and (b) D18, Type 5, D16 and D16 Dyke samples. Two curves are necessary since analyses were performed over two days.